Departament de Física
Grup de Física Teòrica: Informació i Fenòmens Quàntics

Correlations in multipartite systems: From entanglement to localization

Author:

Julia Stasińska

Thesis supervised by:

Prof. Anna Sanpera Trigueros

Thesis written within the Doctoral Programme in Physics
Bellaterra, September 2012

Inside every ugly fact is a beautiful theory trying to escape. (...) Mathematics is the key that allows the hidden beauty of nature to show through.

Steve Jones

List of publications

Articles included in the thesis and published at the moment of its completion:

[Stasińska 12a] *Glass to superfluid transition in dirty bosons on a lattice.*
J. Stasińska, P. Massignan, M. Bishop, J. Wehr, A. Sanpera, M. Lewenstein
Journal ref.: New J. Phys. **14**, 043043 (2012)

[Stasińska 12b] *Beyond pure state entanglement for atomic ensembles.*
J. Stasińska, S. Paganelli, A. Sanpera
Journal ref.: New J. Phys. **14**, 033034 (2012)

[Augusiak 11] *Bell inequalities with no quantum violation and unextendible product bases.*
R. Augusiak, J. Stasińska, Ch. Hadley, J. K. Korbicz, M. Lewenstein, A. Acín
Journal ref.: Phys. Rev. Lett. **107**, 070401 (2011)

[Stasińska 09] *Manipulating mesoscopic multipartite entanglement with atom-light interfaces.*
J. Stasińska, C. Rodó, S. Paganelli, G. Birkl, A. Sanpera
Journal ref.: Phys. Rev. A **80**, 062304 (2009)

Submitted manuscripts included in the thesis:

[Stasińska 12c] *Multipartite entanglement of rotationally invariant states.*
J. Stasińska, B. Rogers, G. De Chiara, A. Sanpera
Submitted to Phys. Rev. A

Articles published during the PhD studies not connected with the subject of the thesis:

1. *Convergence of expansions in Schrödinger and Dirac eigenfunctions, with an application to the R-matrix theory.*
   J. Stasińska
   Journal ref.: J. Math. Phys. **53**, 022101 (2012)

2. *Positive maps, majorization, entropic inequalities, and detection of entanglement.*
   R. Augusiak, J. Stasińska
   Journal ref.: New J. Phys. **11**, 053018 (2009)

Other published articles

1. *A general scheme for construction of scalar separability criteria from positive maps.*
   R. Augusiak, J. Stasińska
   Journal ref.: Physical Review A **77**, 010303(R) (2008)

2. *Beyond the standard entropic inequalities: Stronger scalar separability criteria and their applications.*
   R. Augusiak, J. Stasińska, P. Horodecki
   Journal ref.: Phys. Rev. A **77**, 012333 (2008)

3. *Rotationally invariant bipartite states and bound entanglement.*
   R. Augusiak, J. Stasińska
   Journal ref.: Phys. Lett. A **363**, 182 (2007)

Contents

Chapter 1

Introduction

The notion of entanglement captures the idea that in a a quantum world one may posses a maximal knowledge about a composite (pure) state, yet not have access to such complete information about each individual subsystem. This genuinely quantum feature of physical systems, which was initially perceived as more of a paradox and curiosity than something useful, eventually became one of the marvels of modern science. The theory of entanglement, although far from complete, is now well developed and offers many tools that allow us to test the presence of such correlations and quantify its content in a given state (see [Horodecki 09, Gühne 09] for current reviews of the subject). On the one hand, entanglement is treated as a resource with capacity to enable quantum information tasks like teleportation of quantum states or dense coding of information, which are not achievable within classical theory [Nielsen 00]. It also turns out to be an essential ingredient for quantum computational speed-up in many algorithms; especially multipartite entanglement draws a lot of attention in this context [Vidal 03a, Jozsa 03, Bruß 11]. On the other hand, the apparatus of quantum information proved useful for analysis of complex ground states of, e.g., quantum critical systems providing some insight into their structure and revealing new properties [Amico 08]. Moreover, it helps to develop efficient numerical methods for simulation of complex many-body systems [Verstraete 04b, Vidal 04].

On a more abstract level, quantum correlations, in general not equivalent to quantum entanglement, are studied within the paradigm of device-independent quantum information processing [Barrett 05b, Acín 07, Pironio 10]. There, a central role is played by the notion of correlations between the sets of data, completely detached from their particular physical origin. The parties do not need to know the details of the devices they use to generate the data, the only requirement is that the shared correlations are sufficiently strong to enable a given task. The strength of classical correlations is subject to certain constraints, commonly known as Bell inequalities. Violation of these inequalities is the manifestation of non-locality—displayed, in particular, by quantum mechanics, meaning that quantum mechanics can outperform classical physics at tasks associated with such Bell inequalities. For instance, non-local quantum correlations provide cryptographic security not achievable with classical theory [Ekert 91, Masanes 11] and outperform classical correlations at communication complexity problems [Brukner 04, Buhrman 10]. Interestingly, however, there exist situations in which one does not have any advantage from quantum data and only a stronger type of correlations (supra-quantum correlations) is of benefit [Almeida 10, Acín 12a].

This thesis deals with the study of multipartite correlations in various physical systems such as atomic ensembles of non-interacting atoms, systems of interacting spins and disordered Bose gas in an optical lattice. In each case I emphasize a different aspect of this broad concept. First, I concentrate on generation of multipartite entanglement with atom-light interfaces. Then, the focus is shifted to the analysis of multipartite correlations in spin networks using quantum information tools. Finally, I take a more conventional approach and characterize the disordered Bosonic system with typical observables of Condensed Matter Physics. I also analyse correlations as an abstract concept concentrating on device-independent multipartite tasks for which correlations of quantum origin perform equally well as the classical ones. The thesis is organized as follows.

In chapter 2 I provide a brief survey of the entanglement theory. It begins with the definition of bipartite entanglement and the review of elementary methods of its detection and quantification. Then, I introduce the well-known results concerning multipartite systems and the hierarchy of entangled states in this case, which is much richer than in the bipartite scenario. In particular, in the multipartite case a notion of the maximally entangled state does not exist and, due to this fact, quantification of multipartite correlations becomes an intricate task. In this chapter I also pay special attention to the concept of bound entanglement in the bipartite and multipartite case.

In Chapter 3 I study the physical system of atomic ensembles placing a particular emphasis on the multipartite entanglement that can be induced between them through the atom-light interface. Such set-ups have a huge potential as elements of quantum communication networks since they incorporate two types of quantum systems, the long-living atomic ensembles and the " ying" photons [Briegel 98, Sangouard 11]. We show that they offer a universal toolbox for generation and manipulation of continuous-variable multipartite entanglement proving to be also an efficient experimental playground for quantum information studies of foundational character. The results presented in this chapter are reported in [Stasińska 09] and [Stasińska 12b].

In Chapter 4 we shift our focus to an abstract problem of finding device-independent tasks for which (i) quantum correlations do not outperform the classical ones but (ii) there exist supra-quantum non-signalling correlations that do provide an advantage [Acín 12a]. We demonstrate a systematic way to build such tasks from Unextendible Product Bases — an important concept in entanglement theory [Bennett 99b]. The fundamental importance of UPBs stems from the fact that they allowed for the construction of one of the first examples of bound entangled states [Horodecki 98]——and, furthermore, that they give rise to *nonlocality without entanglement* [Bennett 99a], i.e., the impossibility of perfectly distinguishing orthogonal product states by means of local operations and classical communication. Our results, reported in [Augusiak 11], establish a link between the structure of composite Hilbert spaces, which gives rise to this intriguing phenomenon, and the properties of the sets of correlations.

Chapter 5 is devoted to application of quantum information tools in the study of spin models. I concentrate on entanglement properties of the ground and thermal states of spin graphs, in particular on the presence of genuine tripartite entanglement in their subsystems. The role of entanglement is particularly important in the study of quantum phase transitions (QPT), where multipartite long-range correlations are believed to play a central role. Even though in our analysis we are far from the thermodynamic limit, characterization of tripartite entanglement reveals qualitative differences between ground states of spin systems in different regimes of parameters. The results are reported in [Stasińska 12c].

In Chapter 6 I move to the study of bosonic lattice gases in the presence of disorder. I study a particular type of random potential, the so-called Bernoulli potential, obtained through a random distribution of identical impurities in a lattice. An important advantage of systems with this particular disorder is that they admit rigorous analytical estimates. I focus on the regime of weak to intermediate interactions and explore the properties of the ground and thermal states of 1D and 2D systems characterizing them by means of typical parameters such as the super uid fraction, fractal dimension and correlation function. Most of the results of this chapter are reported in [Stasińska 12a], however, I also include some unpublished results obtained within an ongoing project in collaboration with L. Sanchez-Palencia, P. Massignan and M. Lewenstein.

Finally, in Chapter 7 I summarise the obtained results and sketch future research directions.

Chapter 2

Preliminaries

In this chapter I review the basic concepts of the theory of composite quantum systems, which I use throughout the thesis. I explain the notion of entanglement in the bipartite and multipartite case and introduce the elementary separability criteria. Then I discuss the distillation of maximally entangled states, an important problem in the entanglement theory, devoting special attention to the concept of bound entanglement in multipartite systems. I finish the chapter with a brief survey of a special class of quantum states, the continuous variable Gaussian states. Their importance follows from the fact that they can be efficiently generated, manipulated and detected with the current optical technology. Moreover, many other physical set-ups admit the CV Gaussian description, among others the system of atomic ensembles interfaced with light, which I inspect in more detail in chapter 3.

2.1 Bipartite entanglement

Consider a quantum system composed of two particles each described by a Hilbert space $\mathcal{H}_i$ of dimension d_i ($i = 1\ 2$). The composite bipartite Hilbert space is then a tensor product of the two local spaces $\mathcal{H} = \mathcal{H}_1 \otimes \mathcal{H}_2$ and a general pure state of the system is the superposition of product states, which can be written as

$$\Psi \ = \sum_{i,j=1}^{d_1,d_2} c_{ij}\ i \ \otimes \ j \tag{2.1}$$

with complex coefficient matrix $[c_{ij}]_{i,j=1}^{d_1,d_2}$. A pure state Ψ is called *separable* whenever there exist two local vectors $_1$ $_2$ such that $\Psi = _1 \otimes _2$, i.e., in the pure state case separability is equivalent to being a product state. If this is not the case Ψ is called *entangled*. Note that it is straightforward to produce a pure separable state locally, however generation of an entangled state requires some kind of non-local action. Therefore, local producibility (in the scenario with parties sharing some classical correlations or with allowed communication, so-called LOCC scenario) is what characterizes separable states. Generalizing this notion to mixed states we note that obviously a product of two density matrices can be generated with local resources. Moreover, all convex combinations of such products, giving the most general

separable mixed state in the form

$$\rho = \sum_i p_i \rho_2^{(i)} \otimes \rho_1^{(i)} \tag{2.2}$$

with non-negative p_i. A density matrix that does not admit such decomposition represents an entangled state.

Deciding whether a given bipartite state is entangled or separable using solely the definition is not an easy task and a general solution to the separability problem is not known. Nevertheless, there exist some operational criteria that applied to a density matrix imply separability or entanglement. In what follows I will review the most popular approaches to the separability problem.

2.1.1 Separability criteria

I begin with the structural criteria, i.e., such that require the full knowledge of the density matrix to be applied, and therefore are not directly measurable in experiments. In this class we have, among others, the criteria based on positive maps, on linear contractions and permutations and the algorithmic approaches. I will concentrate on the first of this categories.

Positive linear maps. — Let us denote by $\mathcal{B}(\mathcal{H}_i)$ a space of linear operators acting on $\mathcal{H}_i$. A linear map $\Lambda : \mathcal{B}(\mathcal{H}_1) \quad \mathcal{B}(\mathcal{H}_2)$ is called positive (P) if it maps positive operators onto positive operators. Among all positive maps we distinguish those that preserve positivity of an operator even if applied to its subsystem, i.e., Λ is called completely positive (CP) if for any auxiliary $\mathcal{H}_A$ the map $\mathbb{I}_A \otimes \Lambda$ is positive [$\mathbb{I}_A$ is an identity map on $\mathcal{B}(\mathcal{H}_A)$]. Now, of particular importance in entanglement detection are those maps which are positive, yet not completely positive. Such a map when applied to a separable state returns a positive matrix, however it need not be the case for entangled matrices. It turns out that even a stronger statement is true [Horodecki 96].

Fact 1. The state $\rho \quad \mathcal{B}(\mathcal{H}_1) \otimes \mathcal{B}(\mathcal{H}_2)$ is separable if and only if for all P but not CP maps $\Lambda : \mathcal{B}(\mathcal{H}_2) \quad \mathcal{B}(\mathcal{H}_1)$ the following holds:

$$[\mathbb{I}_1 \otimes \Lambda](\rho) \geqslant 0 \tag{2.3}$$

Consequently, if there exist a P but not CP map for which the above inequality does not hold, then ρ must be entangled.

Partial transposition. — A strong necessary separability condition is provided by the transposition map T [Peres 96, Horodecki 96]. We say that the state ρ is PPT (positive partial transpose) if it fulfils the condition

$$[\mathbb{I}_1 \otimes T](\rho) \geq 0 \qquad [T \otimes \mathbb{I}_2](\rho) \geq 0 \tag{2.4}$$

Otherwise we call the state NPT (non-positive partial transpose). By Fact 1, all NPT states are necessarily entangled. More importantly, as it was shown in [Horodecki 96], for low-dimensional Hilbert spaces, i.e., those of dimensions $2 \otimes 2$ and $2 \otimes 3$, all PPT states are separable, which solves completely the separability problem in this cases.

The other group of tests, the so-called scalar criteria, aims at experimental detection of entanglement. They are formulated in terms of observables on a single or many copies of a state or require a measurement of several quantities, but much less comparing to the full

state tomography. In this category we include such approaches as entropic and entropic-like inequalities, entanglement witnesses, criteria based on variances and covariances *etc* .

Entropic inequalities. — As already pointed out, the concept of entanglement is the manifestation of the fact that in a a quantum world, unlike in classical systems, one may posses more information about the global system than about each individual subsystem. This statement is more precisely expressed through the measure of information, entropy. As proved in [Vollbrecht 02] for all separable states $\mathcal{B}(\mathcal{H}_1) \otimes \mathcal{B}(\mathcal{H}_2)$ it holds that

$$\underset{\alpha>0}{} S_\alpha(\rho) \geqslant S_\alpha(\rho_1) \;\&\; S_\alpha(\rho) \geqslant S_\alpha(\rho_2) \tag{2.5}$$

where $S_\alpha(\rho) = (1-\alpha)^{-1} \log \mathrm{tr}\rho^\alpha$ is the Renyi α-entropy. Violation of an entropic inequality indicates that a given state is entangled. Direct measurement of the Renyi entropy is possible for integer α through a multi-copy observable, and involves α identical and uncorrelated copies of the state [Horodecki 03, Bovino 05].

Entanglement witnesses. — An entanglement witness is, by definition, a Hermitian operator (quantum observable) $\mathcal{W}$ acting on a composite Hilbert space such that it has a non-negative mean value for all separable states, and a negative mean value for at least one entangled state. We say that an entangled state ρ is detected by the witness $\mathcal{W}$ if $\mathrm{tr}\rho\mathcal{W} < 0$.

Due to the Choi-Jamio kowski isomorphism, which links entanglement witnesses and P but not CP maps, entanglement witnesses provide a complete characterization of the set of separable states in a way analogous to Fact 1.

Fact 2. The state ρ $\mathcal{B}(\mathcal{H}_1) \otimes \mathcal{B}(\mathcal{H}_2)$ is separable if and only if for all entanglement witnesses $\mathcal{W}$ $\mathcal{B}(\mathcal{H}_1) \otimes \mathcal{B}(\mathcal{H}_2)$ the following holds:

$$\mathrm{tr}\rho\mathcal{W} \geqslant 0 \tag{2.6}$$

It follows that for each entangled state there exist an entanglement witness detecting it.

2.1.2 Entanglement measures

Entanglement is a fundamental resource of quantum information theory and an essential ingredient for applications such as quantum teleportation or quantum dense coding. The entanglement criteria discussed in the previous subsections give a yes–no answer to the question about the presence of entanglement, however, usually cannot tell how useful this entanglement is or *what is the entanglement contents of a given state*. This is the role of *entanglement measures*.

There exist entanglement measures which inform us how well does a given state perform in a specific quantum information protocol; we call them *operational* measures. For example the entanglement cost E_C is defined as the number of qubits that have to be communicated in order to produce a given state. The other approach to quantification of entanglement is purely *axiomatic*. A function of a state is said to be an entanglement measure if it fulfils the monotonicity condition, namely does not increase if the state is transformed through LOCC. A complete review of entanglement measures and their properties may be found in [Horodecki 09].

2.2 Multipartite entanglement

Multipartite states have a much more complex structure than the bipartite ones. In particular, there the whole hierarchy of separability classes can be distinguished, in contrast to just one type of separable states in the bipartite case [Dür 00]. Another phenomenon not encountered in two-particle systems is the existence of many locally inequivalent types of entangled states, i.e., states that cannot be converted one to another through stochastic local operations and classical communication (SLOCC). For this reason it is also very difficult to quantify this type of correlations, as there is no single representative maximally entangled state.

A direct generalization of the notion of bipartite separability to the N-partite case, based on the local producibility postulate, is the full separability

$$\rho = \sum_i p_i \rho_1^{(i)} \otimes \quad \otimes \rho_N^{(i)} \tag{2.7}$$

where ρ is a density matrix acting on a product Hilbert space $\mathcal{H}_1 \otimes \quad \otimes \mathcal{H}_N$. An entangled state is then one that does not admit this decomposition. However, in the multipartite case a state that is not fully separable is not immediately fully entangled. There exist a notion of partial separability, i.e., separability with respect to partitions of a state. Let us refer to the simplest example of tripartite states to illustrate this concept.

Despite being the simplest multipartite system, the three-qubit states already have the qualities that do not exist in the bipartite scenario, i.e., the presence of partial separability and locally inequivalent fully entangled states. Characterization of this class was given in [Dür 00, Acín 01], where four types of states were distinguished: (i) separable states $\mathcal{S}$, (ii) biseparable states $\mathcal{B}$, (iii) W-type states, and (iv) GHZ-type states. Each of the classes embraces those that are lower in the hierarchy, $\mathcal{S} \subset \mathcal{B} \subset \mathrm{W} \subset \mathrm{GHZ}$. Separable states are those that admit decomposition (2.7). Biseparable states belong to the convex hull of states separable with respect to one of the bipartite partitions 1 23, 2 13 or 3 12 denoted by $\mathcal{B}_1$, $\mathcal{B}_2$, $\mathcal{B}_3$, respectively. Hence, $\mathcal{B} = \mathrm{conv}(\mathcal{B}_1\ \mathcal{B}_2\ \mathcal{B}_3)$. The division between the W-type states and the GHZ-type states stems from the fact that in three qubits there exist two SLOCC inequivalent classes of genuinely entangled states with representative elements being precisely the W state

$$\mathrm{W} = \frac{1}{\sqrt{3}}(\ 100\ +\ 010\ +\ 001\ ) \tag{2.8}$$

and the GHZ state

$$\mathrm{GHZ} = \frac{1}{\sqrt{2}}(\ 000\ +\ 111\ ) \tag{2.9}$$

Therefore, the W-class is defined as those states that are a convex combination of states SLOCC-equivalent to W . Analogously, the GHZ-class contains all SLOCC-transformations of GHZ and is, at the same time, equal to the set of all tripartite states.

The classification of the three-qubit states based on convex sets can be generalized to arbitrary number of parties and any dimension [Dür 99, Dür 00]. This, however, is not the unique classification one may think of. As pointed out in [Gühne 09] identifying a state to belong to one of such sets answers the question: *How many partitions are separable?* Other criteria on which a hierarchy of states may be built include the questions: *How many parties are entangled?* or *How many parties are separable?* Each of these issues becomes important in a different context. For example, the first one tells us what resources are required

to produce a given state and may be more adequate for study of entanglement in macroscopic systems [Gühne 05].

Entanglement detection. — One way of detecting entanglement in the multipartite case is to reduce the problem to detection of bipartite entanglement between different partitions. This strategy, however, does not guarantee success, as there exist states separable with respect to any bipartition, but not fully separable. Several tests have been designed specifically for multi-particle systems, for instance, criteria based on permutations[Clarisse 06], the spin-squeezing inequalities[Korbicz 06, Tóth 07], multipartite entanglement witnesses[Acín 01, Gühne 05, Kaszlikowski 08]. They allow to recognize that a given state belongs to a specific entanglement class (concentrating usually on the two extreme cases: full separability and genuine multipartite entanglement).

2.3 Distillation of entanglement, bound entanglement

Distillation of entanglement is the protocol exploiting LOCC operations to convert n copies of some bipartite entangled state ρ to $m < n$ copies of the (approximately) maximally entangled state. Feasibility of such task is of fundamental importance for quantum information as many basic protocols require pure bipartite entanglement. Moreover, the efficiency of distillation, measured by the rate $r = m\ n$, is a crucial parameter. The first constructive proof that the task is achievable was given in [Bennett 96, Deutsch 96], where the first distillation protocols were proposed.

Then, the question which states are distillable should be answered. Obviously, separable states are undistillable since one cannot create entanglement via LOCC. Therefore, entanglement is a necessary condition for distillability; it turns out, however, *not* to be a sufficient one. As shown in [Horodecki 98], all PPT states are undistillable. As the first example of an entangled PPT state was already known [Horodecki 97], this lead to the astonishing conclusion that there exist undistillable entangled states, i.e., *bound entangled* states.

Bound entangled states require some amount of entanglement to be created, but then the resource becomes so "diluted" that no maximally entangled state can be recovered. One may, therefore, ask whether such states can still be useful. A positive answer to this question was given in [Horodecki 99] and since then many other protocols employing bound entanglement were found. I will come back to this issue in chapter 3, where I discuss a particular example of a bound entangled state, the Smolin state [Smolin 01].

Let us comment here on entanglement distillation from multipartite states. There, the problem can be reduced to distillation of maximally entangled states between each pair. Subsequently, the parties can use the distilled resource to prepare a desired multipartite state (in general, a more efficient strategy converting a number of given states to the desired state may exist, but the presented approach is more universal). The sufficient condition for distillability of pure bipartite entanglement from a number of copies of a given N-partite state was given in [Dür 99, Dür 00]. Precisely, the authors proved that in order to distil entanglement between parties i and j it must hold that every bipartite split dividing i and j is NPT. Consequently if there exist a PPT bipartition of the state such that i and j belong to different sets, the state is undistillable with respect to this two parties. We call a state *multipartite bound entangled* if no bipartite entanglement can be distilled from it.

2.4 Continuous variable states

Discrete or continuous degrees of freedom of quantum systems manifest themselves upon measurement of observables with discrete or continuous spectrum. The latter case imposes a continuous variable description of quantum states which essentially involves infinite-dimensional Hilbert spaces. In such situation, usually the most convenient characterization is provided by a quasi-probability distribution in phase space, e.g., the Wigner function. A system with two canonical degrees of freedom Q and P fulfilling the Canonical Commutation Relation (CCR)

$$[Q\ P] = i\mathbf{1} \tag{2.10}$$

and described by a density matrix is fully characterized by the Wigner function defined as

$$W_\varrho(q\ p) = \frac{1}{\pi}\int_{-\infty}^{\infty} \mathrm{d}x\ \ q + x \quad q - x\ \ e^{2ipx} \tag{2.11}$$

where q are the eigenvectors of $Q : Q\ q\ = q\ q\ $. Such quasi-probability distribution gives a complete description of measurement outcomes statistics for $Q\ P$ and arbitrary functions of these observables. A particular family of CV states, to which belong the systems of atomic ensembles studied in chapter 3, are the Gaussian states. Here I review the most basic concepts needed to efficiently describe such systems, with particular emphasis placed on the atomic ensembles set-up. For a more detailed review of CV systems the reader is referred to [Giedke 02, Braunstein 05, Adesso 07, Andersen 10] and references therein.

2.4.1 Covariance matrix formalism for Gaussian states

Gaussian states are those whose marginals of the quasi-probability distribution for q and p are Gaussian. This is the case, e.g., for collective degrees of freedom describing the atomic ensembles or high-intensity laser beams. They are a sum of identical independent random variables corresponding to single atoms or photons, respectively and due to the Central Limit Theorem admit the Gaussian distribution.

Theorem 2.1. *(Lindeberg-Levy) If independent random variables $Y_1\ Y_2 \quad Y_n$ have the same distribution with mean value μ and variance σ^2 then the distributions of*

$$Z_n = \frac{\dfrac{1}{n}\displaystyle\sum_{i=1}^{n} Y_i - \mu}{(\sigma \quad \overline{n})} \tag{2.12}$$

converge (in distribution) to $\mathcal{N}(0\ 1)$, i.e., the standard normal distribution.

Description of Gaussian states. — Gaussian states are fully characterized by the first and second moments of the canonical coordinates. For a Gaussian quantum system of N pairs of canonical degrees of freedom ("position" and "momentum" called also quadratures) $R = (X_1\ P_1 \quad X_N\ P_N)$, the first moments of R define the displacement vector (DV) d,

$$d_i = \mathrm{tr}(\ R_i) \tag{2.13}$$

and the second moments, the covariance matrix (CM) γ

$$\gamma_{ij} = \mathrm{tr}(\quad R_i - d_i\ R_j - d_j\ \ ) \tag{2.14}$$

The Wigner function of Gaussian states has a general form

$$W(\zeta) = \frac{1}{\pi^N \sqrt{\det \gamma}} \exp\left[-(\zeta - d)^T \gamma^{-1} (\zeta - d)\right] \tag{2.15}$$

where the variable $\zeta = (x_1 \ p_1 \quad \ldots \quad x_N \ p_N)$ is a real phase space vector. The CM corresponding to a quantum state must fulfil the positivity condition

$$\gamma + i\mathcal{J}_N \geqslant 0 \tag{2.16}$$

where $\mathcal{J}_N$ is the symplectic matrix for N modes defined through the commutation relations as

$$(\mathcal{J}_N)_{ij} = \frac{1}{i}[R_i \ R_j] \qquad (i \ j = 1 \quad \ldots \quad 2N) \tag{2.17}$$

Equivalently the positivity condition can be formulated using the notion of symplectic spectrum $\{\nu_k\}_{k=1}^N$, i.e., N quantities constituting the non-negative part of the spectrum of $i\mathcal{J}_N\gamma$. If all the symplectic eigenvalues fulfil

$$\nu_k \geqslant 1 \tag{2.18}$$

the covariance matrix corresponds to a quantum state.

Gaussian operations. — Gaussian operations are those completely positive maps that preserve the Gaussian character of states. All of them can be applied at the level of CM and DV using symplectic transformations and homodyne measurements [Andersen 10].

A symplectic transformation of a CM, $\gamma' = S^T \gamma S$, is the analogue of a Gaussianity-preserving unitary transformation of a density matrix. The matrix S represents a symplectic transformation if it preserves the CCR, i.e., the transformed canonical degrees of freedom $R' = SR$ must still fulfil equation (2.10). Due to relation (2.17) this condition can be shortly written as

$$S^T \mathcal{J} S = \mathcal{J} \tag{2.19}$$

The set of real matrices of dimension $2N \times 2N$ satisfying condition (2.19) forms a symplectic group $\mathsf{Sp}(2N, \mathbb{R})$.

To show how the homodyne measurement of a subsystem in uence a CM and DV, we write a general CM in the form

$$\gamma = \begin{pmatrix} A & C \\ C^T & B \end{pmatrix} \tag{2.20}$$

where B is a 1-mode subsystem of a multi-mode state. Homodyne measurement of the quadrature X_B with outcome $\tilde{x}_B$ leaves the subsystem A in a state described by the covariance matrix

$$\gamma_A' = A - C(DBD)^{-1} C^T \tag{2.21}$$

and the displacement vector

$$d_A' = d_A + C(DBD)^{-1}(\tilde{x}_B \ 0) \tag{2.22}$$

where the inverse is understood as an inverse on the support whenever the matrix is not of full rank, and $D = \mathrm{Diag}(1 \ 0)$. The homodyne detection of any other combination of quadratures can be reduced to the present case by applying prior to the measurement an appropriate symplectic transformation.

2.4.2 Gaussian states of quantized electromagnetic field

Here we review the properties of the fundamental Gaussian states: the single-mode vacuum state, coherent states, squeezed states and the thermal state.

Vacuum state. — The vacuum state, denoted by $|\Omega\rangle$, is defined as the lowest energy eigenstate of the field Hamiltonian $H_{\text{field}} = \sum_n \hbar\omega_n \left(a_n^\dagger a_n + 1/2\right)$. It fulfils the condition

$$a_n |\Omega\rangle = 0 \tag{2.23}$$

which is sometimes used as an alternative definition. From now on we concentrate on a single mode, and determine first and second moments of field quadratures. Since by equation (2.23) the expectation values for both a and $a^\dagger$ vanish, the mean values of X and P also amount to zero, i.e.,

$$\langle X \rangle = \left\langle \frac{1}{\sqrt{2}} \left(a + a^\dagger\right) \right\rangle = 0 \qquad \langle P \rangle = \left\langle \frac{1}{\sqrt{2}i} \left(a - a^\dagger\right) \right\rangle = 0 \tag{2.24}$$

The second moments, i.e., the variances and the covariances, are also easily determined from the definition and read:

$$\mathrm{Var}X = \frac{1}{2} \qquad \mathrm{Var}P = \frac{1}{2} \qquad \langle XP + PX \rangle = 0 \tag{2.25}$$

Using this we immediately write the CM and the DV of the vacuum state

$$\gamma_\Omega = \begin{pmatrix} 1 & 0 \\ 0 & 1 \end{pmatrix} \qquad d_\Omega = (0 \;\; 0) \tag{2.26}$$

Notice that the variances of X and P have a minimum value allowed by the uncertainty principle, hence the vacuum state has minimum fluctuations allowed by quantum mechanics. This is the property shared by all pure Gaussian states.

Coherent states. — By definition the coherent state is an eigenstate of the annihilation operator

$$a\,|\alpha\rangle = \alpha\,|\alpha\rangle \tag{2.27}$$

corresponding to a complex eigenvalue α. One can show that a coherent state is obtained from a vacuum state through the unitary displacement, i.e., $|\alpha\rangle = \mathcal{D}(\alpha)\,|\Omega\rangle$, where

$$\mathcal{D}(\alpha) = \exp(\alpha a^\dagger - \alpha^* a) \tag{2.28}$$

The knowledge of the action of the displacement operator on the creation and annihilation operator, $\mathcal{D}^\dagger(\alpha) a \mathcal{D}(\alpha) = a + \alpha$, allows us to determine the mean values for the quadratures in the coherent state

$$\langle X \rangle = \frac{1}{\sqrt{2}}(\alpha + \alpha^*) = \sqrt{2}\mathrm{Re}\,\alpha \qquad \langle \mathrm{P} \rangle = \frac{1}{\sqrt{2}i}(\alpha - \alpha^*) = \sqrt{2}\mathrm{Im}\,\alpha \tag{2.29}$$

In a similar manner we obtain the second moments which are exactly the same as those for the vacuum state (2.32). Therefore, we arrive at the following CM and the DV

$$\gamma_\alpha = \begin{pmatrix} 1 & 0 \\ 0 & 1 \end{pmatrix} \qquad d_\alpha = \begin{pmatrix} \sqrt{2}\mathrm{Re}\,\alpha & \sqrt{2}\mathrm{Im}\,\alpha \end{pmatrix} \tag{2.30}$$

Squeezed vacuum states. — Squeezed states are pure states of electromagnetic field with reduced uctuations in one of the quadratures. Since as pure Gaussian states they must saturate the uncertainty principle, the reduction is obtained at the cost of enlarging the uctuations of the complementary quadrature, i.e., anti-squeezing. The state can be obtained through a unitary squeezing transformation of the vacuum state $\Omega\ \xi\ = \mathcal{S}(\xi)\ \Omega\ $, with

$$\mathcal{S}(\xi) = \exp\left[\frac{1}{2}\xi^* a^2 - \frac{1}{2}\xi(a^\dagger)^2\right] \tag{2.31}$$

The expectation values for the quadratures in the squeezed vacuum state are the same as those for the vacuum, while the variances must, by definition, be modified. We have

$$\mathrm{Var}X = \frac{1}{2}e^{-2r} \qquad \mathrm{Var}P = \frac{1}{2}e^{-2r} \tag{2.32}$$

where $r = \mathrm{Re}\,\xi$ is the so-called squeezing parameter. Hence, the CM representation of the squeezed vacuum state is

$$\gamma_{\Omega,\xi} = \begin{pmatrix} e^{-2r} & 0 \\ 0 & e^{2r} \end{pmatrix} \qquad d_{\Omega,\xi} = (0\ 0) \tag{2.33}$$

Thermal states. — A thermal state is the equilibrium state of field coupled to a reservoir at temperature T. A single thermal mode of frequency is characterized by an average number of thermal photons which follows the Bose-Einstein statistics

$$n\ _T = \frac{1}{\exp(\beta\ ) - 1} \tag{2.34}$$

where $\beta = 1\ T$, and the following density matrix

$$\rho_T = Z^{-1}\exp(\beta\ a^\dagger a) \tag{2.35}$$

It is then straightforward to determine the moments of the quadratures:

$$X\ =\ P\ = 0 \tag{2.36}$$

and

$$\mathrm{Var}X = \mathrm{Var}P = \frac{1}{2}\frac{e^{\beta\omega}+1}{e^{\beta\omega}-1} =\ n\ _T + \frac{1}{2} \tag{2.37}$$

The symmetrized covariance term equals zero which leads to the following CM and DV:

$$\gamma_T = \begin{pmatrix} 2\ n\ _T + 1 & 0 \\ 0 & 2\ n\ _T + 1 \end{pmatrix} \qquad d_T = (0\ 0) \tag{2.38}$$

2.4.3 Separability of Gaussian states

The covariance matrix and the displacement vector provide a complete knowledge about a Gaussian state, but in fact it is only the CM that carries information about quantum correlations, i.e., entanglement between modes. This makes verification of entanglement amenable to covariance matrix entanglement criteria. The necessary and sufficient separability criterion, which may also serve as a definition of separability for bipartite Gaussian systems, was

given in [Werner 01b]. It states that a CM γ of $N+M$ modes represents a separable state if and only if there exist two CMs γ_1 and γ_2 of N and M modes, respectively, such that

$$\gamma \geqslant \gamma_1 \oplus \gamma_2 \tag{2.39}$$

This criterion, similarly to the definition of separability (2.2), is rather difficult to apply. However, there exist many operational tests applicable at the level of covariance matrix [Simon 00, Duan 00b, Giedke 01a, van Loock 03]. In what follows I recall only those that are used in the thesis.

Partial time reversal map. — A CV counterpart of the PPT criterion, which can only be applied when the full CM is available, is the partial time reversal of the covariance matrix [Simon 00]. It corresponds to a change of the sign of momentum for the chosen modes. We denote the map applied to modes $I = i_1 \quad i_m$ by τ_I. If the partially time reversed covariance matrix does not fulfil the positivity condition (2.16), i.e.,

$$\tau_I(\gamma) \not\geqslant i\mathcal{J} \tag{2.40}$$

the state corresponding to γ is entangled with respect to the partition $I - N \quad I$. This test, however, checks only bipartite entanglement. In the multipartite scenario, a state may be PPT with respect to all its bipartite divisions and still not be fully separable. Such states are bound entangled states. For Gaussian states this criterion is necessary and sufficient to detect entanglement in all partitions of $1 \times N$ modes.

Negativity. — Negativity is a bipartite entanglement measure that quantifies the non-positiveness of a density matrix after the application of the partial transposition map [Zyczkowski 98, Vidal 02]. For a general quantum state it is defined as

$$\mathcal{N}(\ ) = \frac{\left\| \ ^{T_I} \right\|_1 - 1}{2} \tag{2.41}$$

where $\cdot \ _1$ is the trace norm and T_I denotes the partial transposition with respect to parties from set I. Alternatively one can use the logarithmic negativity defined as

$$E_{\mathcal{N}}(\ ) = \log \left\| \ ^{T_I} \right\|_1 \tag{2.42}$$

For Gaussian states both the negativity and the logarithmic negativity can be expressed in terms of the symplectic spectrum $\tilde{\nu}_k$ of the partially time reversed CM $\tau_I(\gamma)$ as follows

$$\mathcal{N}(\gamma) = \begin{cases} \frac{1}{2} \prod_{k:\tilde{\nu}_k<1} \tilde{\nu}_k^{-1} & \text{if} \quad {}_{\mathrm{k}}\tilde{\nu}_{\mathrm{k}} < 1 \\ 0 & \text{if} \quad {}_{\mathrm{k}}\tilde{\nu}_{\mathrm{k}} \geqslant 1 \end{cases} \tag{2.43}$$

and

$$E_{\mathcal{N}}(\gamma) = \begin{cases} -\sum_{k:\tilde{\nu}_k<1} \log \tilde{\nu}_k & \text{if} \quad {}_{\mathrm{k}}\tilde{\nu}_{\mathrm{k}} < 1 \\ 0 & \text{if} \quad {}_{\mathrm{k}}\tilde{\nu}_{\mathrm{k}} \geqslant 1 \end{cases} \tag{2.44}$$

Criterion for full separability of a three-mode state. — In general, it is not an easy task to distinguish between fully separable and fully PPT entangled states for arbitrary number of modes. For three-mode Gaussian states, a CM-based full separability criterion was given in [Giedke 01a]. Its formulation requires several definitions so before we go into the details of the criterion let us set the notation.

We write the three-mode CM in the form

$$\gamma_3 = \begin{pmatrix} A & C \\ C^T & B \end{pmatrix} \tag{2.45}$$

with A corresponding to the first mode. Then the authors define two matrices

$$N = A - C(B - i\mathcal{J})^{-1}C^T \qquad \widetilde{N} = A - C(B - i\widetilde{\mathcal{J}})^{-1}C^T \tag{2.46}$$

where $\widetilde{\mathcal{J}} = \mathcal{J}_2 \oplus -\mathcal{J}_2$. Now, we need to define two-dimensional vectors whose elements are connected to elements of N $\widetilde{N}$

$$L = \begin{pmatrix} N_{11} - N_{22} \\ 2\mathrm{Re}N_{12} \end{pmatrix} \qquad \widetilde{L} = \begin{pmatrix} \widetilde{N}_{11} - \widetilde{N}_{22} \\ 2\mathrm{Re}\widetilde{N}_{12} \end{pmatrix} \tag{2.47}$$

We state the criterion in the following fact:

Fact 3. (adapted from [Giedke 01a]) A three-mode state corresponding to a fully PPT CM γ, i.e., one that fulfils

$$\tau_1(\gamma) \geqslant i\mathcal{J} \qquad \tau_2(\gamma) \geqslant i\mathcal{J} \qquad \tau_3(\gamma) \geqslant i\mathcal{J} \tag{2.48}$$

is fully separable if and only if it holds that

$$\det N \geqslant 0 \qquad \det \widetilde{N} \geqslant 0 \tag{2.49}$$

and at least one of the points $(y\ \ z)$ from the following set:

$$S = \left\{ m_c\ \ m_e\ \ m_{\tilde{e}}\ \ i^{\pm}_{e\tilde{e}}\ \ i^{\pm}_{ce}\ \ i^{\pm}_{c\tilde{e}} \right\} \tag{2.50}$$

fulfils all the inequalities:

$$\min\ \mathrm{tr}N\ \mathrm{tr}\widetilde{N}\ \ \geqslant 2\sqrt{1 + y^2 + z^2} \tag{2.51a}$$

$$\det N + 1 + L^T \begin{pmatrix} y \\ z \end{pmatrix} \geqslant \mathrm{tr}N\sqrt{1 + y^2 + z^2} \tag{2.51b}$$

$$\det \widetilde{N} + 1 + \widetilde{L}^T \begin{pmatrix} y \\ z \end{pmatrix} \geqslant \mathrm{tr}\widetilde{N}\sqrt{1 + y^2 + z^2} \tag{2.51c}$$

The points from the set S are defined as follows

$$\begin{aligned} m_c &= (0\ \ 0) \\ m_e &= \frac{\det N + 1}{k_1} L \\ m_{\tilde{e}} &= \frac{\det \widetilde{N} + 1}{\tilde{k}_1} \widetilde{L} \\ i^{\pm}_x &= g_x + s^{\pm}_x f_x \qquad (x = e\tilde{e}\ \ ce\ \ c\tilde{e}) \end{aligned} \tag{2.52}$$

where

$$k_1 = 4\left[\det N + (\mathrm{Im}N_{12})^2\right] \qquad \tilde{k}_1 = 4\left[\det \widetilde{N} + (\mathrm{Im}\widetilde{N}_{12})^2\right] \tag{2.53}$$

and

$$
\begin{aligned}
g_{e\tilde{e}} &= \left(\frac{\det N + 1}{\mathrm{tr} N} + \frac{\det \widetilde{N} + 1}{\mathrm{tr}\widetilde{N}} \right) \frac{L^{'}}{L^{'}} \qquad L^{'} = \frac{\widetilde{L}}{\mathrm{tr}\widetilde{N}} - \frac{L}{\mathrm{tr} N} \\
g_{ce} &= \left(\mathrm{tr} N \sqrt{r_c^2 + 1} - \det N - 1 \right) \frac{L}{L} \\
g_{c\tilde{e}} &= \left(\mathrm{tr}\widetilde{N} \sqrt{r_c^2 + 1} - \det \widetilde{N} - 1 \right) \frac{\widetilde{L}}{\widetilde{L}} \\
r_c &= \min \left\{ \sqrt{(\mathrm{tr} N)^2 \;\; 4 - 1} \;\; \sqrt{(\mathrm{tr}\widetilde{N})^2 \;\; 4 - 1} \right\}
\end{aligned} \tag{2.54}
$$

The vectors $f_{e\tilde{e}} \;\; f_{ce} \;\; f_{c\tilde{e}}$ are defined to be orthogonal to $L^{'} \;\; L \;\; \widetilde{L}$, respectively, and $s^{\pm}_{e\tilde{e}} \;\; s^{\pm}_{ce} \;\; a^{\pm}_{c\tilde{e}}$ are the real roots of the polynomials

$$
\begin{aligned}
P_{e\tilde{e}}(s) &= \left[L^T (g_{e\tilde{e}} + s f_{e\tilde{e}}) + \det N + 1 \right]^2 - (\mathrm{tr} N)^2 \left(1 + \;\; g_{e\tilde{e}} + s f_{e\tilde{e}} \;\; {}^2 \right) \\
P_x(s) &= r_c^2 - \;\; g_x + s f_x \;\; {}^2 \qquad (x = ce \;\; c\tilde{e})
\end{aligned} \tag{2.55}
$$

Variance inequalities. — Experimentally, it is more convenient to check separability via variances of the combinations of observables, the criterion originally proposed for two mode states in [Duan 00b] and generalized to many-mode states in [van Loock 03]. The separability test states that if an N mode state is separable, then the sum of the variances of the following operators:

$$
\begin{aligned}
U &= h_1 X_1 + \qquad + h_N X_N \\
V &= g_1 P_1 + \qquad + g_N P_N
\end{aligned} \tag{2.56}
$$

is bounded from below by a function of the coefficients $h_1 \qquad h_N \;\; g_1 \qquad g_N$. Mathematically, the inequality is expressed as

$$
\mathrm{Var} U + \mathrm{Var} V \geqslant f(h_1 \qquad h_N \;\; g_1 \qquad g_N) \tag{2.57}
$$

where

$$
f(h_1 \qquad h_N \;\; g_1 \qquad g_N) = \left| h_l g_l + \sum_{r \in I} h_r g_r \right| + \left| h_m g_m + \sum_{s \in I'} h_s g_s \right| \tag{2.58}
$$

In the above formula the two modes, l and m, are distinguished and the remaining ones are grouped into two disjoint sets I and I'. The criterion (2.58) holds for all bipartite splittings of a state defined by the sets of indices $\;\; l \qquad I$ and $\;\; m \qquad I'$.

A particular case of the above general theory is the criterion for two modes proposed in [Duan 00b]. It states that for any two-mode separable state and $\lambda \qquad \mathbb{R} \qquad 0$ the sum of variances of $\;\lambda \; P_1 + \frac{1}{\lambda} P_2$ and $\;\lambda \; X_1 - \frac{1}{\lambda} X_2$ is bounded as

$$
\mathrm{Var}(\; \lambda \; P_1 + \frac{1}{\lambda} P_2) + \mathrm{Var}(\; \lambda \; X_1 - \frac{1}{\lambda} X_2) \geqslant 2 \tag{2.59}
$$

The criterion becomes a necessary and sufficient entanglement test after the CM is transformed into its standard form by local operations [Duan 00b]. This local transformations, however, are determined by the form of the covariance matrix. In this sense, the knowledge of the full covariance matrix is essential in order to decide unambiguously whether the state is entangled.

Chapter 3

Manipulation of entanglement in atomic ensembles

The theory of Quantum Information shows how to carry out certain tasks using the laws of quantum physics for encoding, processing, extracting and transmitting information. Shortly after this new branch of physics emerged a natural question must have been posed: Can we obtain such degree of control over quantum physical systems to implement all these fantastic ideas in reality? Although the quest for a universal quantum device is not yet finished, we already witness a huge progress in quantum technologies [Kok 07, Duan 10, Saffman 10, Singer 10, Buluta 11, Weedbrook 12]. All the requirements that a physical set-up must fulfil to serve the purpose of quantum information processing can be summarized in the form of DiVincenzo conditions originally proposed in [DiVincenzo 00] and later, as new ideas and proposals appeared, revised and discusses in, e.g., [DiVincenzo 01, Pérez-Delgado 11].

First of all one needs a scalable quantum system in which, in principle, arbitrary amount of information can be encoded, manipulated and stored. Here we should distinguish two types of quantum systems: static and " ying" ones. The former type is usually associated with atoms, ions or solid state platforms whose position can be well controlled over long period of time. The latter, with light being a paradigmatic example, is in constant motion. Therefore, static systems are a natural choice for storage of information, i.e., a quantum register, while " ying" ones are more suitable for transmission of quantum information over distance. An ideal set-up should be a hybrid of both types of systems and allow for high-fidelity interconversion of a stationary quantum information and a " ying" one. Another requirement is a long decoherence time of the components. Precisely, the lifetime of the system must be long enough to complete any quantum-information task and perform a readout of its final state, in which the solution is encoded.

It turned out that fulfilling all this conditions and building a universal quantum machine is an extremely hard task. However, in many applications we can settle for a special-purpose quantum set-up, one that cannot perform an arbitrary operation, but is well suited for a specific task. Quantum simulators, quantum repeaters and quantum secret key distribution devices all fall into this category.

In this chapter I will discuss the potential of a quantum set-up consisting of macroscopic samples of non-interacting atoms interfaced with light in such way that the quantum uctuations between the two systems are exchanged. Atomic ensembles are particularly advanta-

geous when it comes to information storage as they have decoherence time on the order of milliseconds. This is due to the fact that for this physical system the relevant degrees of freedom have collective nature which makes them insensitive to single particle losses. Another important inbuilt feature of this set-up is the possibility of interconversion between the static form of information stored in the ensemble and the " ying" one encoded in polarization degrees of freedom of light. Last but not least, the atom-light interface enables the manipulation and readout of the state of the system, making the set-up of atomic ensembles and light a promising candidate for building, at least, some special-purpose quantum devices.

There exist various mechanisms for the quantum interface between an atomic ensemble and light such as the quantum non-demolition-Faraday (QND-Faraday) interaction, Raman interaction, photon echo, and electromagnetically induced transparency (for details see [Hammerer 10] and references therein). In this chapter we will concentrate on the QND-Faraday interaction combined with the homodyne detection. The former refers to the rotation experienced by the polarization of light while it propagates through a magnetic medium. At the quantum level the interaction leads to an exchange of quantum uctuations between matter and light, thus a quantum interface. The seminal results exploiting this scheme include the experimental demonstration of the spin squeezing of a single ensemble [Kuzmich 00], the deterministic entanglement of two atomic samples [Julsgaard 01], the quantum memory for light [Julsgaard 04] and the teleportation protocol [Sherson 06]. This genuine quantum instrument also finds applications beyond the quantum information processing; it was shown to be a powerful tool in quantum metrology and magnetometry [Napolitano 10, Napolitano 11, Wolfgramm 10] and quantum spectroscopy [Eckert 07b, Eckert 07a, Roscilde 09, Greif 11, De Chiara 11, Romero-Isart 12].

In recent years there is a growing interest in the role played by multipartite entanglement in quantum algorithms [Bruß 11], continuous-variable measurement-based quantum computing [Menicucci 06, Gu 09, Ohliger 10], communication protocols [Zhang 09] and high-precision metrology [Tóth 12, Hyllus 12]. Here, we will show that the set-ups based on atomic ensembles offer a versatile toolbox for generation and manipulation of multipartite entanglement in both the pure and mixed-state case. We will also demonstrate that small modification of the very same setting provides an experimentally feasible scheme for the generation of bound entanglement, broadening the applicability of atomic ensembles for quantum information studies of foundational character.

3.1 The QND-Faraday atom-light interface

Efficient atom-photon coupling lays at the heart of storage and retrieval of quantum states of light from a material medium through a matter-light interface. Historically, it was first achieved with few atoms in the regime of cavity quantum electrodynamics (cavity QED), however recent experiments show that it can also be performed with collective degrees of freedom of large samples of non-interacting atoms, i.e., atomic ensembles. In this case strong coupling is obtained through the increase of the optical depth by taking the macroscopic or mesoscopic number of atoms in the sample [Kuzmich 97] and moderate-intensity of light (typical value for atomic-ensemble experiments reported in [Julsgaard 01, Julsgaard 04] was $I = 1\mathrm{mW\ cm}^2$). Figure 3.1 summarizes the Faraday interface set-up. In the next paragraphs we will describe one by one its elements and derive the effective Hamiltonian governing the interaction. We will also discuss possible sources of errors and inbuilt imperfections of the

system.

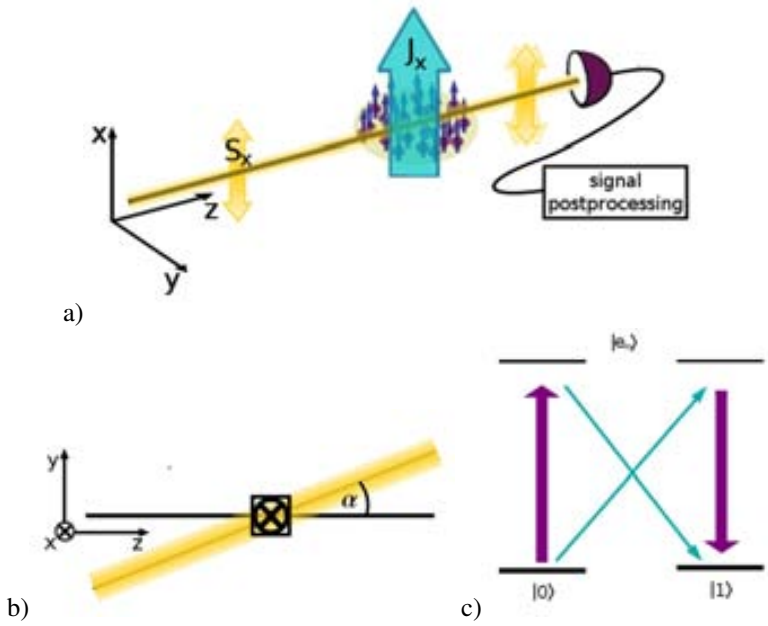

Figure 3.1: Schematic representation of the experimental set-up in which the QND-Faraday atom-light interface is implemented. In figure a) the light beam polarized along direction x and propagating in the YZ plane experiences polarization rotation after the interaction with the polarized atomic ensemble; in figure b) we depict the angle at which the light impinges at the atomic sample. Figure c) shows a schematic structure of atomic levels with degenerate ground state $0 \quad 1$ and excited states e_m .

Atomic ensembles. — The notion of atomic ensembles refers to samples composed of $N_A \sim 10^6 - 10^{12}$ non-interacting atoms, which are typically alkali or alkaline-earth metals [Julsgaard 01, Julsgaard 04, Sherson 06] but also a proper spin-1 $2\ ^{171}\mathrm{Yb}$ could be used [Takeuchi 06]. The description of such multilevel atoms can be reduced to two degenerate levels $0 \quad 1$ and one can define for each atom the angular momentum operator **j** with components (we choose x as a quantization axis):[1]

$$j_x(t\ \mathbf{r}) = \frac{1}{2}(\ 0\ \ 0\ -\ 1\ \ 1\ ) \tag{3.1a}$$

$$j_y(t\ \mathbf{r}) = \frac{1}{2}(\ 0\ \ 1\ +\ 1\ \ 0\ ) \tag{3.1b}$$

$$j_z(t\ \mathbf{r}) = \frac{1}{2i}(\ 0\ \ 1\ -\ 1\ \ 0\ ) \tag{3.1c}$$

[1] Such defined operators fulfil the following commutation rules:

$$[j_i(t,\mathbf{r}), j_j(t,\mathbf{r}')] = i\frac{1}{A\rho}\varepsilon_{ijk}j_k(t,\mathbf{r})\delta(\mathbf{r}-\mathbf{r}').$$

They become convenient microscopic degrees of freedom and the sample as a whole is then characterized by its collective spin $\mathbf{J}(t) = \sum_{i=1}^{N_A} \mathbf{j}_i \approx \int_V \mathrm{d}\mathbf{r}\mathbf{j}(t\ \mathbf{r})\rho(\mathbf{r})$.

Further preparation of the sample involves putting all the atoms in state 0 , making the ensemble polarized along the x direction, as schematically depicted in figure 3.1a. Such state is often referred to as a coherent spin state (CCR). If a macroscopic number of atoms is considered, the uctuations of the macroscopic spin J_x are practically negligible, hence we can approximate the operator with a constant c-number $J_x(t) \approx J_x = N_{\mathrm{A}}\ 2$. Now the orthogonal collective spin components can be rescaled to fulfil the canonical commutation relation $[J_y\ \sqrt{J_x}\ J_z\ \sqrt{J_x}\ ] = i$ and thus define the atomic position and momentum

$$X_A = \frac{J_y}{\sqrt{J_x}} \qquad P_A = \frac{J_z}{\sqrt{J_x}} \tag{3.2}$$

In this way we have defined a continuous-variable system. Furthermore, an ensemble initialized in this way belongs to an important class of continuous-variable states, the Gaussian states. Their significance stems from the fact that they are efficiently generated, manipulated and detected with the current optical technology [Weedbrook 12]. Moreover, Gaussian states are fully characterized by first and second moments, i.e., the mean values and the covariances, of X and P. Hence, rather than describe such system with an infinite-dimensional density matrix, one can use a much simpler covariance matrix formalism, which I brie y introduced in chapter 2. Its application in the particular case of the QND-Faraday interface will be thoroughly discussed in the next section.

In the language of Gaussian states the polarized ensemble is described by zero mean values $X_A = P_A = 0$ and balanced variances saturating the uncertainty principle $\sqrt{\mathrm{Var}X_A}\ \sqrt{\mathrm{Var}P_A} \geqslant 1\ 2$, i.e., $\mathrm{Var}X_A = \mathrm{Var}P_A = 1\ 2$. This minimum uctuation state is the vacuum state denoted usually by Ω [Mandel 95].

Light. — The light is assumed to propagate along a chosen direction in the YZ plane (e.g., along direction z) as depicted in figure 3.1b, be off-resonant from any relevant atomic transition and linearly polarized along the x-direction. Since we are interested in polarization degrees of freedom, a convenient description is given by the microscopic Stokes operators, analogous to single-atom angular momenta $\mathbf{j}$. Precisely speaking, they are defined as:

$$s_x(t\ z) = \frac{1}{2}\left[a_x^\dagger(t\ z)a_x(t\ z) - a_y^\dagger(t\ z)a_y(t\ z)\right] \tag{3.3a}$$

$$s_y(t\ z) = \frac{1}{2}\left[a_x^\dagger(t\ z)a_y(t\ z) + a_y^\dagger(t\ z)a_x(t\ z)\right] \tag{3.3b}$$

$$s_z(t\ z) = \frac{1}{2i}\left[a_x^\dagger(t\ z)a_y(t\ z) - a_y^\dagger(t\ z)a_y(t\ z)\right] \tag{3.3c}$$

where $a_x(t\ z)\ a_y(t\ z)$ are the annihilation operators of modes with linear x and y polarization, respectively[1]. We explicitly write here the time and position-dependence of the variables assuming propagation along direction z. The $x\ y\ z$ Stokes operators correspond to a difference between the number of photons with $x\ y$, $\pm\pi\ 4$ linear polarizations and *left/right* circular polarizations, respectively.

[1]The commutation rules for the Stokes operators following from the creation-annihilation operators read

$$[s_i(t,z), s_j(t,z')] = i\varepsilon_{ijk}s_k(t,z)\delta(z-z').$$

The Stokes operators are well suited for the microscopic description of interaction with atoms, however, effectively only the following macroscopic observables will be relevant: $S_k(z) = \int_0^T \mathrm{d}t s_k(t\ z)$, where T is the duration of the light pulse. The so defined operators obey standard angular momentum commutation rules. Similarly to the case of atomic ensembles, the assumption of linear polarization along direction x allows for the approximation $S_x(z) \approx\ S_x\ \equiv N_{\mathrm{ph}}\ 2$. Once more, the remaining orthogonal components S_y and S_z are appropriately rescaled in order to make them fulfil the CCR, $\left[S_y\ \sqrt{\ S_x\ }\ S_z\ \sqrt{\ S_x\ }\right] = i$. Straightforwardly, a correspondence equivalent to this in equation (3.2) arises:

$$X_L = \frac{S_y}{\sqrt{\ S_x}} \qquad P_L = \frac{S_z}{\sqrt{\ S_x}} \tag{3.4}$$

which allows us to treat the light polarization degrees of freedom on the same footing as the atomic variables. Similarly, the strongly polarized light constitutes a Gaussian mode in the vacuum state.

Interaction. — The choice of atomic ensemble and light with properties described in previous paragraphs makes it possible to approximate the dipole atom-light interaction with the effective QND-Faraday Hamiltonian. In order to derive it we begin by the most general Hamiltonian describing the composite system of a single atom interacting with electromagnetic field

$$H = H_A + H_L + H_{\mathrm{int}} \tag{3.5}$$

where H_A is the Hamiltonian of a single atom, H_L describes the field energy and the coupling term is taken in the dipole approximation $H_{\mathrm{int}} = -\mathbf{E}(\mathbf{R}) \cdot \mathbf{D}$. In the latter $\mathbf{D} = -e\mathbf{r}$ denotes the electric dipole operator of a single atom and $\mathbf{E}(\mathbf{R})$, the electric field at position $\mathbf{R}$ of an atom.

In what follows we present the theory for a general atom described by its atomic eigenstates a and expand the dipole operator in this basis. We also write the field operators in terms of creation and annihilation operators $a^\dagger_{\mathbf{k}\lambda}\ a_{\mathbf{k}\lambda}$ for modes characterized by a wave vector $\mathbf{k}$ and polarization λ obtaining

$$H = \sum_a\ {}_a\, a\ \ a\ + \sum\!\!\!\!\!\!\int_{\mathbf{k},\lambda}\ {}_k a^\dagger_{\mathbf{k}\lambda} a_{\mathbf{k}\lambda} + \sum_{a,b} \sum\!\!\!\!\!\!\int_{\mathbf{k},\lambda} \left[\ a\ \ b\ g_k \mathbf{d}_{ab} \cdot \mathbf{e}_{\mathbf{k}\lambda} a_{\mathbf{k}\lambda} e^{i\mathbf{k}\cdot\mathbf{R}} + \mathrm{h\ c}\ \right] \tag{3.6}$$

where $\mathbf{d}_{ab} = -e\ a\ \mathbf{r}\ b$ are the dipole matrix elements, $\mathbf{e}_{\mathbf{k}\lambda}$ the field polarization vector and $g_k = \sqrt{\ {}_k\ (2\ V)}$, with ${}_k = c\,\mathbf{k}$ and V being the volume of an atom. From this point we work in the interaction picture and consider only the interaction term with time dependent light and atomic variables.

Since the laser beam has a well defined wavelength and we assume it to propagate along a specific direction in the YZ plane, say direction z, we can reduce the sum over all the modes $\mathbf{k}\lambda$ in the interaction Hamiltonian to the sum over two polarizations $x\ \ y$ or equivalently $+\ -$ corresponding to

$$\mathbf{e}_+ = -\frac{\mathbf{e}_x + i\mathbf{e}_y}{\overline{2}} \qquad \mathbf{e}_- = \frac{\mathbf{e}_x - i\mathbf{e}_y}{\overline{2}} \tag{3.7}$$

The interaction Hamiltonian thus becomes

$$H_{\mathrm{int}} = \sum_{a,b} \sum_{\lambda=+,-} \left[\ a\ \ b\ g \mathbf{d}_{ab} \cdot \mathbf{e}_\lambda a_\lambda(t\ z) + \mathrm{h\ c}\ \right] \tag{3.8}$$

where we have written explicitly the time and position dependence of field operators. For a given field frequency we can assume that there are only two relevant atomic states, $0 \quad 1$, i.e., two degenerate atomic ground states (see figure 3.1c). We further reduce the Hamiltonian distinguishing this two levels and leaving some excited states e_m , which will be later eliminated by assuming that light is off-resonant with respect to all atomic transitions. In this step we also substitute $g\mathbf{d}_{ab}$ with $\mathbf{g}_{ab}$ and write explicitly the conjugate terms

$$\begin{aligned} H_{\text{int}} \;=\; \sum_m \sum_{\lambda=+,-} \Big[& 0 \;\; e_m \; \mathbf{g}_{0m} \cdot \mathbf{e}_\lambda a_\lambda(t \;\; z) + \;\; e_m \;\; 0 \; \mathbf{g}^*_{0m} \cdot \mathbf{e}^*_\lambda a^\dagger_\lambda(t \;\; z) \\ & + e_m \;\; 0 \; \mathbf{g}_{m0} \cdot \mathbf{e}_\lambda a_\lambda(t \;\; z) + \;\; 0 \;\; e_m \; \mathbf{g}^*_{m0} \cdot \mathbf{e}^*_\lambda a^\dagger_\lambda(t \;\; z) \\ & + 1 \;\; e_m \; \mathbf{g}_{1m} \cdot \mathbf{e}_\lambda a_\lambda(t \;\; z) + \;\; e_m \;\; 1 \; \mathbf{g}^*_{1m} \cdot \mathbf{e}^*_\lambda a^\dagger_\lambda(t \;\; z) \\ & + e_m \;\; 1 \; \mathbf{g}_{m1} \cdot \mathbf{e}_\lambda a_\lambda(t \;\; z) + \;\; 1 \;\; e_m \; \mathbf{g}^*_{m1} \cdot \mathbf{e}^*_\lambda a^\dagger_\lambda(t \;\; z) \Big] \end{aligned} \tag{3.9}$$

Now we eliminate the non-resonant terms (corresponding to a simultaneous atom excitation and photon emission, and the conjugate term) from the interaction Hamiltonian, which is commonly known as the rotating wave approximation, and obtain

$$\begin{aligned} H_{\text{int}} \;=\; \sum_m \sum_{\lambda=+,-} \Big[& e_m \;\; 0 \; \mathbf{g}_{m0} \cdot \mathbf{e}_\lambda a_\lambda(t \;\; z) + \;\; 0 \;\; e_m \; \mathbf{g}^*_{m0} \cdot \mathbf{e}^*_\lambda a^\dagger_\lambda(t \;\; z) \\ & + e_m \;\; 1 \; \mathbf{g}_{m1} \cdot \mathbf{e}_\lambda a_\lambda(t \;\; z) + \;\; 1 \;\; e_m \; \mathbf{g}^*_{m1} \cdot \mathbf{e}^*_\lambda a^\dagger_\lambda(t \;\; z) \Big] \end{aligned} \tag{3.10}$$

Expressing now the interaction Hamiltonian in terms of the microscopic angular momenta (3.1a)–(3.1c) and the Stokes operators (3.3a)–(3.3c), and taking into account that the excited states can be adiabatically eliminated due to the light detuning we have

$$H_{\text{int}} = -cg \left[a_0 \rho(t \;\; z) + a_1 s_z(t \;\; z) j_z(t \;\; z) \right] \tag{3.11}$$

where the term containing a_0 corresponds to the Stark shift proportional to photon density ρ, while the term containing a_1 is responsible for the Faraday rotation. The coupling constant is expressed through the system parameters as $g = \frac{\delta}{4A\Delta} \frac{\lambda^2}{2\pi}$, with A being the cross section, λ the wave length of light, Δ the detuning energy and δ the frequency width of the atomic excited state. Due to the approximations made, this Hamiltonian is valid only for time scales much longer than Δ^{-1} and light detuning significantly larger than the width of the atomic excited state.

So far we have concentrated on a single-atom description. In order to obtain the Hamiltonian governing the evolution of the total atomic ensemble of length L (along the direction of light propagation) and the light, we need to integrate equation (3.11) in the interval $[0 \;\; L]$ with respect to z assuming the interaction cross section A and density of atoms ρ. By doing this we obtain a general Hamiltonian describing the interaction of the atomic sample with off-resonant light propagating along direction z. Since we concentrate on a QND-Faraday interaction, we have neglected in this derivation the higher order terms, leaving only the bilinear coupling:

$$H_{\text{int,sample}} = -\int_0^L \mathrm{d}z A \rho c g \left[a_0 \rho(t \;\; z) + a_1 s_z(t \;\; z) j_z(t \;\; z) \right] \tag{3.12}$$

Using the Heisenberg equation and neglecting the retardation effects we obtain the general propagation equations for $j_k(t\ z)\ s_k(t\ z)\ (k = x\ y\ z)$ [1]

$$\frac{}{t} j_x(z\ t) = cga_1 s_z(z\ t) j_y(z\ t) \tag{3.13a}$$

$$\frac{}{t} j_y(z\ t) = -cga_1 s_z(z\ t) j_x(z\ t) \tag{3.13b}$$

$$\frac{}{t} j_z(z\ t) = 0 \tag{3.13c}$$

$$c\frac{}{z} s_x(z\ t) = cga_1 s_y(z\ t) j_z(z\ t) \tag{3.13d}$$

$$c\frac{}{z} s_y(z\ t) = -cga_1 s_x(z\ t) j_z(z\ t) \tag{3.13e}$$

$$c\frac{}{z} s_z(z\ t) = 0 \tag{3.13f}$$

Only now we are in the point where we can make use of the fact that both the light and the atomic ensemble are strongly polarized, and substitute the operators with their mean values $j_x(t\ z) \qquad j_x(z)$ and $s_x(t\ z) \qquad s_x$. We also integrate the above equations and introduce new integrated variables $J_k(t) = \int_0^L \mathrm{d}z j_k(z\ t)$ and $S_k(z) = c\int_0^T \mathrm{d}t s_k(z\ t)$ (T is the duration of the light pulse), obtaining

$$J_y^{\mathrm{out}} = J_y^{\mathrm{in}} - ga_1 S_z^{\mathrm{in}} J_x^{\mathrm{in}} \tag{3.14a}$$

$$J_z^{\mathrm{out}} = J_z^{\mathrm{in}} \tag{3.14b}$$

$$S_y^{\mathrm{out}} = S_y^{\mathrm{in}} - ga_1 S_x^{\mathrm{in}} J_z^{\mathrm{in}} \tag{3.14c}$$

$$S_z^{\mathrm{out}} = S_z^{\mathrm{in}} \tag{3.14d}$$

where we have introduced the variables with indices $\mathrm{in}\ \mathrm{out}$ for input and output variables corresponding to $z = 0\ \ L$ for light and $t = 0\ \ T$ for atoms.

As demonstrated in previous paragraphs the new variables $S_k(z)\ \ J_k(t)$ fulfil, after rescaling, the canonical commutation rules, hence the equations and the effective Hamiltonian can be rewritten in terms of the canonical variables X and P. Moreover, we introduce an additional parameter α which specifies the direction of the beam propagation in the YZ plane as depicted in figure 3.1b. This can be easily included in the equations through rotation of the reference frame for atoms as $J_y = J'_y \cos\alpha - J'_z \sin\alpha$ and $J_z = J'_y \sin\alpha + J'_z \cos\alpha$. All

[1] The evolution equations are different for the Stokes operators and the spin operators:

$$\frac{\partial}{\partial t} j_k(t,z) = [s_k(t,z), H_{\mathrm{int,sample}}],$$

$$\left(\frac{\partial}{\partial t} + c\frac{\partial}{\partial z}\right) s_k(t,z) = [s_k(t,z), H_{\mathrm{int,sample}}].$$

Neglecting of retardation effects reduces to omitting the term $\frac{\partial}{\partial t}$ in the second equation.

these steps lead to the following set of equations

$$X_A^{\text{out}} = X_A^{\text{in}} - \kappa P_L^{\text{in}} \cos\alpha \tag{3.15a}$$

$$P_A^{\text{out}} = P_A^{\text{in}} + \kappa P_L^{\text{in}} \sin\alpha \tag{3.15b}$$

$$X_L^{\text{out}} = X_L^{\text{in}} - \kappa (P_A^{\text{in}} \cos\alpha + X_A^{\text{in}} \sin\alpha) \tag{3.15c}$$

$$P_L^{\text{out}} = P_L^{\text{in}} \tag{3.15d}$$

with the parameter $\kappa = g a_1 \sqrt{\begin{array}{cc} J_x & S_x \end{array}}$ being a new coupling constant. Note that the effective interaction Hamiltonian can be now rewritten in the form

$$H_{\text{int}}^{\text{eff}} = -\kappa P_L (P_A \cos\alpha + X_A \sin\alpha) \tag{3.16}$$

We observe from equation (3.15c) [or equation (3.14c)] that the rotation of light polarization is proportional to the atomic spin in the direction of propagation, as in the classical Faraday effect. Note that this property enables probing of the atomic spin component in the direction of light propagation in a quantum-non-demolition manner, i.e., with minimum disturbance of the measured system. This is due to the fact that the measured observable commutes with the interaction Hamiltonian (3.16), hence the name QND-Faraday interface. One should also note that the Hamiltonian is bilinear in atomic and light variables, leading thus to linear propagation equations. Transformation induced by such Hamiltonian is a Gaussian operation, therefore if the state of the system is Gaussian at the beginning (which is the case for the system under consideration) it remains Gaussian after the interaction. This important property will allow us to describe the system with an elegant and simple covariance matrix formalism, which we introduce in the next subsection.

By now we have considered only a single sample interacting with a single light beam, which is useful for a quantum memory set-up or generation of spin squeezing. However, the situations like generation of entanglement essentially involve multiple samples. To deal with the multi-sample set-up we treat the output light from one ensemble as an input to another one. In this way, the one-sample scheme provides a universal description which can be applied to more complicated situations. We denote the variables characterizing the nth sample by $(X_{A,n}\ P_{A,n})$ and α_n corresponds to the angle at which the light beam propagates through the nth ensemble. For completeness we write here the most general Hamiltonian for a single beam interacting consecutively with N_s samples

$$\hat{H}_{\text{int}}(\boldsymbol{\alpha}\ \boldsymbol{\kappa}) = -\sum_{i=1}^{N_s} \kappa_i P_L \left(P_{A,i} \cos\alpha_i + X_{A,i} \sin\alpha_i\right) \tag{3.17}$$

and the corresponding propagation equations:

$$X_{A,i}^{\text{out}} = X_A^{\text{in}} - \kappa_i P_L^{\text{in}} \cos\alpha_i \tag{3.18a}$$

$$P_{A,i}^{\text{out}} = P_A^{\text{in}} + \kappa_i P_L^{\text{in}} \sin\alpha_i \tag{3.18b}$$

$$X_L^{\text{out}} = X_L^{\text{in}} - \sum_{i=1}^{N_s} \kappa_i (P_{A,i}^{\text{in}} \cos\alpha_i + X_{A,i}^{\text{in}} \sin\alpha_i) \tag{3.18c}$$

$$P_L^{\text{out}} = P_L^{\text{in}} \tag{3.18d}$$

where $\boldsymbol{\alpha} = (\alpha_1 \qquad \alpha_{N_s})$ refers to the incident angles at which the light impinges at each atomic samples, and we include the possibility of having a different coupling constant for

every atomic ensemble using $\boldsymbol{\kappa} = (\kappa_1 \qquad \kappa_{N_s})$. This is a starting point for the geometric scheme, which we discuss further in the next section.

Measurement. — In many applications of the QND-Faraday interface a polarimetric (polarization homodyne) measurement of light following the interaction and a subsequent feedback onto atoms is a central part of the protocol. The class of such "measurement-based" schemes includes spin squeezing [Braginsky 96, Kuzmich 97, Kuzmich 00], generation of pure-state entanglement [Duan 00a, Julsgaard 01, Stasińska 09] and quantum memory [Julsgaard 04]. The main idea behind this method is that the light beam serves as a probe of the spin components (see equation (3.15c)). Its homodyne measurement, by providing information about the spin component, reduces the uctuations of the spin.

Another possibility, which was discussed in [Stasińska 12a], is the situation in which the light beam is not measured after the interaction. Such action corresponds to a truly random displacement of atomic variables that has a Gaussian distribution [see equations (3.15a) and (3.15b)]. One cannot produce entanglement through such procedure, however it enables manipulation of the entanglement already present in the system. In this way one obtains mixed entangled states, in particular exploiting this technique we are able to explore the important class of bound entangled states.

Imperfect atom-light interface. — An experimental system is never a perfect implementation of the theoretical model presented in previous paragraphs. In practice it is always subject to certain imperfections due to particle loss, spontaneous emission, uctuations of the laser amplitude, population of atomic excited states due to photon absorption, inhomogeneities of the sample and light beam, *etc* . Moreover, the polarized atomic samples have a finite life-time due to collisions and spin relaxation.

A complete description of the effect of inhomogeneities on atom-light interfaces is provided in [Koschorreck 09]. Here, following [Madsen 04, Sherson 05, Julsgaard 03], we will assume our systems to be homogeneous and analyse the errors due to the decay of the atomic spin-polarized state modelled as:

$$X_{A,n}^{\mathrm{in}'} = \sqrt{1-\eta_\tau} X_{A,n}^{\mathrm{in}} + \quad \overline{\eta_\tau} V_x \tag{3.19a}$$

$$P_{A,n}^{\mathrm{in}'} = \sqrt{1-\eta_\tau} P_{A,n}^{\mathrm{in}} + \quad \overline{\eta_\tau} V_p \tag{3.19b}$$

where $V_p \;\; V_x$ are the vacuum modes. The parameter η_τ is a decay rate during the time interval of length τ hence its value is bounded as $0 \leq \eta_\tau \leq 1$. Since the interaction time is much shorter than the atomic spin relaxation time, we safely assume the interaction to be instantaneous. Thus, the atomic decoherence corresponds to the time window between the different pulses applied in the protocol. In such case it is safe to consider $\eta_\tau < 0\ 1$. In the next subsection we will introduce the covariance matrix formalism for the QND-Faraday interface, therefore, going a bit beforehand, we show the effect of decoherence at this level; it can be expressed as:

$$\gamma^{'}(\eta_\tau) = (1-\eta_\tau)\gamma + \eta_\tau \mathbf{1} \tag{3.20}$$

Additionally, we study the effect of the uncertainty in the coupling constant, $\kappa \pm \Delta\kappa$, and the uncertainty in the homodyne detection measuring process. Typical values and uncertainties for the coupling strengths, atomic spin decay rate, and for the light and spin variances are based on recent experimental results [Appel 09].

3.1.1 QND-Faraday interface with the covariance matrix formalism

Our aim in this chapter is to discuss the generation of multipartite entanglement between the atomic ensembles. To this end, we will need a convenient description of the system consisting of many samples that interact with multiple light beams. It should incorporate both the sample-light interaction and the possibility of light measurement, as well as enable to include decoherence effects. The atomic ensembles and the light are in a Gaussian state at each stage of the discussed protocols. For such systems, the suitable description is given in terms of the covariance matrix (CM) formalism, which I brie y introduced in chapter 2. Here, I present all the steps of the QND-Faraday interface in terms of covariance matrices, symplectic transformations and Gaussian measurements.

Let us first characterize with this formalism the initial state of the system. As previously explained the state of both the light and the atomic ensembles directly after preparation is a Gaussian vacuum state Ω represented by the following CM

$$\gamma_\Omega = \begin{pmatrix} 1 & 0 \\ 0 & 1 \end{pmatrix} \tag{3.21}$$

where the diagonal elements are proportional to the variances of X and P, both equal $1\ 2$. The mean values of the canonical variables define the displacement vector (DV). In the case of the vacuum state these, by definition, equal zero giving the initial DV $d_\Omega = (0\ 0)$. In multipartite protocols, we begin with uncorrelated ensembles, each in a vacuum state. The corresponding multi-mode CM is, therefore, a direct sum of γ_Ωs.

The next step of the interface is the atom-light interaction. We demonstrate how to reconstruct the equations of evolution at the level of the covariance matrix from the most general propagation equations (3.18), i.e., find the corresponding symplectic transformation. Due to the bilinearity of the interaction Hamiltonian, the variables characterizing the system after the interaction (out) are expressed as a linear combination of the initial ones (in). Let us denote this linear transformation by $\mathcal{K}$

$$\mathcal{K}: \begin{pmatrix} X^{\text{out}}_{A,1} \\ P^{\text{out}}_{A,1} \\ \vdots \\ X^{\text{out}}_{A,N_s} \\ P^{\text{out}}_{A,N_s} \\ X^{\text{out}}_{L} \\ P^{\text{out}}_{L} \end{pmatrix} = \mathcal{K} \begin{pmatrix} X^{\text{in}}_{A,1} \\ P^{\text{in}}_{A,1} \\ \vdots \\ X^{\text{in}}_{A,N_s} \\ P^{\text{in}}_{A,N_s} \\ X^{\text{in}}_{L} \\ P^{\text{in}}_{L} \end{pmatrix} \tag{3.22}$$

Comparing equation (3.22) and equations (3.18) we immediately see that the transformation reads:

$$\mathcal{K} = \begin{pmatrix} & & & & 0 & -\kappa_1 \cos\alpha_1 \\ & & & & 0 & \kappa_1 \sin\alpha_1 \\ & & \mathbf{1}^{(A)}_{2N_s} & & & \vdots \\ & & & & 0 & -\kappa_{N_s} \cos\alpha_{N_s} \\ & & & & 0 & \kappa_{N_s} \sin\alpha_{N_s} \\ -\kappa_1 \sin\alpha_1 & -\kappa_1 \cos\alpha_1 & & -\kappa_{N_s} \sin\alpha_{N_s} & -\kappa_{N_s} \cos\alpha_{N_s} & \\ 0 & 0 & & 0 & 0 & \mathbf{1}^{(L)}_2 \end{pmatrix} \tag{3.23}$$

The matrix $\mathcal{K}$ can be directly applied to a phase space vector $\zeta = (x_1\ p_1 \quad \cdots \quad x_{N_s}\ p_{N_s}\ x_L\ p_L)$ and correspondingly to the covariance matrix, however, the sign of the coupling constants κ_i should be changed. This is due to the fact that the phase space variables evolve according to the Schrödinger picture, whereas the quadratures, being operators transform according to the Heisenberg picture. Therefore, we define $\widetilde{\mathcal{K}} = \mathcal{K}\big|_{\boldsymbol{\kappa}\to(-\boldsymbol{\kappa})}$, which we apply to the phase space vector and the covariance matrix as

$$\zeta_{\rm out}^T\gamma_{\rm in}^{-1}\zeta_{\rm out} = \zeta_{\rm in}^T\widetilde{\mathcal{K}}^T\gamma_{\rm in}^{-1}\widetilde{\mathcal{K}}\zeta_{\rm in} = \zeta_{\rm in}^T\left[\widetilde{\mathcal{K}}^{-1}\gamma_{\rm in}(\widetilde{\mathcal{K}}^T)^{-1}\right]^{-1}\zeta_{\rm in} = \zeta_{\rm in}^T\gamma_{\rm out}^{-1}\zeta_{\rm in} \tag{3.24}$$

and obtain $S = (\widetilde{\mathcal{K}}^T)^{-1}$. Hence, a general symplectic matrix describing the QND-Faraday interaction is given by:

$$S_{\rm int} = \left(\begin{array}{ccc|c} & & & G_1 \\ & \mathbf{1}_{2N_s}^{(A)} & & \vdots \\ & & & G_{N_s} \\ \hline M_1 & \cdots & M_{N_s} & \mathbf{1}_2^{(L)} \end{array}\right) \tag{3.25}$$

with

$$G_i = \begin{pmatrix} -\kappa_i\sin\alpha_i & 0 \\ -\kappa_i\cos\alpha_i & 0 \end{pmatrix} \qquad M_i = \begin{pmatrix} 0 & 0 \\ -\kappa_i\cos\alpha_i & \kappa_i\sin\alpha_i \end{pmatrix} \tag{3.26}$$

Now the covariance matrix of the output state is straightforwardly obtained through the formula:

$$\gamma_{\rm out} = S_{\rm int}^T\gamma_{\rm in}S_{\rm int} \tag{3.27}$$

and at the same time the DV of the system after the interaction is calculated as follows:

$$d_{\rm out} = S_{\rm int}^T d_{\rm in} \tag{3.28}$$

Note that if the initial state of the atoms and the light is the vacuum, the displacement does not change due to the interaction. However, looking at equations (3.18a) and (3.18b) we observe that the atomic quadratures are modified by a random variable with Gaussian distribution $P_L^{\rm in}$, which can be expressed in the following manner

$$d_{A,\rm out} = d_{A,\rm in} + (-\kappa\left\langle P_L^{\rm in}\right\rangle\cos\alpha\ \ \kappa\left\langle P_L^{\rm in}\right\rangle\sin\alpha) \tag{3.29}$$

Due to this fact, any subsequent manipulation of the light mode may affect the DV and, quite obviously, also the CM corresponding to the atomic ensemble. As we will see in the next section, the reason for that is the entanglement generated between the sample and the light through the interaction.

A particular example of such manipulation of the light mode is the homodyne detection of the field. In the case of the QND-Faraday interface it is the variable $X_L^{\rm out}$ that is measured, leaving the sample in the state characterized by the CM [compare equation (2.21)]

$$\gamma_{A,\rm fin} = \gamma_{A,\rm out} - C(D\gamma_{L,\rm out}D)^{-1}C^T \tag{3.30}$$

and the DV [compare equation (2.22)]

$$d_{A,\rm fin} = d_{A,\rm out} + C(D\gamma_{L,\rm out}D)^{-1}(\tilde{x}_L\ \ 0) \tag{3.31}$$

where $\tilde{x}_L$ is the measurement outcome, the subscript $A\ L$ corresponds to atomic and light modes in the CM $\gamma_{\rm out}$, C is the rectangular submatrix containing the atom–light correlation terms, and $D = {\rm Diag}(1\ 0)$.

In the case when the light is not measured, but just discarded from the system, the final state can be interpreted as a mixture of pure states corresponding to all possible outcomes of the homodyne measurement. The corresponding CM and DV are obtained from (3.27) and (3.28) by choosing only the submatrix containing the atomic modes.

Throughout the chapter I will use the following notation for the covariance matrix and the displacement vector:

$$\gamma_{i,x} \qquad d_{i,x}$$

with $i = 1 \qquad n$ denoting the step of the protocol and $x \qquad {\rm in\ out\ fin}$, its stage. The index ${\rm in}$ corresponds to the initial state of the system, note that it does not have to be the vacuum state, but rather $\gamma_{i,{\rm in}} = \gamma_{i-1,{\rm fin}} \oplus \gamma_L$, $i = 2\ 3 \qquad$. The index ${\rm out}$ denotes the state after the interaction and ${\rm fin}$ the final state after the ith step of the protocol is complete.

3.2 Pure multipartite entanglement

3.2.1 Bipartite entanglement: a brief review

Figure 3.2: A picture of the experimental set-up with two atomic ensembles used to demonstrate bipartite entanglement in [Julsgaard 01]. The visible elements are the magnetic shields which protect the cells with Caesium atoms from magnetic disturbance. One can also notice that the laser access is possible from orthogonal directions.

We begin by brie y reviewing the seminal experiment demonstrating bipartite entanglement between two spatially separated macroscopic objects. The experiment was aimed at generation of the paradigmatic EPR state, which is by definition a pure state with suppressed uctuations in $X_{A,1} - X_{A,2}$ and $P_{A,1} + P_{A,2}$. Note that these particular combinations can be squeezed simultaneously because their commutator vanishes. A crucial part of the task was the verification of the presence of entanglement, which was done through the variance inequalities criterion. The set-up in which the entangling protocol was implemented is shown in figure 3.2 and the details of the scheme are summarized in figure 3.3. The system consists of two atomic ensembles of approximately 10^{12} atoms at room temperature and strongly polarized along the x-axis. They are interfaced with the linearly polarized light propagating

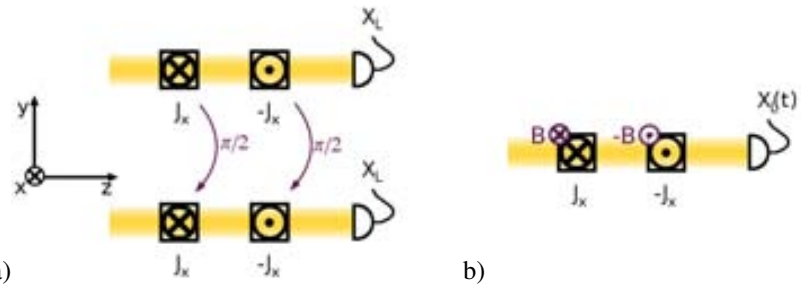

Figure 3.3: Two possible set-ups for generation of EPR-like entanglement between the oppositely polarized atomic ensembles as proposed in [Julsgaard 01, Julsgaard 03]. In set-up a) the first beam squeezes the combination $P_1 + P_2$ then the atomic spins are rotated and the second beam probes the combination $X_1 + X_2$. In figure b) a parallel magnetic field causes the Larmor precession of atomic spin which enables to squeeze both combinations of variables with a single beam.

along direction z which leads to an exchange of quantum uctuations between the beam and the ensembles. The subsequent measurement of light establishes entanglement between the samples by projecting them on a squeezed state.

The detailed procedure is the following. The atomic ensembles are prepared in a spin-polarized state such that their collective spin has a strong, classical component along x. The spins are pointing in the opposite directions which makes the combinations of field quadratures $X_{A,1} + X_{A,2}$ and $P_{A,1} + P_{A,2}$ commute. Then, the first beam applied along direction z (figure 3.3a upper picture), probes the variable $P_{A,1} + P_{A,2}$ imprinting it in quadrature X_L [see equation (3.18c)]. The subsequent homodyne detection of X_L establishes entanglement between the samples. In order to squeeze the other combination, $X_{A,1} + X_{A,2}$, the second beam along the y direction is applied and measured. Equivalently, the atomic spins can be rotated by π 2 around the x-axis using magnetic field and probed with the light pulse propagating along direction z (figure 3.3a).

As an alternative to the above scheme, which requires two light passes to produce optimal amount of entanglement, the authors of [Julsgaard 01] propose to use a magnetic field parallel to spin polarization to cause the Larmor precession of spin components (figure 3.3b). The advantage of this approach is that the information about both transverse atomic spin components is accumulated in a single light beam and can be then separated through signal post-processing. This is possible because the period of spin precession is much shorter than T, the duration of the light pulse.

Note that in this measurement-based scheme, entanglement is generated irrespectively of the outcome of the measurement. However, the result has to be recorded to make the produced correlations useful. To show it we consider the method used in [Julsgaard 01, Julsgaard 03] to verify that entanglement was indeed generated by the first pulse. The criterion applied for this purpose is the variance inequality (2.59) for $X_{A,1} + X_{A,2}$ and $P_{A,1} + P_{A,2}$. Let us denote by $M_1^{(x)}$ $M_1^{(p)}$ the outcomes of the first, entangling, measurements. In the verification step, the two combinations are probed again (using either two consecutive beams or a single beam in the protocol using the magnetic field) and the results $M_2^{(x)}$ $M_2^{(p)}$ are obtained. Now the variances of $M_2^{(x)}$ $M_2^{(p)}$, conditioned on the outcomes $M_1^{(x)}$ $M_1^{(p)}$ need to be determined.

Precisely speaking, it is assumed that

$$\left\langle M_2^{(x)} \right\rangle \quad M_1^{(x)} \qquad \left\langle M_2^{(p)} \right\rangle \quad M_1^{(p)} \tag{3.32}$$

and therefore

$$\begin{aligned} \mathrm{Var}\left(X_{A,1} + X_{A,2}\right) + \text{light noise} &= \mathrm{Var}\left(M_2^{(x)} \middle| M_1^{(x)}\right) \\ &= \left\langle \left(M_2^{(x)} - \left\langle M_2^{(x)} \right\rangle\right)^2 \right\rangle \\ &= \left\langle \left(M_2^{(x)} - \quad M_1^{(x)}\right)^2 \right\rangle \qquad (3.33a) \\ \mathrm{Var}\left(P_{A,1} + P_{A,2}\right) + \text{light noise} &= \left\langle \left(M_2^{(p)} - \quad M_1^{(p)}\right)^2 \right\rangle \qquad (3.33b) \end{aligned}$$

The mean values in equations (3.33b) and (3.33a) are obtained by averaging over many repetitions of the experiment. If instead the variances of $M_2^{(x)}$ $M_2^{(p)}$ were computed, without taking into account the outcome of the first measurement, the obtained results would not re ect the squeezing of the variables $X_{A,1} + X_{A,2}$ and $P_{A,1} + P_{A,2}$. This is because the variables $M_2^{(x)}$ $M_2^{(p)}$ have distribution corresponding to the initial state of ensembles, i.e., the product of the vacuum states [Julsgaard 03].

Covariance matrix analysis. — The CM formalism can be straightforwardly applied to the bipartite entanglement protocol and the amount of entanglement produced can be easily quantified using, for instance, the logarithmic negativity. We use this simple example also to demonstrate the utility of the CM formalism.

We begin with the set-up in which both the atomic ensembles and the light are in the vacuum state, i.e., the one characterized by zero displacement and the following CM

$$\gamma_{1,\mathrm{in}} = \mathbf{1}_4^{(A)} \oplus \mathbf{1}_2^{(L)} \tag{3.34}$$

and we assume that both atomic samples couple to light with the same strength κ ($\kappa_1 = \kappa_2 = \kappa$) simplifying the symplectic matrix (3.25). In the first step of the interaction (figure 3.3a) the angles α_1 α_2 are both equal zero, hence we obtain the following output CM of the system:

$$\begin{aligned} \gamma_{1,\mathrm{out}} &= S_1^T \gamma_{1,\mathrm{in}} S_1 \\ &= \left(\begin{array}{cccc|cc} 1+\kappa^2 & 0 & \kappa^2 & 0 & 0 & \kappa \\ 0 & 1 & 0 & 0 & \kappa & 0 \\ \kappa^2 & 0 & 1+\kappa^2 & 0 & 0 & \kappa \\ 0 & 0 & 0 & 1 & \kappa & 0 \\ \hline 0 & \kappa & 0 & \kappa & 1+2\kappa^2 & 0 \\ \kappa & 0 & \kappa & 0 & 0 & 1 \end{array}\right) \end{aligned} \tag{3.35}$$

Now, using, e.g., the logarithmic negativity it is easy to check that due to the interaction both atomic modes are entangled with light; however, the reduced state of the two ensembles [represented by the 4×4 upper left block matrix of equation (3.35)] is separable (figure 3.4a). This indeed indicates that entanglement between atomic samples is not produced through sole interaction with light. Next, the quadrature of light $X_L^{(\mathrm{out})}$ is measured with outcome $\tilde{x}_{L,1}$

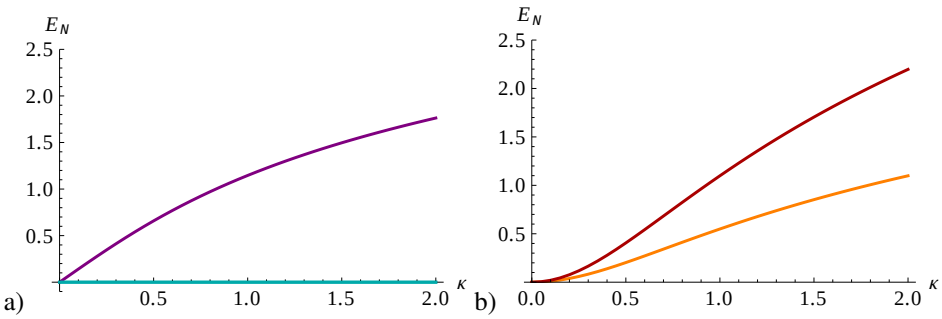

Figure 3.4: Amount of entanglement generated in the bipartite entanglement protocol [Julsgaard 01] quantified by the logarithmic negativity. In figure a) the purple line corresponds to the amount of entanglement between the samples and the light while the blue line is the amount of entanglement in the reduced state of two atomic ensembles. Figure b) shows the logarithmic negativity of the state of ensembles after the homodyne detection is performed. There, the orange line corresponds to a single step protocol (the first line of figure 3.3a), while the red line to the complete procedure depicted in figure 3.3a.

and one obtains the final state of the system described by the CM [see equations (3.30) and (3.31)]

$$\gamma_{1,\mathrm{fin}} = \begin{pmatrix} 1+\kappa^2 & 0 & \kappa^2 & 0 \\ 0 & \frac{\kappa^2+1}{2\kappa^2+1} & 0 & -\frac{\kappa^2}{2\kappa^2+1} \\ \kappa^2 & 0 & 1+\kappa^2 & 0 \\ 0 & -\frac{\kappa^2}{2\kappa^2+1} & 0 & \frac{\kappa^2+1}{2\kappa^2+1} \end{pmatrix} \tag{3.36}$$

and the displacement vector

$$d_{1,\mathrm{fin}} = \begin{pmatrix} 0 & -\dfrac{\tilde{x}_{L,1}\kappa}{2\kappa^2+1} & 0 & -\dfrac{\tilde{x}_{L,1}\kappa}{2\kappa^2+1} \end{pmatrix} \tag{3.37}$$

The logarithmic negativity of the state after the homodyne detection of light is depicted in figure 3.4b.

In the second step, introducing more entanglement, the ensembles again interact with a light beam in the vacuum state, hence we add one mode to the final CM of the previous step obtaining:

$$\gamma_{2,\mathrm{in}} = \gamma_{1,\mathrm{fin}} \oplus \mathbf{1}_2^{(L)} \tag{3.38}$$

The interaction at angles $\alpha_1 = -\alpha_2 = \pi$ 2 with the same coupling constant κ leads to the state characterized by the following matrix

$$\gamma_{2,\mathrm{out}} = \left(\begin{array}{cccc|cc} 1+\kappa^2 & 0 & \kappa^2 & 0 & -\kappa & 0 \\ 0 & \frac{2\kappa^4+2\kappa^2+1}{2\kappa^2+1} & 0 & -\frac{2\kappa^2\left(\kappa^2+1\right)}{2\kappa^2+1} & 0 & \kappa \\ \kappa^2 & 0 & 1+\kappa^2 & 0 & \kappa & 0 \\ 0 & -\frac{2\kappa^2\left(\kappa^2+1\right)}{2\kappa^2+1} & 0 & \frac{2\kappa^4+2\kappa^2+1}{2\kappa^2+1} & 0 & -\kappa \\ \hline -\kappa & 0 & \kappa & 0 & 1+2\kappa^2 & 0 \\ 0 & \kappa & 0 & -\kappa & 0 & 1 \end{array}\right) \tag{3.39}$$

Finally, the homodyne measurement of $X_L^{\rm out}$, this time with outcome $\tilde{x}_{L,2}$, leads to the expected EPR-like state with CM

$$\gamma_{2,\rm fin} = \begin{pmatrix} \frac{2\kappa^4+2\kappa^2+1}{2\kappa^2+1} & 0 & \frac{2\kappa^2\left(\kappa^2+1\right)}{2\kappa^2+1} & 0 \\ 0 & \frac{2\kappa^4+2\kappa^2+1}{2\kappa^2+1} & 0 & -\frac{2\kappa^2\left(\kappa^2+1\right)}{2\kappa^2+1} \\ \frac{2\kappa^2\left(\kappa^2+1\right)}{2\kappa^2+1} & 0 & \frac{2\kappa^4+2\kappa^2+1}{2\kappa^2+1} & 0 \\ 0 & -\frac{2\kappa^2\left(\kappa^2+1\right)}{2\kappa^2+1} & 0 & \frac{2\kappa^4+2\kappa^2+1}{2\kappa^2+1} \end{pmatrix} \tag{3.40}$$

and displacement vector

$$d_{2,\rm fin} = \begin{pmatrix} -\frac{\kappa\tilde{x}_{L,2}}{2\kappa^2+1} & -\frac{\kappa\tilde{x}_{L,1}}{2\kappa^2+1} & \frac{\kappa\tilde{x}_{L,2}}{2\kappa^2+1} & -\frac{\kappa\tilde{x}_{L,1}}{2\kappa^2+1} \end{pmatrix} \tag{3.41}$$

It is important to note that the covariance matrix is independent of the measurement outcomes, but the latter are clearly present in the displacement vector of the atomic modes. This is a general rule in this kind of protocols indicating once more that the entanglement is generated independently of the results of the measurements, nevertheless, can be used only if those results are recorded. The logarithmic negativity of the state generated in the two-step procedure is depicted in figure 3.4b. Clearly, as expected, the squeezing of the complementary combination of variables step increases the amount of entanglement between the ensembles.

Variance inequalities are strong and experimentally-friendly criteria to test the presence of entanglement in the CV system [Duan 00b, van Loock 03]. However, their efficiency is limited, which we will demonstrate here. The simplest inequality, yet most useful in our case, reads [see also equation (2.59)]:

$$\mathrm{Var}(P_1+P_2)+\mathrm{Var}(X_1-X_2) \geqslant 2 \tag{3.42}$$

The required variances can be immediately computed from matrix elements of CMs (3.36) and (3.40) as follows:

$$\begin{aligned} \mathrm{Var}\left(P_{A,1}+P_{A,2}\right)\big|_{\gamma_{j,\rm fin}} &= \frac{1}{2}\left[(\gamma_{j,\rm fin})_{22}+(\gamma_{j,\rm fin})_{44}+2(\gamma_{j,\rm fin})_{24}\right] \\ \mathrm{Var}\left(X_{A,1}-X_{A,2}\right)\big|_{\gamma_{j,\rm fin}} &= \frac{1}{2}\left[(\gamma_{j,\rm fin})_{11}+(\gamma_{j,\rm fin})_{33}-2(\gamma_{j,\rm fin})_{13}\right] \quad (j=1\ 2) \end{aligned} \tag{3.43}$$

In figure 3.5 we depict the left-hand side of inequality (3.42) as a function of the coupling constant. The plot shows that the criterion based on variances is efficient in this case since it detects entanglement for arbitrarily small $\kappa > 0$. Note, however, that the variances are measured with finite precision and this establishes a lower bound on κ for which we can trust the obtained result.

To determine experimentally the required sum of variances one can simply repeat the two steps used for entanglement generation (or a single step in the set-up with magnetic field), record the result and compute the conditional variance as it was described in equations (3.33). In such case we obtain

$$\mathrm{Var}X_{L,1}^{\rm out} = \mathrm{Var}X_{L,1}^{\rm in}+\kappa^2\mathrm{Var}(P_{A,1}+P_{A,2}) \tag{3.44a}$$

$$\mathrm{Var}X_{L,2}^{\rm out} = \mathrm{Var}X_{L,2}^{\rm in}+\kappa^2\mathrm{Var}(X_{A,1}-X_{A,2}) \tag{3.44b}$$

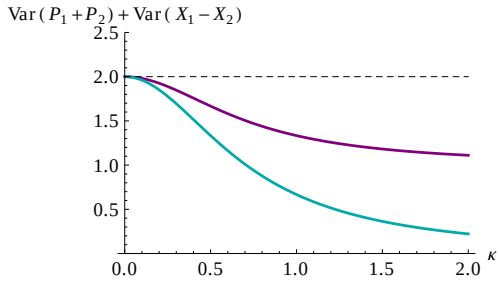

Figure 3.5: We plot the left-hand side of equation (3.42) in order to show the efficiency of the entanglement criterion base on variances of squeezed variables. The purple line corresponds to the state produced in the first step of the protocol, and the blue line to the final EPR-like state. The dashed line is the bound below which the variance inequality criterion is violated.

Since there are two separate measurements of each variance, the uncertainty of the obtained result increases. In [Stasińska 09] we proposed an alternative *geometric* scheme in which a single beam is used as depicted in figure 3.6 to probe the following combination of variables

$$X_L^{\text{out}} = X_L^{\text{in}} - \frac{\kappa}{2}\left(P_{A,1} + P_{A,1} + X_{A,1} - X_{A,2}\right) \tag{3.45}$$

Now, since the atomic variables $X_{A,j}$ and $P_{A,j}$ were not correlated by the entangling pulses, we have $X_{A,i}P_{A,j} = X_{A,i}\ P_{A,j}\ (i\ j = 1\ 2)$ and the variance of (3.45) amounts to

$$\text{Var}X_L^{\text{out}} = \text{Var}X_L^{\text{in}} + \frac{\kappa^2}{2}\left[\text{Var}(P_{A,1} + P_{A,1}) + \text{Var}(X_{A,1} - X_{A,2})\right] \tag{3.46}$$

Figure 3.6: Set-up for verification of bipartite entanglement.

We see that the sum of the variances, which we will denote by F, is proportional to the variances of $X_L^{\text{in/out}}$, hence in the error analysis we treat it as a complex expression depending on a number of experimental values q_i with relative errors δ_i and determine the cumulative relative error through the formula

$$\delta(F) = \sqrt{\sum_i \left(\frac{}{q_i}F\right)^2 \delta_i^2} \tag{3.47}$$

with

$$\mathbf{q} = \left(\text{Var}X_L^{\text{in}}\ \ \text{Var}X_L^{\text{out}}\ \ \kappa\right) \tag{3.48}$$

and we take the relative error of variances and κ to be 5%. The error computed in this way is smaller than 10% for $\kappa \geqslant 1$, however grows quickly for smaller κ. This values suggest that in order to to certify the presence of entanglement the coupling constant should be greater than 1 and in this case the measured variances must give the total smaller then $1\ 8$, which is well within reach of today s technology [Appel 09].

3.2.2 Geometric scheme for multipartite entanglement

There exist experimental situations in which it is not possible to address each sample with individual magnetic field. For instance, the atomic ensembles of mesoscopic size produced in the set-up of optical micro-traps are too close to each other to achieve individual addressing [Kruse 10, Schlosser 11]. Moreover, the scheme with oppositely polarized atomic ensembles and magnetic fields fails to preserve the QND character when an odd number of samples is involved, since in this case it is not possible to make the total spin along x equal zero. These restrictions can be overcome with the *geometric scheme* for multipartite set-up [Stasińska 09, Stasińska 12b] in which light passes through the ensembles at specific angles. We will demonstrate how using this scheme one can explore the multipartite scenario and not only produce GHZ-like and cluster-like states but also verify their entanglement. In contrast to the bipartite case, where only one type of entanglement exists, the issue of detection of multipartite entanglement with variance inequalities (2.57) becomes an intricate task, however in the pure-state scenario, which we study in this section, it is still feasible.

GHZ-like states. — By definition the CV GHZ state is an eigenstate of zero total momentum $P_1 + \quad + P_{N_s}$ and zero pairwise relative positions $X_i - X_j$ ($i\ j = 1 \qquad N_s$, $i < j$) [van Loock 00]. Note that all such combinations of variables commute which, in turn, implies they can be squeezed simultaneously. Generation of this state is feasible in the set-up of atomic ensembles for any number N_s of atomic samples. The first step, being a trivial extension of the bipartite entangling strategy [figure 3.3a (upper picture)], is the following. A single beam passes through all the samples along direction z (see figure 3.7a) and the light quadrature $X^{\text{out}}_{1,L}$ is measured afterwards. The state produced in this way possesses entanglement of GHZ type, however it is squeezed in a single combination of variables $P_1 + \quad + P_{N_s}$, which clearly leads to weak correlations. In order to increase the amount of entanglement,

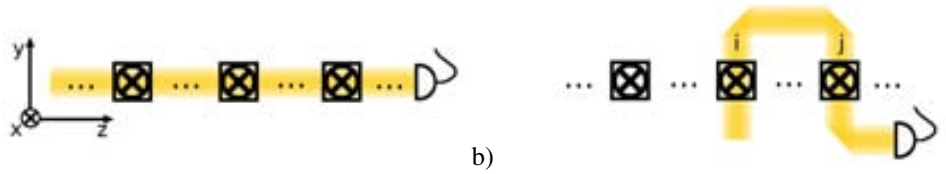

a) b)

Figure 3.7: Set-up for generation of multipartite GHZ-like entanglement. In figure a) the geometry for squeezing the combination $P_1 + \quad + P_{N_s}$; in b) the way to introduce more entanglement between the samples by squeezing all the combinations $X_i - X_j$ ($i < j$).

all the combinations of variables defining the GHZ state should be squeezed. Note, however, that this requires $N_s(N_s - 1)\ 2$ separate beams and measurements, which may be feasible for several parties but becomes problematic for larger systems due to the decay of the atomic spin-polarized state in time windows between the consecutive beams (3.19).

For an ideal system, the final genuine N_s-partite entangled state is characterized by the variances

$$\mathrm{Var}\,(P_1 + \quad + P_{N_s}) = \frac{N_s}{2 + 2N_s\kappa^2} \tag{3.49a}$$

$$\mathrm{Var}\,(X_i - X_j) = \frac{1}{1 + N_s\kappa^2} \qquad (i < j) \tag{3.49b}$$

which violate the variance inequalities of the type (2.57)

$$\mathrm{Var}\,(P_1 + \quad + P_{N_s}) + \mathrm{Var}\,(X_i - X_j) \geqslant 2 \qquad (i < j) \tag{3.50}$$

certifying the presence of entanglement. If the system is subject to some kind of decoherence, we model the process by appropriately modifying the CM [see equation (3.20)] after each interaction–measurement step. The effects of decoherence are displayed in figure 3.8, where we plot the value of the left-hand side of equation (3.50) for different values of parameter η_t and κ, and compare the results with those for the perfect system, i.e., $\eta_t = 0$.

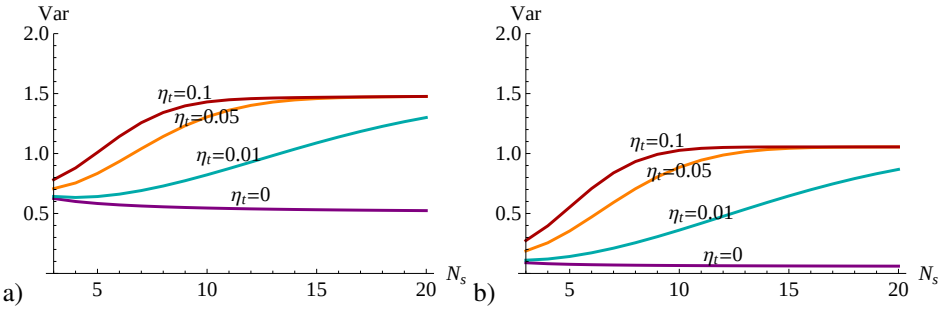

Figure 3.8: Violation of the variance inequality criterion for GHZ state (3.50) generated in a system subject to spin decay measured by parameter η_t depicted in the pictures. The coupling constants are a) $\kappa = 1$, b) $\kappa = 3$. Value below 2 indicates the presence of GHZ entanglement.

We observe that decoherence does not destroy the GHZ-type entanglement in the system even for large number of samples N_s where numerous light passages are required and the generation process becomes long. On the contrary, for large N_s the sum of the variances (3.50) saturates to a value well below the threshold (equal 2) indicating that the proposed procedure is efficient even if a large number of ensembles is involved, especially for strong coupling $\kappa > 1$. Note, however, that in order to determine the variances (3.49) one needs to perform another $N_s(N_s - 1)$ 2 measurements of the same variables once the state is generated. Therefore, the whole generation-verification procedure becomes complicated with increasing number of parties.

To overcome the problem of such large number of measurements we again exploit the geometric scheme. The alternative protocol still generates multipartite entanglement, and at the same time the number of light-beam passes is significantly reduced. Nevertheless, it is valid only for an even number of ensembles $N_s = 2M$ [Stasińska 09].

The set-up is depicted in figure 3.9a. In the first step we generate squeezing in $P_{A,1} + \quad + P_{A,2M}$. Next we squeeze the observables $X_{A,1} - X_{A,2} + \quad + (-1)^{2M-1}X_{A,2M}$ with the second beam passing through the ith sample at an angle $(-1)^{i-1}\pi$ 2. In order to detect the

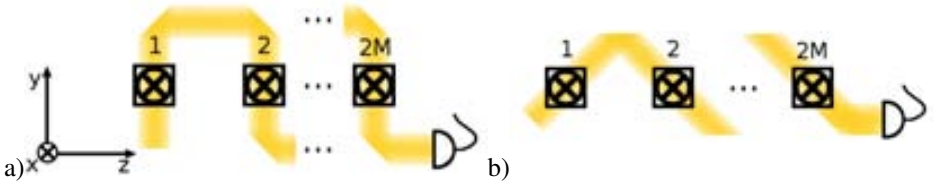

Figure 3.9: Alternative scheme for generation of multipartite entanglement.

entanglement of this state we use the variance inequality for two squeezed variables discussed in this paragraph. To probe them, we generalize the scheme described in the previous section (see figure 3.6) in the way summarized in figure 3.9b.

The measurement of light propagating through the ith sample at an angle $(-1)^{i-1}\pi$ 4 gives at the level of variances

$$\begin{aligned}\mathrm{Var}X_L^{\mathrm{out}} &= \mathrm{Var}X_L^{\mathrm{in}} \\ &+ \frac{\kappa^2}{2}\mathrm{Var}(X_{A,1} - X_{A,2} + \quad + (-1)^{2M-1}X_{A,2M}) \\ &+ \frac{\kappa^2}{2}\mathrm{Var}(P_{A,1} + \quad + P_{A,2M})\end{aligned} \tag{3.51}$$

Therefore, only a single beam is required for verification of entanglement. The same criterion and the above measurement scheme can be applied not only to detect the entanglement in the above set-up but also in those proposed before, i.e., (i) the state with squeezing only in $P_{A,1} + \quad + P_{A,2M}$ (after interaction and measurement of the first beam), and (ii) the state with squeezing in $P_{A,1} + \quad + P_{A,2M}$ and all combinations $X_{A,i} - X_{A,j}$ $(i = j)$. The reduction in the number of measurements in the verification step is significant.

Optimization of the scheme for odd number of atomic ensembles within this geometric approach is to our knowledge not possible. Even though it is possible to find independent variables involving all the samples, it is not clear what geometry should be applied in order to squeeze these operators.

Cluster-like states. — Continuous-variable cluster states were introduced in [Zhang 06] and further explored in a number of works including [van Loock 07, Yukawa 08, Menicucci 10, Aolita 11]. Their efficient generation and further manipulation is particularly important in the context of universal measurement-based scheme for quantum computation with Gaussian cluster states [Nielsen 04, Menicucci 06, Gu 09, Ohliger 10]. By definition a cluster state is a graph state based on a connected graph. One associates with each vertex of a graph $\mathcal{G}$ a CV mode. The edges between the vertices define the notion of the nearest neighbour. By $\mathcal{N}_a$ we denote the set of nearest neighbours of the vertex a. Graph states in CV are defined only asymptotically as those with infinite squeezing in the variables

$$P_a - \sum_{b\in\mathcal{N}_a} X_b \qquad \text{for all } a \quad \mathcal{G} \tag{3.52}$$

We talk about graph-like or cluster-like states when the squeezing is finite.

Given a set of atomic ensembles, it is possible to create a chosen cluster-like state by squeezing the required combinations of variables (3.52). Since they commute, it is possible to squeeze them sequentially. The procedure is as follows.

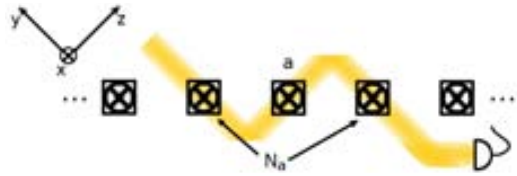

Figure 3.10: A unit entangling operation for graph states. The light beam probes the combination (3.52) for a particular vertex labelled by a which has two neighbours N_a.

1. Each graph vertex is associated with an atomic ensemble.

2. For every vertex a a unit entangling operation is executed. It consists of (i) probing the atomic momentum of the ensemble associated with a by passing a beam at the angle $\alpha = 0$ and (ii) probing the positions of the adjacent vertices by propagating a beam at the angle $\alpha = -\pi\ \ 2$ through the samples corresponding to elements of $\mathcal{N}_a$ (as schematically depicted in figure 3.10).

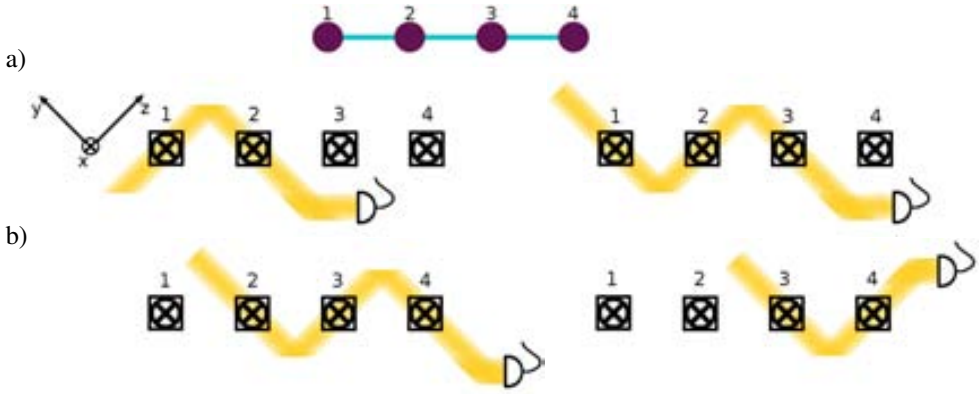

Figure 3.11: The set-up for generation of the cluster state corresponding to the linear graph depicted in figure a).

We illustrate the method by considering a simple example consisting in the four-mode linear cluster state, yet the protocol is general. The corresponding graph is depicted in figure 3.11a while figures 3.11b show how the light should propagate through the samples in order to squeeze the required combinations of variables. For example, the squeezing of $P_{A,1} - X_{A,2}$ is generated by passing light through samples 1 and 2 at angles 0 and $-\pi\ \ 2$, respectively.

In order to verify that the state is entangled it is enough to check the set of variance inequalities that involve the variables squeezed in the protocol [Yukawa 08]. Explicitly, the criteria read:

$$\mathrm{Var}\left(P_{A,1} - X_{A,2}\right) + \mathrm{Var}\left(P_{A,2} - X_{A,1} - X_{A,3}\right) > 2 \tag{3.53a}$$

$$\mathrm{Var}\left(P_{A,2} - X_{A,1} - X_{A,3}\right) + \mathrm{Var}\left(P_{A,3} - X_{A,2} - X_{A,4}\right) > 2 \tag{3.53b}$$

$$\mathrm{Var}\left(P_{A,3} - X_{A,2} - X_{A,4}\right) + \mathrm{Var}\left(P_{A,4} - X_{A,3}\right) > 2 \tag{3.53c}$$

It turns out that the so generated linear cluster state violates all the inequalities if the coupling constant $\kappa > 0\ 4$.

It is interesting to perform the analysis of the protocol assuming that the atomic spins decay in the time window between the entangling pulses. The analysis is analogous to the one for the GHZ state, namely we compute the maximal value attained by the left-hand sides of the inequalities (3.53) generalized to an arbitrary number of atomic ensembles. The results are depicted in figure 3.12 for different values of parameters κ and η_t.

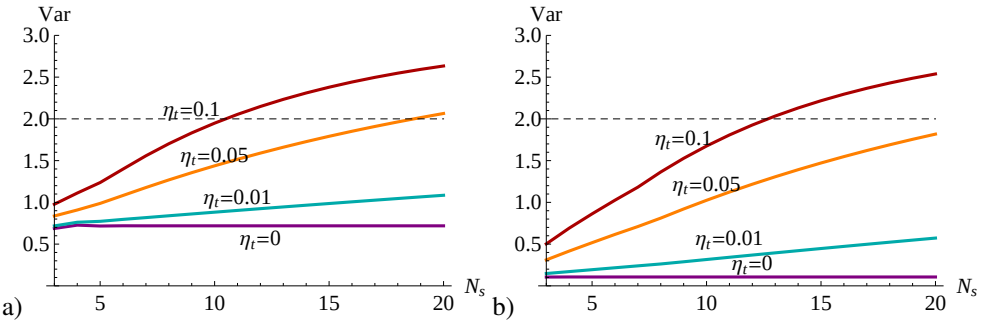

Figure 3.12: The maximum of the left-hand sides of inequalities of type (3.53) generalized to arbitrary number of parties for values of parameter η_t depicted in the picture and a) $\kappa = 1$, b) $\kappa = 3$.

Comparing figures 3.8 and 3.12 we see that the two types of entanglement behave completely differently under decoherence during the generation process. For large systems the linear cluster-like entanglement is completely destroyed by strong decoherence, unlike the GHZ-like entanglement which is present even in large systems and $\eta_t \approx 0\ 1$. However, one sees that the cluster states are more robust to small atomic decay $\eta_t \approx 0\ 01$. We should also mention that the atomic spin decay destroys the purity of the generated state which, as we will see in the next section, affects detectability of entanglement by the variance inequalities.

3.3 Extension to mixed entangled states

The generation of pure Gaussian entangled states analysed so far is important for quantum information protocols [Braunstein 05, Andersen 10, Weedbrook 12]. Therefore, it is crucial to evaluate its experimental feasibility with novel systems such as atomic ensembles. However the QND-Faraday interface offers also all the tools necessary to generate mixed-state entanglement, in particular bound entanglement [Stasińska 12b]. In this section we show two possible approaches to generation of mixed states. The first one demonstrates the robustness of the entanglement induced via QND-Faraday interface when the initial state of atoms is thermal instead of pure (vacuum). In such case the subsequent standard entangling operations cannot purify the state of the samples, consequently the obtained state is mixed. The second method consists in generation of pure state entanglement and its manipulation through interaction with a light beam that is not measured afterwards. This procedures introduces a random displacement classically correlated between the samples. Both methods can lead to various types of bound entangled states. In what follows we show how a three-mode state generated through cluster-like procedure from thermal samples changes its entanglement prop-

erties with the temperature parameter. Then we illustrate the potential of the second method showing how to create a four-mode Smolin-like state [Zhang 11], which possesses a special type of entanglement, *unlockable bound entanglement*.

3.3.1 Initial mixedness

Let us start with the set-up in which the atomic samples are not in the minimum- uctuation coherent state (vacuum), but in a general thermal state. The thermal uctuations can be imposed in a controlled way, for instance, by mapping to each sample separately a thermal state of light. The initial state of the composite system is in this case given by the following covariance matrix for atoms and light

$$\gamma_{\text{in}} = n_1 \mathbf{1}_2^A \oplus \cdots \oplus n_{N_s} \mathbf{1}_2^A \oplus \mathbf{1}_2^L \tag{3.54}$$

where the parameters n_1 n_N are related to temperature as $n_i = \coth[\beta_i \quad 2]$ ($i = 1 \cdots N$), β is the inverse of the temperature, and is the effective frequency of the local oscillator of a single sample.

Bipartite entanglement of thermal states. — In this paragraph we generalize the bipartite set-up of section 3.2.1. Starting from two ensembles in thermal states characterized by n_1 and n_2, and performing the first entangling step analogous to equations (3.35)-(3.36) we obtain the state characterized by the CM

$$\gamma_{1,\text{fin}} = \begin{pmatrix} n_1+\kappa^2 & 0 & \kappa^2 & 0 \\ 0 & \frac{n_1 n_2 \kappa^2 + n_1}{(n_1+n_2)\kappa^2+1} & 0 & -\frac{n_1 n_2 \kappa^2}{(n_1+n_2)\kappa^2+1} \\ \kappa^2 & 0 & n_2+\kappa^2 & 0 \\ 0 & -\frac{n_1 n_2 \kappa^2}{(n_1+n_2)\kappa^2+1} & 0 & \frac{n_1 n_2 \kappa^2 + n_2}{(n_1+n_2)\kappa^2+1} \end{pmatrix} \tag{3.55}$$

and the displacement vector

$$d_{1,\text{fin}} = \begin{pmatrix} 0 & -\dfrac{\tilde{x}_{L,1}\kappa n_1}{(n_1+n_2)\kappa^2+1} & 0 & -\dfrac{\tilde{x}_{L,1}\kappa n_1}{(n_1+n_2)\kappa^2+1} \end{pmatrix} \tag{3.56}$$

For $n_1 = n_2 = 1$ we reproduce trivially the results for the pure state case. In the second step, in order to increase the amount of entanglement we perform the squeezing operation on the complementary combination of quadratures obtaining:

$$\gamma_{2,\text{fin}} = \begin{pmatrix} \frac{a+n1}{\kappa^2(n_1+n_2)+1} & 0 & \frac{a}{\kappa^2(n_1+n_2)+1} & 0 \\ 0 & \frac{a+n_1}{\kappa^2(n_1+n_2)+1} & 0 & \frac{-a}{\kappa^2(n_1+n_2)+1} \\ \frac{a}{\kappa^2(n_1+n_2)+1} & 0 & \frac{a+n_2}{\kappa^2(n_1+n_2)+1} & 0 \\ 0 & \frac{-a}{\kappa^2(n_1+n_2)+1} & 0 & \frac{a+n_2}{\kappa^2(n_1+n_2)+1} \end{pmatrix} \tag{3.57}$$

with $a = \kappa^4(n_1+n_2) + \kappa^2(1+n_1 n_2)$, and

$$d_{2,\text{fin}} = \begin{pmatrix} \dfrac{-\kappa n_1 \tilde{x}_{L,2}}{\kappa^2(n_1+n_2)+1} & \dfrac{-\kappa n_1 \tilde{x}_{L,1}}{\kappa^2(n_1+n_2)+1} & \dfrac{\kappa n_2 \tilde{x}_{L,2}}{\kappa^2(n_1+n_2)+1} & \dfrac{-\kappa n_2 \tilde{x}_{L,1}}{\kappa^2(n_1+n_2)+1} \end{pmatrix} \tag{3.58}$$

In order to see the effect of the initial thermal noise imposed on the samples, we now quantify the entanglement produced in each step with logarithmic negativity. We also check

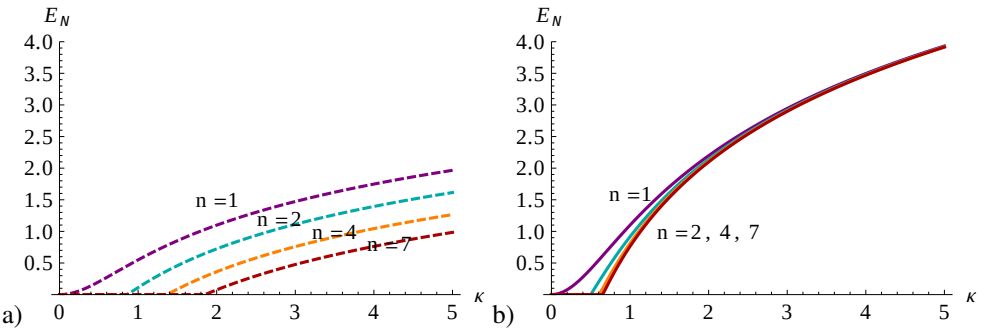

Figure 3.13: The negativity of the states produced in the bipartite entangling protocol in a) the first and b) the second step for the values of thermal noise depicted in the pictures.

if the noise affects the detectability of entanglement with variance inequality (3.42). In figure 3.13 we depict the negativities of the states produced in both steps as a function of $n_1 = n_2 = n$ and the coupling constant κ. This analysis shows that, contrary to the case of initially pure states ($n = 1$), in which an arbitrarily small coupling produces entanglement, the protocol beginning with thermal states requires a stronger coupling with light to be successful.

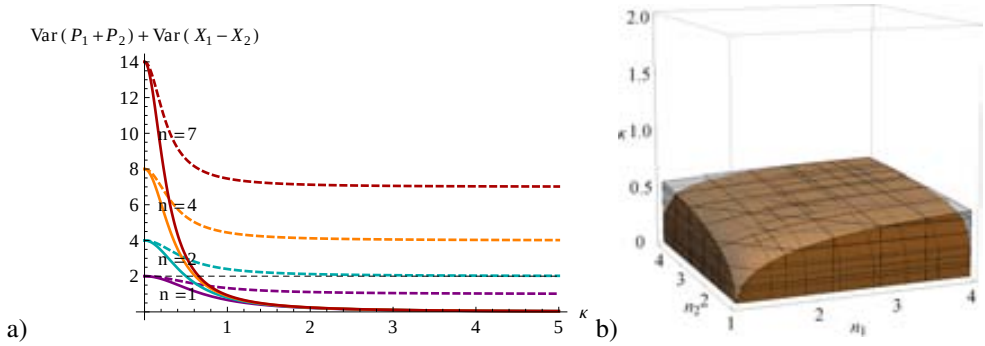

Figure 3.14: The value of the left-hand side of inequality (3.42) for the states produced in the bipartite entangling protocol in the first (dashed) and the second (continuous) step for the values of thermal noise depicted in the pictures. In figure b) we compare the set of parameters κ n_1 n_2 for which the state $\gamma_{2,\mathrm{fin}}$ of the ensembles remains separable (brown inner region) and the one for which the state is not detected by the variance criterion (transparent outer region).

In figure 3.14a we show the corresponding plots for the left-hand side of the bipartite variance inequality. Comparing the curves of the negativity with those of the variance test, we notice that the latter performs particularly poor for the weakly entangled state produced after the first step of the protocol, where it does not detect any entanglement for $n \geqslant 2$. This is due to the fact that only one combination of variables, i.e., $P_1 + P_2$ is squeezed and the thermal uctuations, still present in $X_1 - X_2$, keep the sum in equation (3.42) above the bound. The detectability very much improves when the two-step procedure is applied. There, the inequality detects all the states with positive negativity for the choice $n_1 = n_2 = n$.

In figure 3.14b we compare the set of states with positive negativity and the set of states not detected by the variance inequality. We observe that some states with $n_1 = n_2$ are not detected.

If we consider the decay of atomic spin in the course of the protocol, as in equation (3.20), we see that the amount of entanglement is not affected significantly. For the decay constant $\eta \approx 0\ 05$ the region of entangled states shrinks very little, especially for the admissible parameter $\kappa \geqslant 1$. The feasibility of the detection of entanglement through the variance inequality was studied already in section 3.2.1 and the obtained results remain valid for the protocol with thermal samples. For achievable parameters, i.e, $\kappa \geqslant 1$ and $\eta \approx 0\ 05$ detection is always feasible in the set-up consisting of two light beams, however is limited to $n_1 + n_2 \approx 2$ (initial vacuum state) if only one entangling beam is used.

Bipartite entanglement eraser. — In [Stasińska 09, Stasińska 12b] we have shown that the measurement-induced entanglement between two atomic samples reported in the previous paragraphs can be deleted by exploiting the squeezing and anti-squeezing mechanism. Let us recall here the results for the bipartite entanglement generated from initially mixed states with CM (3.55) and DV (3.56).

Figure 3.15: The geometric set-up for entanglement eraser.

For simplicity we begin with the entangled state produced in the one-step protocol. Then, interaction with strength κ with a second light beam impinging on each atomic sample at $\alpha_1 = \alpha_2 = \pi\ 2$ (as depicted in Figure 3.15) followed by the light measurement erases the entanglement produced by the interface with the first light beam if the properties of light are appropriately adjusted. To this aim, it is sufficient to take the erasing light beam characterized by the covariance matrix

$$\gamma_L = \begin{pmatrix} 2\mathrm{Var}X & 0 \\ 0 & 2\mathrm{Var}P \end{pmatrix} \tag{3.59}$$

with

$$2\mathrm{Var}X = \kappa^2(n_1 + n_2) + n_1 n_2 \tag{3.60a}$$

$$2\mathrm{Var}P = \frac{n_1 n_2}{\kappa^2(n_1 + n_2) + 1} \tag{3.60b}$$

The covariance matrix of the final state is then given by:

$$\gamma_{1,\mathrm{er}} = \begin{pmatrix} \frac{\kappa^2(n_1+n_2)+n_1n_2}{2\kappa^2+n_2} & 0 & 0 & 0 \\ 0 & \frac{n_1\left(2\kappa^2n_2+1\right)}{\kappa^2(n_1+n_2)+1} & 0 & 0 \\ 0 & 0 & \frac{\kappa^2(n_1+n_2)+n_1n_2}{2\kappa^2+n_1} & 0 \\ 0 & 0 & 0 & \frac{n_2\left(2\kappa^2n_1+1\right)}{\kappa^2(n_1+n_2)+1} \end{pmatrix} \tag{3.61}$$

and the corresponding displacement is:

$$d_{1,\mathrm{er}} = \left(-\frac{\kappa\tilde{x}_{L,\mathrm{er}}}{2\kappa^2+n_2} \; -\frac{\kappa n_1\tilde{x}_{L,1}}{\kappa^2(n_1+n_2)+1} \; -\frac{\kappa\tilde{x}_{L,\mathrm{er}}}{2\kappa^2+n_1} \; -\frac{\kappa n_1\tilde{x}_{L,1}}{\kappa^2(n_1+n_2)+1} \right) \tag{3.62}$$

where $\tilde{x}_{L,\mathrm{er}}$ is the outcome of the measurement of the erasing beam. Note that the state (3.61) is separable. It is identical to the initial one, however, only if $n_2 = n_1 = 1$.

An analogous procedure can be applied to the state generated in the two-step protocol characterized by CM (3.57) and DV (3.58). In this case the properties of light should be chosen as

$$2\mathrm{Var}X = \frac{\kappa^2(n_1+n_2)+n_1n_2}{\kappa^2(n_1+n_2)+n_1n_2+1} \tag{3.63a}$$

$$2\mathrm{Var}P = \frac{\kappa^2(n_1+n_2)+n_1n_2+1}{\kappa^2(n_1+n_2)+1} \tag{3.63b}$$

In this case, after the interaction and the light detection the state of the ensembles is characterized by the CM

$$\gamma_{2,\mathrm{er}} = \begin{pmatrix} \frac{\kappa^2(n_1+n_2)+n_1n_2}{2a+n_2} & 0 & 0 & 0 \\ 0 & \frac{2a+n_1}{\kappa^2(n_1+n_2)+1} & 0 & 0 \\ 0 & 0 & \frac{\kappa^2(n_1+n_2)+n_1n_2}{2a+n_1} & 0 \\ 0 & 0 & 0 & \frac{2a+n_2}{\kappa^2(n_1+n_2)+1} \end{pmatrix} \tag{3.64}$$

with $a = \kappa^4(n_1+n_2)+\kappa^2(n_1n_2+1)$, and

$$d_{2,\mathrm{er}} = d_{2,\mathrm{fin}} + \left(-\frac{a\tilde{x}_{L,\mathrm{er}}}{\kappa(2a+n_2)} \; 0 \; -\frac{a\tilde{x}_{L,\mathrm{er}}}{\kappa(2a+n_1)} \; 0 \right) \tag{3.65}$$

Again we see that the entanglement was erased, however the initial state is not recovered even for the pure-state case, i.e., $n_1 = n_2 = 1$. In the latter case, each sample after the erasing protocol is in a squeezed vacuum state.

Bound entanglement in three-mode states. — We move now to the truly multipartite entanglement and aim at analysing bound entanglement, which exist only in the mixed state case. We focus on the simplest scenario of the three atomic samples, since the entanglement of this states was already fully classified by Giedke and co-workers in [Giedke 01b]. There are five classes of states: states inseparable with respect to every bipartite splitting are denoted as class 1. States which are biseparable with respect to one (and only one) bipartition belong to class 2. States that are biseparable with respect to two or three bipartitions, but still entangled, belong to class 3 and class 4, respectively. These two classes of states are bound entangled. Finally, class 5 are the separable states. While classes 1-3 are fully characterized by the PPT criterion, in order to distinguish class 4 and 5, a different strategy is necessary. The authors of [Giedke 01b] provide the necessary and sufficient test for full separability which we summarized in section 2.4.3 of chapter 2. It will allow us to distinguish unambiguously the two classes.

Using the geometric set-up for cluster states described in section 3.2.2 we analyse two states, one based on the linear graph and the other based on the triangular one (corresponding graphs are depicted in figure 3.16), however produced from initially thermal samples as in

equation (3.54). For simplicity we choose the same temperature parameter and coupling constant for each sample. We demonstrate that in such set-up bound entangled states of various types are produced for certain choices of temperature and coupling. This research can be placed in the context of [Cavalcanti 10] where the authors study the presence of undistillable entanglement in thermal finite-dimensional systems.

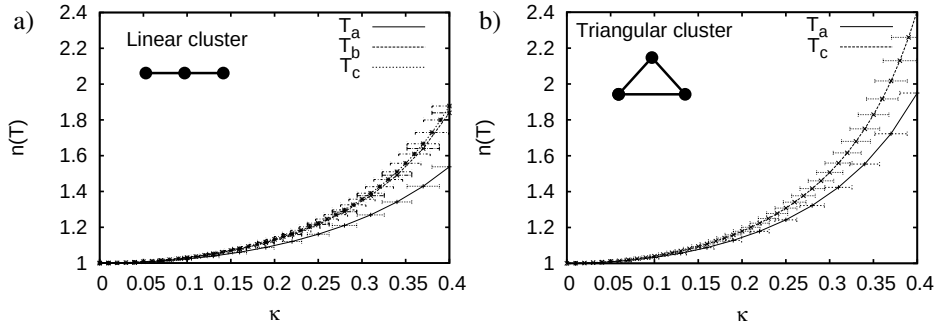

Figure 3.16: Range of parameters for a) the linear and b) the triangular cluster state for which the produced state belongs to different entanglement classes (see explanation it the text).

In figure 3.16 we summarize our results. We depict sets of states with different entanglement types as a function of the temperature T through $n(T) = 1 \ \tanh(\ \ 2T)$ and coupling κ. In the case of the linear cluster state (figure 3.16a), for a fixed value of the parameter κ, the state is NPT with respect to all the three cuts in the interval $0 < T < T_a$, meaning that it belongs to class 1. For $T_a < T < T_b$ the state is PPT with respect to the bipartition $2 - (1\ 3)$ and NPT with respect to others. Hence, it belongs to bound entangled class 3. For $T > T_b$ the state becomes PPT with respect to all the cuts. Using the full-separability criterion, we see that within the range $T_b < T < T_c$ the state is class-4, while for $T > T_c$ it becomes fully separable. Figure 3.16b shows different entanglement classes for a triangular cluster state. In this case, because of the permutational invariance, class 3 is never recovered. Nevertheless, a class-4 region still appears between the genuine tripartite class-1 states and the fully separable states of class 5.

Even though at the level of covariance matrix we are able to distinguish all the entanglement classes it may be challenging to recover them in experiment. On one hand, the uctuations of the coupling constant ($\delta\kappa \approx 0\ 05$) that are always present in the system due to particle loss, spontaneous emission, uctuations of laser intensity *etc* make the states belonging to class-4 practically undistinguishable from those belonging to class-3 and -5. On the other hand bound entangled states belonging to entanglement class-3 are well separated from other types of states, hence experimentally distinguishable.

3.3.2 Manipulation of pure entanglement

So far, all the presented protocols were "measurement-based", i.e., involved a final projective measurement on the light, and only in this type of procedures, the entanglement can be generated. In this section we look closer at the situation in which the light beam is not measured after the interaction. In this case, the interaction with the light beam mixes all the possible outcomes of the measurement-based experiment with a Gaussian weight. We propose to ex-

ploit this Gaussian randomness that is inherently present in the system, due to uncertainty of the outcome of the light measurement, to manipulate the entanglement previously created in the system. Using this procedure, starting from two pure bipartite entangled states, it is possible to produce the CV analogue of the so-called Smolin state [Smolin 01, Zhang 11] which is an example of an unlockable bound entangled state.

The CV Smolin state. — The Smolin state introduced in [Smolin 01] for qubits an experimentally demonstrated in [Amselem 09, Lavoie 10] is an interesting example of an undistillable multipartite entangled state that can be unlocked if several parties perform a collective measurement and send the outcome to the remaining parties. The Smolin state is formed by an equal-weight mixture of products of the four Bell states $_i(i = 1 \quad 4)$

$$_{\text{Smolin}} = \sum_{i=1}^{4} \quad _i \quad _i \; _{AB} \otimes \quad _i \quad _i \; _{CD} \tag{3.66}$$

One sees that parties AB and CD share the same Bell state but none of the pairs know which one it is. Such state is clearly separable with respect to partition $AB\ CD$. Moreover, since it is permutationally invariant, the above statement holds for every two pairs, not only for AB and CD. Hence, according to the definition, the state is undistillable with respect to two arbitrary parties, since there always exists a separable bipartition dividing them.

The fact that two arbitrary pairs share the same, yet unknown Bell state makes the entanglement present in the Smolin state unlockable. Imagine the situation in which two of the parties, say C and D, meet in one laboratory and perform collectively a discriminating measurement in the Bell basis, identifying thus the state they possess. This measurement projects the state shared by AB to be the same one. Hence, if A and B, still being in separate laboratories, obtain (by classical communication) the information about the outcome of CD, they can use their maximally entangled state. We emphasize that the otherwise unknown Bell state is useless.

The Smolin state possesses many other interesting features. Apart from being unlockable, its entanglement can be activated through a cooperation of five parties sharing two copies of the state [Shor 03]. Despite being bound entangled, the Smolin state has several applications, among others, it can be used in the remote quantum information concentration protocol [Murao 01]. It was also shown to maximally violate a Bell inequality being at the same time useless for the secret key distillation [Augusiak 06]. This particular result implies that in the multipartite scenario the security of key distribution is not equivalent to violation of Bell inequalities, unlike in the bipartite case [Ekert 91].

Recently, Zhang has generalized the discrete Smolin state to the Gaussian CV scenario using the mathematical formalism of stabilizers [Zhang 11]. It turns out that the state proposed by Zhang can be understood as a mixture of products of the continuous variables maximally entangled states, only this intuitive definition must be appropriately interpreted. Let us consider two EPR(-like) states with known displacement and randomly displace both of them in the opposite *unknown* directions in the phase space, as schematically depicted in figure 3.17. The only constraint imposed on the random displacement is that it has a Gaussian distribution. In this way we obtain a Gaussian mixture of two displaced EPR pairs.

The properties of the CV Smolin state are slightly different from those of the qubit state. First and most important, we loose the permutational invariance [Zhang 11]. Second, since the maximally entangled EPR-state corresponds to infinite squeezing, which is not physical, we always have to deal with EPR-like states and therefore it is necessary to analyse the effect

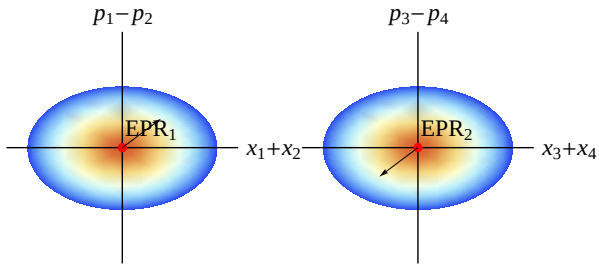

Figure 3.17: The intuitive explanation of how the CV Smolin state is generated. Different shades denote the Gaussian distribution of the displacement centred at 0.

of the finite squeezing on the separability properties of the Smolin-like state. It turns out that the state is bound entangled only within a particular range of the squeezing parameter and width of the Gaussian distribution characterizing the random displacement.

Let us demonstrate how the set-up generating the Smolin-like state proposed in [Zhang 11] greatly simplifies in the atomic-ensemble realization. We characterize each step of the procedure using the CM and the DV. Finally, we demonstrate the unlocking of entanglement and analyse the entanglement of the obtained state as a function of the system parameters.

The Smolin-like state can be generated in two steps [Zhang 11]:

1. generation of two EPR-like pairs with reduced uctuations (squeezing) in $X_1 + X_2$ and $P_1 - P_2$ ($X_3 + X_4$ and $P_3 - P_4$ for modes 3 and 4) and known displacement
2. displacement of the EPR pairs by random Gaussian variables λ_1 and λ_2 such that the quadratures transform in the following way:

$$X_1 + X_2 + X_3 + X_4 \qquad (X_1 - \lambda_1) + (X_2 - \lambda_1) + (X_3 + \lambda_1) + (X_4 + \lambda_1) \quad (3.67)$$

and

$$P_1 - P_2 + P_3 - P_4 \qquad (P_1 + \lambda_2) - (P_2 - \lambda_2) + (P_3 - \lambda_2) - (P_4 + \lambda_2) \quad (3.68)$$

Note that indeed the squeezed combinations in modes $1-2$ and $3-4$ are displaced in the opposite directions. Moreover, implementation of each of these steps is experimentally feasible in the geometrical set-up of atomic ensembles. Step 1 concerns the generation of EPR-like states with known displacement which is achieved as described in section 3.2.1. Step 2 corresponds to the generation of random Gaussian displacements correlated between the samples. In our geometrical set-up this can be achieved by shining two light beams so that they interact with the ensembles at angles

$$\left(\alpha_1^{(1)} \;\; \alpha_2^{(1)} \;\; \alpha_3^{(1)} \;\; \alpha_4^{(1)}\right) = (0 \;\; 0 \;\; \pi \;\; \pi) \quad (3.69)$$

and

$$\left(\alpha_1^{(2)} \;\; \alpha_2^{(2)} \;\; \alpha_3^{(2)} \;\; \alpha_4^{(2)}\right) = \left(\frac{\pi}{2} \;\; -\frac{\pi}{2} \;\; -\frac{\pi}{2} \;\; \frac{\pi}{2}\right) \quad (3.70)$$

A straightforward application of (3.18) shows that the procedure modifies the quadratures of the atomic ensembles in the following way:

$$X_1+X_2+X_3+X_4 \qquad (X_1-\kappa P_{L,1})+(X_2-\kappa P_{L,1})+(X_3+\kappa P_{L,1})+(X_4+\kappa P_{L,1}) \quad (3.71)$$

and

$$P_1 - P_2 + P_3 - P_4 \qquad (P_1 + \kappa P_{L,2}) - (P_2 - \kappa P_{L,2}) + (P_3 - \kappa P_{L,2}) - (P_4 + \kappa P_{L,2}) \quad (3.72)$$

Comparing now equations (3.67) and (3.68) to equations (3.71) and (3.72), respectively, one observes that our set-up reproduces precisely the required displacements. Now, if the output light is *not measured*, $\kappa P_{L,1}$ and $\kappa P_{L,2}$ remain *unknown*, i.e., become the aforementioned random Gaussian displacement with expectation value and variance that can be easily adjusted by choosing the input light with specific properties (vacuum squeezed, thermal *etc*). From now on we will denote these random variables by $\overline{P}_{L,1}$ $\overline{P}_{L,2}$. It should be emphasized that, since this procedure does not involve the final projective measurement, it cannot produce extra entanglement. Its only effect is introduction of randomness in the system, which makes the entanglement bound.

We switch to the covariance matrix formalism that allows us to get a better insight into the process and the properties of the final state. We begin directly with two EPR pairs with zero displacement and characterized by the squeezing parameter r, and a general light mode characterized by the variances: $\mathrm{Var}X_{L,1}$ $\mathrm{Var}P_{L,1}$ and zero displacement. The initial state of the set-up is thus described by:

$$\gamma_{1,\mathrm{in}} = \gamma_{\mathrm{EPR}_1} \oplus \gamma_{\mathrm{EPR}_2} \oplus \begin{pmatrix} 2\mathrm{Var}X_{L,1} & 0 \\ 0 & 2\mathrm{Var}P_{L,1} \end{pmatrix} \quad (3.73)$$

The interaction between the atomic ensembles and the light leads to the following CM for atoms

$$\gamma_{1,\mathrm{out}} = \begin{pmatrix} a_1 & 0 & c_1 & 0 & e_1 & 0 & e_1 & 0 \\ 0 & b & 0 & d & 0 & 0 & 0 & 0 \\ c_1 & 0 & a_1 & 0 & e_1 & 0 & e_1 & 0 \\ 0 & d & 0 & b & 0 & 0 & 0 & 0 \\ e_1 & 0 & e_1 & 0 & a_1 & 0 & c_1 & 0 \\ 0 & 0 & 0 & 0 & 0 & b & 0 & d \\ e_1 & 0 & e_1 & 0 & c_1 & 0 & a_1 & 0 \\ 0 & 0 & 0 & 0 & 0 & d & 0 & b \end{pmatrix} \quad (3.74)$$

with

$$a_1 = 2\kappa^2 \mathrm{Var}P_{L,1} + \mathrm{ch2r} \qquad b = \mathrm{ch2r} \qquad c_1 = 2\kappa^2 \mathrm{Var}P_{L,1} - \mathrm{sh2r}$$
$$d = \mathrm{sh2r} \qquad e_1 = -2\kappa^2 \mathrm{Var}P_{L,1}$$

Interaction with the second light beam characterized by variances $\mathrm{Var}X_{L,2}$ and $\mathrm{Var}P_{L,2}$, leads to the following CM:

$$\gamma_{2,\mathrm{out}} = \begin{pmatrix} a_1 & 0 & c_1 & 0 & e_1 & 0 & e_1 & 0 \\ 0 & a_2 & 0 & -c_2 & 0 & e_2 & 0 & -e_2 \\ c_1 & 0 & a_1 & 0 & e_1 & 0 & e_1 & 0 \\ 0 & -c_2 & 0 & a_2 & 0 & -e_2 & 0 & e_2 \\ e_1 & 0 & e_1 & 0 & a_1 & 0 & c_1 & 0 \\ 0 & e_2 & 0 & -e_2 & 0 & a_2 & 0 & -c_2 \\ e_1 & 0 & e_1 & 0 & c_1 & 0 & a_1 & 0 \\ 0 & -e_2 & 0 & e_2 & 0 & -c_2 & 0 & a_2 \end{pmatrix} \quad (3.75)$$

with

$$a_1 = 2\kappa^2 \mathrm{Var} P_{L,1} + \mathrm{ch2r} \qquad c_1 = 2\kappa^2 \mathrm{Var} P_{L,1} - \mathrm{sh2r} \qquad e_1 = -2\kappa^2 \mathrm{Var} P_{L,1}$$
$$a_2 = 2\kappa^2 \mathrm{Var} P_{L,2} + \mathrm{ch2r} \qquad c_2 = 2\kappa^2 \mathrm{Var} P_{L,2} - \mathrm{sh2r} \qquad e_2 = -2\kappa^2 \mathrm{Var} P_{L,2}$$

and the displacement of the final state is given by:

$$d_{2,\mathrm{out}} = \left(-\kappa \overline{P}_{L,1} \;\; \kappa \overline{P}_{L,2} \;\; -\kappa \overline{P}_{L,1} \;\; -\kappa \overline{P}_{L,2} \;\; \kappa \overline{P}_{L,1} \;\; -\kappa \overline{P}_{L,2} \;\; \kappa \overline{P}_{L,1} \;\; \kappa \overline{P}_{L,2}\right) \tag{3.76}$$

We verify separability of the obtained state using the PPT criterion and see that the state has the following properties:

1. It is PPT with respect to partition $12\ 34$ for any choice of $\kappa \;\; r \;\; \mathrm{Var} P_{L,1} \;\; \mathrm{Var} P_{L,2}$.

2. It is always NPT with respect to partition $13\ 24$.

3. The state is PPT with respect to partition $14\ 23$ only if

$$\kappa^2 \mathrm{Var} P_{L,1} \geq \frac{1}{8}\left(e^{2r} - e^{-2r}\right) \qquad \text{or} \qquad \kappa^2 \mathrm{Var} P_{L,2} \geq \frac{1}{8}\left(e^{2r} - e^{-2r}\right) \tag{3.77}$$

4. All the partitions one vs three modes are always NPT, in agreement with the results obtained in [Zhang 11].

By definition it is not possible to distil a maximally entangled state between two parties A_i and A_j belonging to some N-partite state if there exists a PPT bipartition of the N parties such that A_i and A_j belong to different sets [Dür 99, Dür 00]. We see that in the case of the CV Smolin state with parameters that fulfil condition (3.77) there exists a PPT bipartition of the state for *every* pair of modes. This indicates that no maximally entangled bipartite state can be distilled from it.

We mentioned at the beginning of the section that the bipartite entanglement of the Smolin state can be unlocked by means of a collective measurement performed by two of the parties. In the case of the discrete state this is true for any choice of parties, however, in the CV scenario only the entanglement between modes $1-2$ (equivalently $3-4$) can be straightforwardly unlocked. This is due to the lack of the permutational invariance. In what follows we demonstrate the unlocking protocol for pair $1-2$. It is not clear if an analogous procedure exists for for other bipartite splittings.

Unlocking protocol. — In order to show the unlockability of the obtained state, we write the CM and the DV in the basis in which the EPR states are diagonal, i.e., $R_{\mathrm{EPR}} = (1 \quad \overline{2})\,(X_1 + X_2 \qquad P_3 - P_4)$. For simplicity we also assume that $\mathrm{Var} X_{L,1} = \mathrm{Var} X_{L,2} = \mathrm{Var} X_L$ and $\mathrm{Var} P_{L,1} = \mathrm{Var} P_{L,2} = \mathrm{Var} P_L$. Then we have

$$\gamma_{\mathrm{S}} = \begin{pmatrix} e^{-2r}+f & 0 & 0 & 0 & -f & 0 & 0 & 0 \\ 0 & e^{2r} & 0 & 0 & 0 & 0 & 0 & 0 \\ 0 & 0 & e^{2r} & 0 & 0 & 0 & 0 & 0 \\ 0 & 0 & 0 & e^{-2r}+f & 0 & 0 & 0 & -f \\ -f & 0 & 0 & 0 & e^{-2r}+f & 0 & 0 & 0 \\ 0 & 0 & 0 & 0 & 0 & e^{2r} & 0 & 0 \\ 0 & 0 & 0 & 0 & 0 & 0 & e^{2r} & 0 \\ 0 & 0 & 0 & -f & 0 & 0 & 0 & e^{-2r}+f \end{pmatrix} \tag{3.78}$$

with $f = 4\kappa^2 \mathrm{Var} P_L$, and

$$d_{\mathrm{S}} = \left(- \ \overline{2}\kappa \overline{P}_{L,1} \ 0 \ 0 \quad \overline{2}\kappa \overline{P}_{L,2} \quad \overline{2}\kappa \overline{P}_{L,1} \ 0 \ 0 \ - \ \overline{2}\kappa \overline{P}_{L,2} \right) \tag{3.79}$$

Now inspection of equations (3.78) and (3.79) shows clearly that we have two correlated EPR pairs displaced by random vectors pointing in the opposite directions in the phase space of the squeezed variables, exactly as depicted in figure 3.17. Since we do not know where in the phase space are the EPR pairs, we cannot use them for quantum tasks. Therefore, by analogy to the discrete case [Smolin 01, Augusiak 06], unlocking of entanglement is understood as learning which of the displaced EPR pairs is shared by pair $1-2$ by measuring the displacement of the other EPR pair shared by $3-4$.

The unlocking protocol for the Smolin state can be performed within the operations available in the QND-Faraday atom-light interface. We will demonstrate all the steps of the procedure, i.e., the measurement of the displacement of $X_3 + X_4$ and $P_3 - P_4$ using the CM formalism. This can be done in a quantum non-demolition way with two probe light beams (each with quadratures $X_P^{(i)} \ P_P^{(i)}$, $i = 1 \ 2$) with reduced uctuations in $X_P^{(i)}$, i.e., such that $\mathrm{Var} X_P^{(i)} \leq 1 \ 2$ [Sørensen 98]. The probe beams pass through the samples $3-4$ at the angles

$$\left(\alpha_3^{(1)} \ \alpha_4^{(1)} \right) = \left(\frac{\pi}{2} \ \frac{\pi}{2} \right) \qquad \left(\alpha_3^{(2)} \ \alpha_4^{(2)} \right) = (0 \ \pi)$$

respectively, and $X_P^{(i)}$ is measured afterwards. If the measurement outcomes are $\tilde{x}_+$, $\tilde{p}_-$, the final state of modes $1-2$ is characterized by the following CM and DV (still in the EPR basis), where for simplicity we put $\mathrm{Var} X_P^{(1)} = \mathrm{Var} X_P^{(2)} = \mathrm{Var} X_P$:

$$\gamma_{12} = \begin{pmatrix} e^{-2r} + f(1 - g\kappa) & 0 & 0 & 0 \\ 0 & e^{2r} & 0 & 0 \\ 0 & 0 & e^{2r} & 0 \\ 0 & 0 & 0 & e^{-2r} + f(1 - g\kappa) \end{pmatrix} \tag{3.80}$$

and

$$d_{12} = (g p_- \ 0 \ 0 \ g x_+) \tag{3.81}$$

with

$$g = \frac{f \kappa e^{2r}}{\kappa^2 + e^{2r} \left(2 \mathrm{Var} X_P + f \kappa^2 \right)}$$

The smaller the variance of the probe beam $\mathrm{Var} X_P$ the better the precision of the measurement. In the limit $\mathrm{Var} X_P \quad 0$ [$\mathrm{Var} X_P = o\left(e^{-2r}\right)$] we obtain:

$$g\Big|_{\mathrm{Var} X_P \to 0} = \frac{f e^{2r}}{\kappa + f \kappa e^{2r}} = \frac{1}{\kappa} \frac{1}{e^{-2r} \ f + 1} \tag{3.82}$$

Remembering that f is constrained by equation (3.77) we see that for large initial squeezing r, the term converges to $1 \ \kappa$. Therefore, if the initial EPR pairs were entangled strongly enough, the outcomes $\tilde{x}_+ \ \tilde{p}_-$ obtained for the displacement of $X_3 + X_4$ and $P_3 - P_4$, respectively, approximate very well the displacement of $X_1 + X_2$ and $P_1 - P_2$. Otherwise, the displacement is still a function of known parameters. In comparison to the initial EPR state, the covariance matrix (3.80) has an additional positive term in diagonal elements, which makes the state less

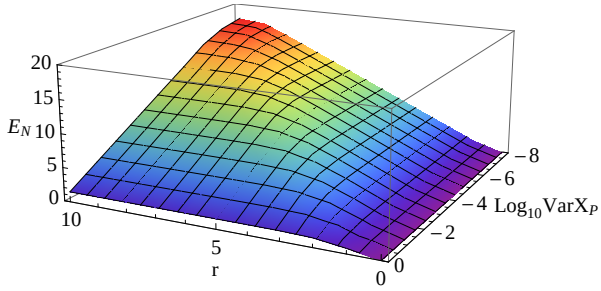

Figure 3.18: Negativity of the unlocked state (3.80) as a function of the squeezing parameter and the variance of the probe beam.

entangled and mixed. The above analysis shows that in the limit of high squeezing r and perfect measurement $1 - \kappa g$ vanishes recovering thus the initial EPR-like state. Nevertheless, we check that for admissible values of parameters the obtained state, even though not pure, is still distillable, which is equivalent to being NPT (see figure 3.18 where we plot the negativity of the unlocked state).

3.4 Conclusions

In this chapter, by exploiting the geometrical setting for the quantum atom-light interface we have demonstrated that atomic ensembles may successfully serve for quantum information processing in protocols that require multipartite entanglement of various types. Moreover, we have shown that slight modification of the typical setting provides an experimentally feasible scheme for generation of mixed states, broadening the applicability of atomic ensembles for quantum information studies.

The analysed set-ups admit the Gaussian continuous-variable description which enables a complete study of correlations between the ensembles and the light beam induced at each step of the considered protocols. Using the covariance matrix formalism, we have assessed the robustness of the multipartite set-ups against the atomic spin decay and the noisy input. We conclude that the atomic spin decay affects very little the generation of bipartite and multipartite entangled states with several ensembles, however may become problematic if more atomic samples are involved. We observe a particularly strong effect in the case of the linear cluster state. The in uence of the noisy input on the generation of entanglement is twofold. First, it affects the feasibility of experimental detection of entanglement through variance inequalities. Second, for sufficient amount of noise the generated state becomes undistillable.

Last but not least, we have studied the properties of continuous variable Smolin state. We have applied the covariance matrix criteria to shown its undistillability and analyse the unlocking protocol. Our results provide, to the best of our knowledge, the first experimentally feasible way to generate and unlock this bound entangled state in the Gaussian scenario.

Chapter 4

Multipartite correlations

Quantum non-local correlations and quantum entanglement are both resources of Quantum Information Theory (QIT) [Horodecki 09, Barrett 05b], however they cannot be considered equivalent [Brunner 05, Cerf 05, Acín 12b]. While the presence of entanglement is a necessary condition for non-locality of the measurement statistics of a state, the seminal work of Werner [Werner 89] proves that it is not a sufficient one. In order to show this, the author provided the first example of entangled states, the famous Werner states, for which any local projective measurement gives outcomes compatible with some classical model. Another striking fact showing the inequivalence of this two resources is that the most entangled states are at the same time *not* the most non-local ones according to all known measures of non-locality (see [Methot 07] and the references therein). For multipartite entanglement and multipartite non-local correlations the situation is even less clear, as the notion of maximally entangled state is not precise. Hence, it seems that presently the main goal of QIT is to distinguish which quantum features manifest themselves in quantum information protocols, identify the resources necessary to accomplish a given information tasks, and understand the interconversion rules between the quantum resources.

The notion of correlations detached from their particular physical origin plays the central role in device-independent quantum information processing [Barrett 05a, Acín 07, Pironio 10, Horodecki 10, Masanes 11, Colbeck 11]. In this paradigm, one concentrates on achieving an information task and not on the particulars of the devices used by the participants. In the most general scenario, schematically depicted in figure 4.1, we consider N non-communicating distant observers having access to N physical systems. Observer i ($i = 1 \quad N$) can perform on his system one of M_i possible measurements. His choice of the measurement is denoted by x_i, and the obtained result by a_i. Each measurement has a specified number of different outcomes d_{ix_i}. In the device-independent scenario each user has access to a black box, which upon input x_i returns output a_i. The correlations among the parties are described by the conditional probabilities $p(\mathbf{a}\ \mathbf{x})$, where we introduce a short notation $\mathbf{x} = (x_1 \quad x_n)$ and $\mathbf{a} = (a_1 \quad a_n)$. We will use the short and full notation interchangeably, depending which is more convenient.

The existence of correlations is an inherent property of composite physical systems and, as such, is fundamental to our understanding of physical phenomena. On the other hand, physical principles impose limits on the correlations between the results of measurements performed on distant systems. If the measurements correspond to space-like separated events,

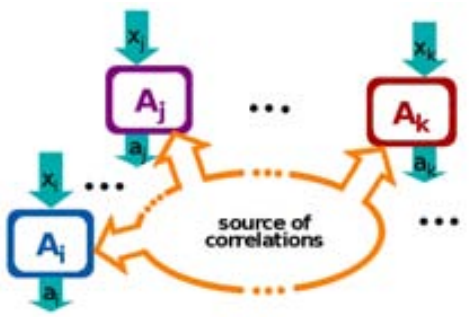

Figure 4.1: Schematic depiction of the most general multipartite scenario.

the observed correlations should obey *the principle of no signalling*, which prevents any instantaneous information transmission among the parties. Formally, this intuitive notion is expressed as follows

$$\begin{aligned} {}_{j\ x_j,x_j'}\sum_{a_j} P(a_1 \quad a_j \quad a_N\ x_1 \quad x_j \quad x_N) \\ = \sum_{a_j} P(a_1 \quad a_j \quad a_N\ x_1 \quad x_j' \quad x_N) \end{aligned} \tag{4.1}$$

which means that the marginal probability distribution obtained by tracing out the jth party is independent of the measurement choices $x_j\ x_j'$ of this party. And this must hold for every party j, and all choices of $\mathbf{a}\ \mathbf{x}$. The no-signalling condition in this form implies that the marginal probability for each subset of observers is independent of the measurement settings of the remaining parties.

Among all the non-signalling correlations there are those that can be achieved through local measurements of a global quantum state , *the quantum correlations* (QC). We write them as follows

$$P(a_1 \quad a_N\ x_1 \quad x_N) = \mathrm{tr}\left(\ M_{a_1}^{x_1} \otimes \quad \otimes M_{a_N}^{x_N}\right) \tag{4.2}$$

where $M_{a_1}^{x_1} \quad M_{a_N}^{x_N}$ are generalized local measurements[1]. Interestingly, what distinguishes the quantum correlations among the general non-signalling correlations (NC) is an axiom telling us how to reconstruct the outcome probabilities. So far, we are not able to tell what physical principle limits the strength of quantum correlations, except in the bipartite case [Barnum 10, Acín 10].

Finally, the observed correlations are said to be *classical* (or local) if they are attainable with shared classical randomness, i.e., reproduced by a local hidden-variable model. The corresponding conditional probabilities can be always written as

$$P(a_1 \quad a_N\ x_1 \quad x_N) = \sum_{\lambda} P(\lambda) P(a_1\ x_1\ \lambda) \quad P(a_N\ x_N\ \lambda) \tag{4.3}$$

where λ is a local variable (or a set of local variables) common to all parties distributed among them with probability $P(\lambda)$ and correlating the outcomes of their measurements.

[1] Generalized positive semi-definite operators on a local Hilbert space such that $\sum_{a_i} M_{a_i}^{x_i} = \mathbf{1}$ $(i = 1, \ldots, N)$.

It was John Bell who first pointed out that classical correlations (CC) are constrained by certain inequalities (the famous Bell inequalities) [Bell 64]. Correlations which violate a Bell inequality, and thus do not correspond to any classical model, are known as non-local (as opposed to classical/local correlations). Bell s theorem guarantees the existence of quantum correlations that are non-local. However, as shown by Popescu and Rohlich [Popescu 94], there exist non-local correlations which fulfil the no-signalling condition but are not quantum (they are called supra-quantum). All this results contribute to our current understanding of the hierarchy of correlations.

The three kinds of correlations correspond to sets of probabilities of measurement outcomes and, as such, form convex sets, represented schematically in Fig. 4.2. From equation (4.3) we infer that the set of classical correlations is a polytope with vertices corresponding to local deterministic strategies $P(a_1 \quad a_N\ x_1 \quad x_N) = P(a_1\ x_1) \quad P(a_N\ x_N)$, where the local conditional probabilities can be either 0 or 1. This polytope is strictly smaller than the set of quantum correlations which itself is not a polytope. The quantum set, in turn, is a proper subset of the set of all non-signalling probabilities. The latter is fully characterized by linear conditions: (i) equation (4.1), (ii) normalization and positivity of all conditional probabilities $P(\mathbf{a}\ \mathbf{x})$, and therefore forms a polytope.

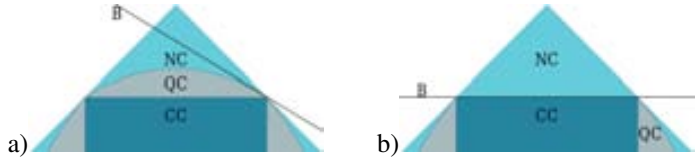

Figure 4.2: Schematically depicted sets of classical, quantum and non-signalling correlations. Tight Bell inequalities correspond to facets of the classical set. $\mathcal{B}$ denotes a Bell inequality with no quantum violation which is a) not tight, b) tight. Note that a tight Bell inequality guarantees that a region in which quantum and classical correlations coincide is a facet. A non-tight inequality may define a common region of the classical and quantum sets that does not have maximal dimension.

In order to distinguish between the different types of correlations one designs a family of Bell tests for a specific scenario (number of parties, measurements and outcomes). It takes the form of an inequality for linear combinations of conditional probabilities:

$$\sum_{\mathbf{x},\mathbf{a}} T_{\mathbf{x},\mathbf{a}} P(\mathbf{a}\ \mathbf{x}) \leqslant \beta_C \tag{4.4}$$

where $T_{\mathbf{x},\mathbf{a}}$ is a $2N$-index matrix of coefficients and β_C is the maximum value of the left-hand side attainable with any local model. Analogously, for QC and NC we obtain bounds $\beta_Q \ \beta_N$. Such inequalities constrain the respective sets of correlations. They are *non-trivial* if the bounds do not coincide with general non-signalling correlations, i.e., , $\beta_{\mathrm{N}} > \beta_{\mathrm{C}}$. A Bell inequality (with bound β_C) is called *tight* if it corresponds to a facet[1] of a classical set (see figure 4.2). Hence, we need a finite number of tight bell inequalities to fully characterize the polytope of CC. Since, as we said before, the quantum set has a more complicated structure, its full characterization requires an infinite number of Bell tests (with a quantum bound β_Q).

[1] A facet is a face of a polytope P with dimension $\dim P - 1$.

Apart from its fundamental importance, understanding the relations among the sets of correlations is crucial from a practical point of view, since correlations find application as an information resource. In particular, one of the goals of quantum information theory is to understand when QC give an advantage over CC. For instance, non-local QC provide cryptographic security not achievable with classical theory [Ekert 91, Barrett 05a, Acín 07, Masanes 11]. They can also be used to certify the presence of randomness [Pironio 10, Colbeck 11] and outperform CC at communication complexity problems [Brukner 04, Buhrman 10].

While QC are in general more powerful than CC, there are some intriguing situations in which CC and QC perform equally well. This equivalence can be detected by Bell inequalities which are not violated by QC, i.e., for them $\beta_C = \beta_Q < \beta_N$. Of particular interest are tight inequalities with this property since they guarantee that the classical and quantum correlations coincide in a non-trivial region, i.e., share a facet of the classical polytope as depicted in figure 4.2b. The first examples of such inequalities were given in [Linden 07] for two parties. Unfortunately, none of these is tight [Almeida]. The first example of tight multipartite Bell inequalities with no quantum violation was provided later in [Almeida 10, Acín 12a] (see also [Augusiak 12]).

In [Augusiak 11] we provided a general construction of Bell inequalities that cannot be violated by quantum mechanics and demonstrate an *a priori* unexpected link between such inequalities and Unextendible Product Bases (UPBs) [Bennett 99b], which is an important notion in the theory of bound entanglement. Our construction covers some of the inequalities previously derived in [Almeida 10] which indicates that it can lead to tight Bell inequalities (*cf.* [Augusiak 12].

4.1 Preliminaries

4.1.1 Basic properties of Bell polytopes

In the introduction we have mentioned that all possible conditional probabilities for a given scenario form a convex set. Here I am going to give a more detailed description of these sets discussing, in particular, the dimensions of the sets of correlations (CC, QC and NC) and the notion of tightness. In general, full characterization of the set of non-signalling correlations is a hard task and was solved only for various bipartite scenarios [Fine 82, Khalfin 85, Pitowsky 01, Śliwa 03, Werner 01a, Barrett 05b] and the simplest tripartite case [Pironio 11]. The notation used is based on the work [Pironio 05].

Each scenario is characterized by a number of parties, possible measurements and outcomes, which we denote by a triple $(N\ \mathbf{M}\ \mathbf{d})$. The number of measurements may be different for each party, which is expressed as $\mathbf{M} = (M_1 \quad M_N)$, and each measurement may yield different number of possible outcomes specified by $\mathbf{d} = [(d_{11} \quad d_{1M_1})$ $(d_{N1} \quad d_{NM_N})]$. We are going to use short notation for situations in which the number of measurements per site or outcomes per measurement is the same. For instance the scenario with $M_1 = \quad = M_N = 2$ will be denoted by $(N\ 2\ \mathbf{d})$ and the scenario in which each observable has three outcomes will be $(N\ \mathbf{M}\ 3)$. Now the number of all possible conditional probabilities within a given scenario is equal to

$$t = \prod_{i=1}^{N} \left(\sum_{j=1}^{M_i} d_{ij} \right) \tag{4.5}$$

and is defining the dimension of the real space $\mathbb{R}^t$ in which the convex sets of correlations are built.

We lower the dimension of the considered structures by imposing the following equality conditions: the normalization of probabilities and the non-signalling defined in equation (4.1). Note that the former implies that we are not going to deal with a subspace of $\mathbb{R}^t$, but rather with an affine space[1], since the zero vector is excluded. The dimension[2] of this affine set is

$$D = \prod_{i=1}^{N} \left(\sum_{j=1}^{M_i} (d_{ij} - 1) + 1 \right) - 1 \tag{4.6}$$

Now in such defined affine space, the polytope of all non-signalling correlations is constrained by the inequality conditions: the positivity of all conditional probabilities. It is said that the inequalities *support* its facets. This is the region of all correlations fulfilling the no-signalling constraint.

The region of local correlations, called a Bell polytope, defined in equation (4.3) is strictly smaller than the polytope of all non-signalling correlations, however it has the same affine dimension. It is fully characterized by a finite set of inequalities of type (4.4) supporting its facets, themselves affine sets of dimension $D - 1$. There are, however, two kinds of facets delimiting the polytope. The first kind are given by trivial Bell tests and overlap with the facets of the non-signalling polytope. The second type, are the proper tight Bell inequalities which can be violated by non-local correlations. In order to identify a tight Bell test one needs to check that among the probabilities that saturate the inequality there are exactly D affinely independent points corresponding to extreme product probabilities.

$$P(\mathbf{a}\ \mathbf{x}) = P(a_1\ x_1) \qquad P(a_N\ x_N) = \delta_{a_1,\tilde{a}_1(x_1)} \qquad \delta_{a_N,\tilde{a}_N(x_N)} \tag{4.7}$$

where $\tilde{\mathbf{a}}(\mathbf{x})$ is a fixed choice of predetermined outcomes.

4.1.2 Gleason s theorem

Gleason s theorem is a seminal result at the foundations of quantum mechanics. It implies that having a complete set of measurement operators $M_a^x\ {}_{x=1}^{k}$ on a Hilbert space $\mathcal{H}$ ($k \leqslant \dim \mathcal{H}$) and assuming that (i) the probability of each outcome is non-negative and (ii) sum of all these probabilities equals one, we recover the Born rule for quantum probabilities $p(a\ x) = \mathrm{tr}\ M_a^x$, where is a density matrix.

The generalization of this result to multipartite composite systems was studied in [Wallach 02]. In this scenario, except for natural extension of the positivity and normalization conditions (i) and (ii), an additional requirement must be fulfilled, i.e., (iii) the no-signalling principle defined in (4.1). It turns out that in the multipartite scenario all the probabilities fulfilling constraints (i)–(iii) are recovered through the following trace formula

$$p(\mathbf{a}\ \mathbf{x}) = \mathrm{tr}(\mathcal{W} M_{a_1}^{x_1} \otimes \qquad \otimes M_{a_N}^{x_N}) \tag{4.8}$$

[1] A set S is an affine space in $\mathbb{R}^n$ if for any points $v_1, \ldots, v_k \in S$ ($k > 0$) and for any scalars $\lambda_1, \ldots, \lambda_k \in \mathbb{R}$ satisfying $\sum_{i=1}^{k} \lambda_i = 1$, the point $v = \sum_{i=1}^{k} \lambda_k v_k$ belongs to S.

[2] We say that the points $v_1, \ldots, v_k$ in $\mathbb{R}^n$ are affinely independent if the unique solution to $\sum_{i=1}^{k} \lambda_i v_i = 0 \& \sum_{i=1}^{k} \lambda_i = 0$ is $\lambda_1 = \ldots = \lambda_k = 0$. The *dimension* of an affine set is one less than the maximum number of affinely independent points it contains.

where $\mathcal{W}$ is a Hermitian operator fulfilling for all product vectors Ψ: $\Psi\,\mathcal{W}\,\Psi \;\geqslant 0$ and $\mathrm{tr}\mathcal{W} = 1$. We see immediately that this coincides with the definition of a normalized *entanglement witness*. As the set of entanglement witnesses is strictly larger then the set of density matrices, there must exist probability distributions which cannot be reproduced from quantum states, but fulfilling conditions (i)–(iii). A single exception is the bipartite scenario for which it was shown that for every bipartite witness there exists a quantum state giving the same correlations [Barnum 10, Acín 10]. Nevertheless, for more than two parties there always exist witnesses giving correlations not compatible with quantum mechanics [Almeida 10, Augusiak 11].

Consequently, as mentioned in the previous section, for truly multipartite correlations, the three principles are not sufficient to distinguish the quantum set and we still await formulation of a physical principle which would complement conditions (i)-(iii) and single out quantum mechanics from the more general non-signalling model.

4.1.3 Unextendible Product Bases

The fundamental physical importance of Unextendible Product Bases (UPBs) [Bennett 99b] stems from the fact that they lay at the heart of the first systematic procedure for the construction of bound (i.e., undistillable) entangled states——being one of the most intriguing concepts in quantum information theory [Horodecki 98]. By definition a UPB in a composite Hilbert space $\mathcal{H}$ is a set of orthogonal *product* vectors with the property that the complementary (non-zero) subspace *does not* contain any product states. We will denote this set by $\mathcal{S}_{\mathrm{UPB}}$.

The bound entangled state constructed from a UPB is supported on the complementary subspace, i.e.,

$$\rho_{\mathrm{BE}} = \frac{1}{\dim(\mathcal{H}) - \;\mathcal{S}_{\mathrm{UPB}}}\,(\mathbf{1}_{\mathcal{H}} - \Pi_{\mathrm{UPB}}) \tag{4.9}$$

where Π_{UPB} is a projector on S_{UPB} and $\mathcal{S}_{\mathrm{UPB}}$ denotes the number of vectors in the set. Clearly, the state is entangled, since by definition the subspace $\mathbf{1} - \Pi_{\mathrm{UPB}}$ does not contain any product states. In order to verify that ρ_{BE} is undistillable, one needs to check that it remains positive under partial transposition (PT) with respect to any bipartite cut. This is straightforward since all vectors from $\mathcal{S}_{\mathrm{UPB}}$ transform under PT to orthogonal product vectors and $\mathbf{1}$ is PT-invariant. It is easy to construct an entanglement witness for this class of states and we provide it here since we are going to use it in the next section

$$\mathcal{W} = \frac{1}{\mathcal{S}_{\mathrm{UPB}} \;- \epsilon\dim(\mathcal{H})}\,(\Pi_{\mathrm{UPB}} - \epsilon\mathbf{1}) \tag{4.10}$$

with $\epsilon = \min_{\psi_{\mathrm{prod}}} {}_{\mathrm{prod}}\,\Pi_{\mathrm{UPB}}\;{}_{\mathrm{prod}}$ [Lewenstein 01].

Another interesting property of UPBs is the impossibility to distinguish the states from this set through local measurements and classical communication. The phenomenon is called non-locality without entanglement and was first studied by Bennett [Bennett 99a]. As we will see in the next section the properties of UPBs can be translated to correlations leading to uncompletable sets of orthogonal conditional probabilities.

4.2 From Unextendible Product Bases to Bell inequalities

We start the construction for general sets of product vectors and only later restrict our attention to UPBs. Consider an N-partite composite Hilbert space $\mathcal{H} = \bigotimes_{i=1}^{N} \mathbb{C}^{d_i}$ and a set $\mathcal{S}$ of orthogonal product vectors from $\mathcal{H}$: $\mathcal{S} =$ $\begin{matrix}(1)\\ j\end{matrix} \otimes \cdots \otimes \begin{matrix}(N)\\ j\end{matrix}$ $_{j=1}^{|\mathcal{S}|}$ with $\begin{matrix}(i)\\ j\end{matrix}$ $\mathbb{C}^{d_i}$. We group the $\mathcal{S}$ local states belonging to each party to N local sets, each denoted by $\mathcal{S}^{(i)}$. In the next step we further partition each $\mathcal{S}^{(i)}$ into disjoint subsets $\mathcal{S}_k^{(i)}$ ($k = 1 \ldots$) containing mutually orthogonal vectors (we remove repeating elements); the range of k depends on the specific choice of $\mathcal{S}$. In order to remove the ambiguity in splitting the local sets $\mathcal{S}^{(i)}$ into subsets, we restrict ourselves to sets $\mathcal{S}$ having the property that *no two vectors belonging to different subsets $\mathcal{S}_k^{(i)}$ are orthogonal.* Henceforth, we refer to this property as (P). Next, we label all vectors within sets $\mathcal{S}_k^{(i)}$ with numbers from the set $\left\{1 \ldots \left|\mathcal{S}_k^{(i)}\right|\right\}$.

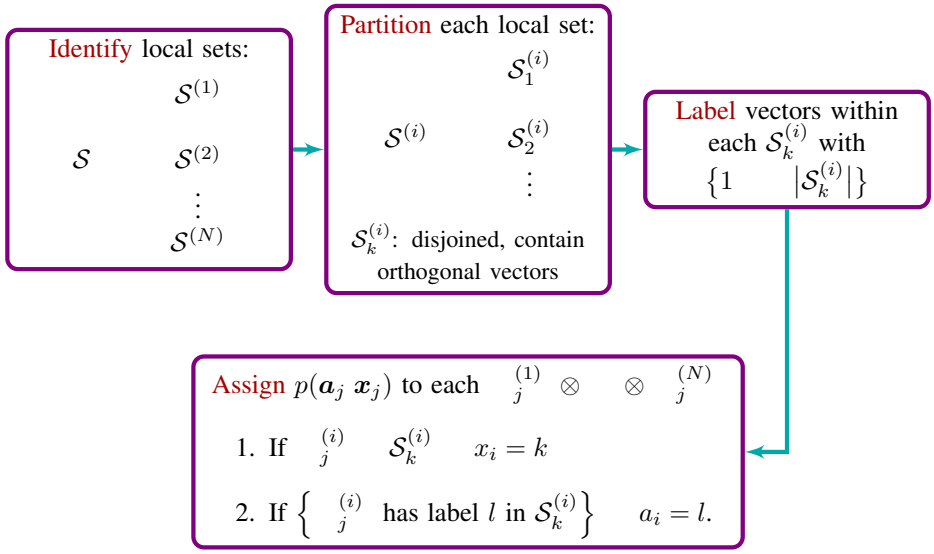

Figure 4.3: Construction of conditional probabilities from set of product vectors with property (P).

We make $\mathcal{S}_k^{(i)}$ define a measurement (input), while the different vectors within every such subset are associated to the measurement outcomes (output). Now, in order to assign to each vector $\begin{matrix}(1)\\ j\end{matrix} \otimes \cdots \otimes \begin{matrix}(N)\\ j\end{matrix}$ from $\mathcal{S}$ a sequence of inputs and outputs for conditional probability $p(\boldsymbol{a}_j\ \boldsymbol{x}_j)$ we do the following for each i: identify the set $\mathcal{S}_k^{(i)}$ to which $\begin{matrix}(i)\\ j\end{matrix}$ belongs and put $x_i = k$; identify the label given to $\begin{matrix}(i)\\ j\end{matrix}$ and substitute it for a_i. The scheme is summarized in figure 4.3. In this way we obtain a set of orthogonal probabilities. Indeed, due to (P), orthogonality of any two vectors from $\mathcal{S}$ means that at some position they have different vectors from the same local subset. At the level of probabilities, this means that if one of them, say $p(\mathbf{a}_j\ \mathbf{x}_j)$, equals unity, the rest have to be zero, as they always have at some position the same input but a different output.

We now consider linear combinations of the conditional probabilities with such defined

$\mathbf{a}_j$ and $\mathbf{x}_j$ and weights q_j

$$\sum_{j=1}^{|\mathcal{S}|} q_j p(\mathbf{a}_j\ \mathbf{x}_j) \leq \beta_C \tag{4.11}$$

This expression constitutes a Bell test, hence we write a classical bound β_C that we now derive. In order to find the maximum of such a linear combination over all local strategies it is enough to consider the deterministic scenarios, i.e., $p(\mathbf{a}_j\ \mathbf{x}_j) = p(a_j^{(1)}\ x_j^{(1)}) \quad p(a_j^{(N)}\ x_j^{(N)})$. Due to the local orthogonality of the probabilities, if we choose one of $p(\mathbf{a}_j\ \mathbf{x}_j)$ equal 1, all the others are immediately zero. Therefore, the maximum of such a linear combination over all local strategies corresponds to assigning 1 to probability with the maximal coefficient q_j, i.e., $\beta_C = \max\ q_j$.

We will now prove that the maximum value achievable within quantum mechanics is the same, as the classical bound, i.e., that the inequality is not violated by quantum correlations.

Fact 1. Let $\mathcal{S}$ be a set of orthogonal product vectors possessing the property (P). Then for the corresponding Bell inequality (4.11) it holds that $\beta_C = \beta_Q = \max\ q_j$.

Proof. Finding the maximum value attained by (4.11) for quantum correlations consists in finding the maximal eigenvalue of the corresponding Bell operator. The latter is constructed from measurement operators $M_{a_i}^{x_i}$ and for a general Bell inequality (4.4) takes form:

$$\mathcal{B} = \sum_{\mathbf{x},\mathbf{a}} T_{\mathbf{x},\mathbf{a}} M_{a_1}^{x_1} \otimes \quad M_{a_N}^{x_N} \tag{4.12}$$

where we sum over all possible configurations $\mathbf{x}\ \mathbf{a}$, however some of the weights $T_{\mathbf{x},\mathbf{a}}$ may equal zero. Since the dimension of a Hilbert space is arbitrary, we can restrict the analysis to projective measurements.

Let us assign projectors $P_j^{(i)}$ (we enumerate them in the same way as the vectors $_j^{(i)}$) to the outcomes of the local observables, and construct the Bell operator

$$\mathcal{B}_{\mathcal{S}} = \sum_{j=1}^{|\mathcal{S}|} q_j \bigotimes_{i=1}^{N} P_j^{(i)} \tag{4.13}$$

In general, $P_j^{(i)}$ can be multidimensional projectors, nevertheless, they must inherit the local orthogonality properties of the vectors from $\mathcal{S}$, encoded in the input and the output of conditional probabilities. Precisely, any pair of projectors $\bigotimes_{i=1}^{n} P_j^{(i)}$ have at some position local projectors corresponding to the same observable but different outcomes, meaning that all of them are orthogonal. Thus the maximal eigenvalue of $\mathcal{B}_{\mathcal{S}}$ is $\max\ q_j$, and $\beta_Q = \beta_C = \max\ q_j$. ■

Our construction offers a systematic and easy way of generating Bell inequalities with no quantum violation from sets of orthogonal product vectors. However, it could be the case that all the derived inequalities are trivial, in the sense that they are not violated by any non-signalling correlations. This is where the concept of UPB becomes relevant. To show it we prove the following fact

Fact 2. *If $\mathcal{S} = \mathcal{S}_{\mathrm{UPB}}$ is a UPB with the property (P), the resulting Bell inequality (4.11) with $_j q_j = 1$ is violated by non-signalling correlations.*

Proof. The multipartite Gleason theorem ensures that every probability of outcome measurements for a composite system fulfilling the no-signalling condition can be obtained through trace formula (4.8). Consequently, to prove the violation of (4.11) by general non-signalling correlations it is enough to find a Bell operator and a normalized entanglement witness such that $\mathrm{tr}\mathcal{W}\mathcal{B}_{\mathcal{S}} > 1$. We will show that in the case when $\mathcal{S}$ is a UPB, the witness given in equation (4.10) gives rise to correlations violating the corresponding Bell inequality.

Let Π_{UPB} be a projector onto the subspace of $\mathcal{H}$ spanned by $\mathcal{S}_{\mathrm{UPB}}$. Then, the simplest Bell operator $\mathcal{B}_{\mathcal{S}}$ with all $q_j = 1$ and the measurements defined by projectors on vectors from local sets $\mathcal{S}_{(i)}$ is exactly Π_{UPB}. We consider now the normalized entanglement witness (4.10) and compute its trace with our Bell operator

$$\begin{aligned}\mathrm{tr}\mathcal{W}\mathcal{B}_{\mathcal{S}} &= \mathrm{tr}\mathcal{W}\Pi_{UPB} \\ &= -\mathrm{tr}\mathcal{W}(\mathbf{1} - \Pi_{UPB}) + \mathrm{tr}\mathcal{W}\mathbf{1} \\ &= -(\dim(\mathcal{H}) - \ \mathcal{S}_{UPB}\ )\mathrm{tr}\mathcal{W}\rho_{BE} + 1 \\ &> 1 \end{aligned} \tag{4.14}$$

In the third line we use the normalization of the entanglement witness and the definition of the bound entangled state ρ_{BE} associated with UPB [see equation (4.9)]. Since the state is detected by the witness, we have $\mathrm{tr}\mathcal{W}\rho_{\mathrm{BE}} < 0$ and the first term becomes positive giving rise to violation of the bound $\beta_C = 1$. ■

The converse statement was proven in [Augusiak 12], where it was shown that for sets $\mathcal{S}$ completable to a full product basis in $\mathcal{H}$ the corresponding Bell inequality is trivial, i.e., never violated.

Our construction, shows how to derive non-trivial Bell inequalities with no quantum violation from any UPB with property (P). Any Bell inequality can also be seen as a non-local game, in which the parties are given the input $\mathbf{x}$ and have to produce the output $\mathbf{a}$, in a distributed manner, all the possibilities being weighted by the tensor $T_{\mathbf{x},\mathbf{a}}$. The maximum values of the inequalities give the optimal winning probability for the different sets of correlations. One can, therefore, view our results as a general construction of non-local games for which access to quantum correlations does not provide any advantage.

Examples. — Let us illustrate the construction with several examples. For two parties there does not exists any UPB with property (P) as otherwise there would exist a bipartite witness violating a Bell inequality beyond the quantum bound, contradicting the results of [Barnum 10, Acín 10] (see discussion in section 4.1.2).

Moving to three parties we have one class of UPBs for qubits with representative set called Shifts UPB [DiVincenzo 03]

$$\mathcal{S}_3 = \quad 000 \quad 1e_2^{\perp}e_3 \quad e_1 1 e_3^{\perp} \quad e_1^{\perp}e_2 1 \tag{4.15}$$

where $e_i \ = \ 0 \quad 1$ and $e_i^{\perp}\ e_i \quad = 0$ $(i = 1\ 2\ 3)$. As it was shown in [Bravyi 04] all other three-qubit UPBs can be brought to this one by local unitary operations and permutations of particles.

Following the algorithm summarized in figure 4.3, at each site we identify the following vectors $\mathcal{S}^{(i)} = \quad 0 \quad 1 \quad e_i \quad e_i^{\perp} \quad$. Now we see that each set $\mathcal{S}^{(i)}$ can be partitioned to two subsets of mutually orthogonal vectors, namely $\mathcal{S}_1^{(i)} = \quad 0 \quad 1 \quad$ and $\mathcal{S}_2^{(i)} = \quad e_i \quad e_i^{\perp} \quad$. We label vectors 0 and e_i with 1 and 1 and $e_i^{\perp}$ with 2. Then, following the recipe, we

assign to each element in $\mathcal{S}_3$ the following probabilities:

$$000 \qquad p(111\ 111) \tag{4.16a}$$
$$1e_2^{\perp}e_3 \qquad p(221\ 122) \tag{4.16b}$$
$$e_1 1 e_3^{\perp} \qquad p(122\ 212) \tag{4.16c}$$
$$e_1^{\perp}e_2 1 \qquad p(212\ 221) \tag{4.16d}$$

Summing them up, we obtain the inequality

$$p(111\ 111) + p(221\ 122) + p(122\ 212) + p(212\ 221) \leq 1 \tag{4.17}$$

which corresponds to the three-partite non-local game called Guess Your Neighbours Input (GYNI)[1] studied in reference [Almeida 10]. We know it is *tight* [Śliwa 03], which confirms that the construction indeed can produce tight Bell tests.

However, we know that not all UPBs can be associated to tight Bell inequalities. We tested our construction on several examples known from the literature. In [DiVincenzo 03] the Shifts UPB were generalized to arbitrary odd number of qubits (GenShifts). We have checked that the corresponding inequality for $n = 5$ is not tight. It also does not correspond any more to the GYNI game. Moving to dimensions larger than two, we have examples of UPB given in [Niset 06]. We verified the tightness of the inequalities obtained from the four-partite qutrit UPB and got a negative result. Therefore, additional conditions are required to conclude that a Bell test derived from a UPB is tight.

4.3 From Bell inequalities to Unextendible Product Bases

Clearly, the above procedure can be reversed: given a Bell inequality (4.11) with locally orthogonal probabilities, one can derive, following analogous rules, a set of product vectors. The number of different inputs x_i at each position gives the number of different local subsets for each party, while the number of different outputs a_i for a particular input x_i corresponds to the number of elements in the subset. The maximal number of different outputs at the ith position gives the dimension of the local Hilbert space d_i. Note that in the general case, i.e., for general Bell tests, the derived vectors need not be orthogonal. It is the local orthogonality of the conditional probabilities that ensures the success of the procedure.

In what follows, we consider the set of GYNI Bell inequalities with no quantum violation [Almeida 10] for arbitrary number of parties. Remarkably, as we will see shortly, one can derive from it a new class of UPBs. We consider odd and even number of parties separately. The explicit form of these inequalities for odd N reads

$$p(\mathbf{1}\ \mathbf{1}) + \sum_{k=1}^{(N-1)/2} \sum_{i_1<\ldots<i_{2k}=1}^{N} D_{i_1\ldots i_{2k}} p(\mathbf{1}\ \mathbf{1}) \leq 1 \tag{4.18}$$

where $\mathbf{1} = (1 \qquad 1)$ and $D_{i_1,\ldots,i_n}$ ips (1 2) the inputs and outputs at positions $i_1 \qquad i_n$ and $i_1 - 1 \qquad i_n - 1$, respectively (if $i_j = 1$ then $i_j - 1 = N$). For even N the structure is

[1] Note that for each probability the output $\mathbf{a}$ is equal to the left-shifted input $\mathbf{x}$, hence the name of the game: Guess Your Neighbour s Input.

slightly more complicated, but the principle is the same. We have

$$p(\mathbf{1}\ \mathbf{1}) + p(1 \quad 12\ 21 \quad 1) + \sum_{k=1}^{(N-2)/2} \sum_{i_1<\ldots<i_{2k}=2}^{N} D_{i_1\ldots i_{2k}}[p(\mathbf{1}\ \mathbf{1}) + p(1 \quad 12\ 21 \quad 1)] \leq 1 \tag{4.19}$$

We now derive the product vectors corresponding to the configurations of inputs and outputs appearing in the inequality. Note that in the GYNI inequalities there are always two different inputs and outputs for each party. Therefore we obtain N-qubit product vectors with two different local bases per party. Without any loss of generality, we can take the bases to be equal for all sites; say $\mathcal{S}_1^{(i)} = \ 0 \quad 1\ $ and $\mathcal{S}_2^{(i)} = \ e \quad e^{\perp}\ $ with $e = 0 \quad 1$.

To write the vectors in a concise way we define a unitary operation V, which changes the local basis from $\mathcal{S}_1^{(i)}$ to $\mathcal{S}_2^{(i)}$

$$V = e\ 0 + e^{\perp}\ 1 \tag{4.20}$$

We associate the in-out sequence $(\mathbf{1}\ \mathbf{1})$ with vector $0\ ^{\otimes N}$, while $(1 \quad 12\ 21 \quad 1)$ becomes $e\ \ 0\ ^{\otimes N-2}\ 1\ = V_1\sigma_N\ 0\ ^{\otimes N}$. In the latter we apply V to the first subsystem, and the qubit ip σ to the last one. We observe that each shift operator $D_{i_1,\ldots,i_n}$ can be translated to qubits with the help of σ and V in the following manner

$$D_{i_1,\ldots,i_n} \quad V_{i_1} \quad V_{i_n}\sigma_{i_1-1} \quad \sigma_{i_n-1} \tag{4.21}$$

Then, the 2^{N-1} product vectors derived from (4.18) can be written as

$$0\ ^{\otimes N} \tag{4.22a}$$

$$V_{i_1} \quad V_{i_k}\sigma_{i_1-1} \quad \sigma_{i_k-1}\ 0\ ^{\otimes N} \tag{4.22b}$$

$$i_1 < \quad < i_k = 1 \quad N \quad k = 2\ 4 \quad N-1$$

while those corresponding to even number of parties (4.19) are

$$0\ ^{\otimes N} \tag{4.23a}$$

$$V_1\sigma_N\ 0\ ^{\otimes N} \tag{4.23b}$$

$$V_{i_1} \quad V_{i_k}\sigma_{i_1-1} \quad \sigma_{i_k-1}\ 0\ ^{\otimes N} \tag{4.23c}$$

$$V_1V_{i_1} \quad V_{i_k}\sigma_{i_1-1} \quad \sigma_{i_k-1}\sigma_N\ 0\ ^{\otimes N} \tag{4.23d}$$

$$i_1 < \quad < i_k = 2 \quad N \quad k = 2\ 4 \quad N-2$$

We have constructed sets of product vectors, however we still need to demonstrate that they are orthogonal to each other for each N and that there does not exist any other product vector orthogonal to all of them. Therefore, we prove the following fact:

Fact 3. The vectors (4.22) and (4.23), form N-qubit UPBs.

Proof. The proof consists of two steps. First we show that for any N, the above vectors can be generated from the Shifts UPB by a recursive protocol. Then we prove that this protocol preserves the property of being a UPB.

Let us start with the case of odd N. We denote the set of vectors in equation (4.22) by U_1 and divide it into two subsets $U_1^{(j)}$ $(j = 1\ 2)$ consisting of vectors with the first qubit

from $\mathcal{S}_j^{(1)}$. Then, we create another group of vectors $U_2^{(j)}$ by ipping the last qubit of $U_1^{(j)}$ to the orthogonal one (this action will be referred to as *orthogonalization*), we also define $U_2 = U_2^{(1)} \quad U_2^{(2)}$. Finally, direct algebra shows that the following set of vectors

$$\left\{ 0 \otimes U_1^{(1)} \quad 1 \otimes U_2^{(2)} \quad e \otimes U_2^{(1)} \quad e^{\perp} \otimes U_1^{(2)} \right\} \tag{4.24}$$

is exactly the same as the vectors in (4.23) with $N+1$ parties.

Almost exactly the same procedure produces $(N+1)$-partite vectors (4.22) from N-partite set with even N. The only difference is that to obtain U_2 from U_1 one has to orthogonalize the last but one qubit and apply the transformation $0 \quad e^{\perp}$ and $1 \quad e$ to the last one. Starting with three-qubits Shifts UPB, we can now generate recursively any of the sets of vectors (4.22) and (4.23). We demonstrate the first two steps in the diagram below. In what follows we show that the algorithm preserves the UPB property.

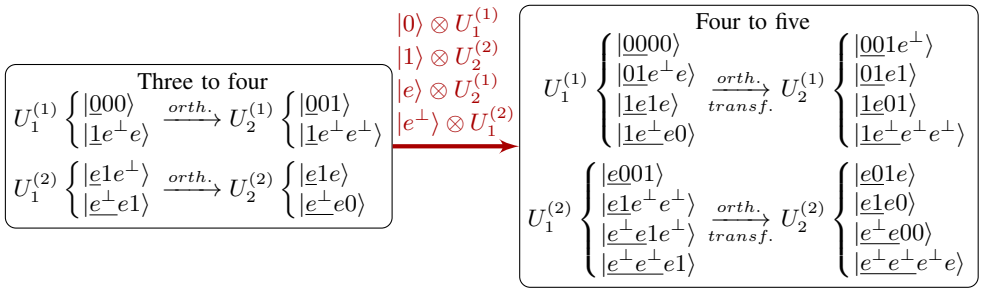

First, we prove that all the vectors (4.24) are orthogonal. For odd number of parties it suffices to demonstrate that vectors from $U_1^{(1)}$ and $U_2^{(1)}$ are orthogonal and that the same holds for $U_1^{(2)}$ and $U_2^{(2)}$ (notice that $U_j^{(1)} \quad U_j^{(2)}$ by definition). The orthogonality can be inferred immediately if we recall that $U_2^{(j)}$ is obtained from $U_1^{(j)}$ (a set of mutually orthogonal product vectors) through orthogonalization of the last qubit. Hence, for a specific vector from $U_2^{(j)}$ the orthogonality to all but one vectors from $U_1^{(j)}$ holds due to first $N-1$ qubits and to the remaining one, due to the last (orthogonalized) qubit.

For even N, similarly to the previous case, the sets $U_1^{(1)}$ and $U_1^{(2)}$ are orthogonal by definition. Since to construct the sets $U_2^{(j)}$ $(j = 1 \ 2)$ we consistently applied local unitary operations on the last two qubits, the vectors remain orthogonal between each other. Therefore, we only need to prove orthogonality of vectors from $U_1^{(j)}$ and $U_2^{(j)}$ $(j = 1 \ 2)$. Note that due to the recursive construction, orthogonality of vectors within one set is assured on first $N-2$ qubits (underlined in the diagram). Due to this fact the operation on the last qubit does not affect orthogonality between sets $U_1^{(j)}$ and $U_2^{(j)}$. Again for a specific vector from $U_2^{(j)}$ the orthogonality to all but one vectors from $U_1^{(j)}$ holds due to first $N-2$ qubits and to the remaining one, due to the last but one (orthogonalized) qubit.

Second, we show that there does not exist any product vector orthogonal to the set (4.24) if U_1 is a UPB (note that in such case U_2 is also a UPB). For this purpose, assume the contrary and write the vector orthogonal to all vectors in the set defined by equation (4.24) as x with $x \quad \mathbb{C}^2$ and denoting the product state of the remaining $N-1$ qubits. If $x = 0$,

then has to be orthogonal to $U_1^{(1)}$, $U_1^{(2)}$ and $U_2^{(1)}$. However, $U_1^{(1)}$ $U_1^{(2)} = U_1$ is a UPB, which leads to contradiction. A similar argument holds for $x = 1$ e $e^{\perp}$. In the case x 0 1 e $e^{\perp}$, must be orthogonal to both UPBs U_1 U_2, which also leads to contradiction. ■

This example shows that indeed the inverse procedure can lead to UPB. Note, however that we have considered the simplest scenario with two observables and two outcomes per site. In the general case, the obtained set of vectors has a weaker property: PUPB, i.e., is unextendible within the vectors from the local sets $\mathcal{S}^{(i)}$ [Augusiak 12].

4.4 Conclusions

Non-trivial Bell inequalities lacking a quantum violation are rare and intriguing objects. In this chapter we have demonstrated a systematic way to build inequalities of this kind with the property $\beta_{\mathrm{C}} = \beta_{\mathrm{Q}} < \beta_{\mathrm{N}}$ from Unextendible Product Bases — themselves an important concept in entanglement theory. Moreover, due to the connection with UPBs we have been automatically able to provide entanglement witnesses which reproduces the non-signalling correlations violating the inequalities. A still open problem is to understand when the construction leads to tight Bell inequalities, and whether one can infer this fact from some properties of UPBs.

These findings are strongly related to recent work on the relationship between quantum correlations and multipartite versions of Gleason s theorem [Barnum 10, Acín 10]. Precisely, we provide further examples of multipartite Bell scenarios for which correlations reproduced by an entanglement witness are not equivalent to quantum correlations.

Finally, we have shown that the construction can be applied in the reverse direction, i.e., starting from a Bell inequality known to have the same classical and quantum bound and consisting of locally orthogonal conditional probabilities, one can derive a set of product vectors that constitutes a UPB. Applying this connection we have derived a new class of UPBs, and consequently a new class of bound entangled states, from the existing GYNI Bell inequalities.

Chapter 5

Multipartite entanglement in spin-1/2 systems

The characterization of quantum correlations in multi-particle systems is crucial for understanding the structure of many-body quantum states. Typical methods used so far to study many-body systems were developed within the field of condensed matter and include the response to external perturbation, the behaviour of order parameters and the analysis of the excitation spectrum. Recently, a new family of tools emerged from quantum information theory. They are based on the qualitative and quantitative study of bipartite and multipartite entanglement between parts of the multi-particle state and have proved useful for revealing the structure of many-body states [Amico 08].

The role of entanglement becomes particularly clear in the study of quantum phase transitions (QPT), where correlations play a crucial role. For instance, a measure of the nearest-neighbour pairwise entanglement allows one to detect the critical point in the Ising model in 1D [Osborne 02, Osterloh 02]. An important notion is also the scaling of the entanglement between two disjoint connected parts of the system A and $S \quad A$ [Vidal 03b, Audenaert 02]. This quantity is deeply connected to the range of quantum correlations in strongly correlated systems. For those with finite correlation length the entanglement between blocks, as measured by the entropy of entanglement, fulfils the so called *area law*, i.e., depends only on the surface separating A and $S \quad A$ (*cf.* [Hastings 07a, Hastings 07b] for rigorous results in 1D). In critical 1D systems when the correlation length becomes infinite, the area law is violated indicating the presence of long-range entanglement. Yet another way to adapt the bipartite techniques to the analysis of the multipartite systems is the concept of localizable entanglement introduced in [Verstraete 04a]. The study of this quantity in the vicinity of critical points shows that there exist situations in which the correlation length is finite, nevertheless the (localizable) entanglement length diverges, which supports the idea that global entanglement plays an important role in QPT.

While these examples regard bipartite entanglement, the multipartite scenario is much less explored, even though it is believed to play an important role in many-body systems. The multipartite correlations are much richer than the bipartite ones and thus this type of entanglement is much more difficult to detect and quantify [Gühne 09]. Nevertheless, several works demonstrate the presence of genuine multipartite entanglement in ground states of certain spin models [Wang 02, Štelmachovic 04, Bruß 05, Gühne 05]. More importantly, as it

was shown in [Wei 03, de Oliveira 06], some multipartite entanglement measures are sensitive to the presence of a quantum phase transition signalling that the quantum critical point is indeed connected to emergence of multi-particle entanglement.

Here we focus on quite specific systems, ground and thermal states of rotationally invariant spin Hamiltonians. A prominent example is the Heisenberg interaction Hamiltonian which arises from a particle exchange mechanism in tight-binding models in solid-state systems. The same interaction can be implemented in quantum simulators of condensed matter models: ultracold atoms in optical lattices. We will concentrate on the presence of genuine tripartite entanglement in the subsystems of the ground and thermal states of spins networks (spin systems with nearest neighbours defined through the edges of a graph), with and without defects in the coupling constant. To this end we use the fact that for spin-1 2 particles the rotational invariance is equivalent to $SU(2)$ symmetry. This allows us to use the results of Eggeling [Eggeling 01] and unambiguously characterize the entanglement properties of an arbitrary three-party reduction of a given rotationally invariant state with the set of scalar inequalities. In particular, the inequalities will allow us to distinguish fully separable states from those biseparable with respect to each partition. Moreover, we demonstrate that the inequalities detect genuine tripartite entanglement also in states without the rotational symmetry. To this end we use the twirling map, i.e., project a given state on the rotationally invariant subspace and subsequently apply the test. It should be emphasized, however, that in this situation the inequalities provide only a necessary separability test.

5.1 Representation and classi cation of rotationally invariant states

We begin the characterization of separability properties of tripartite rotationally invariant states by brie y recalling the class of bipartite rotationally symmetric states described by Schliemann [Schliemann 03, Schliemann 05] and Breuer [Breuer 05, Breuer 06]. Let us consider the quantum state of a system composed of two spins $j_i = (d_i - 1)\ 2\ (i = 1\ 2)$, where d_i is the dimension of the ith local space. The state is then represented by a density matrix acting on a product Hilbert space $\mathcal{H}_1 \otimes \mathcal{H}_2 = \mathbb{C}^{d_1} \otimes \mathbb{C}^{d_2}$. A class of rotationally (or $SO(3)$) invariant states is defined through the following relation

$$\underset{\hat{\boldsymbol{n}},\theta}{} \left[\mathcal{D}^{j_1}(\hat{\boldsymbol{n}}\ \theta) \otimes \mathcal{D}^{j_2}(\hat{\boldsymbol{n}}\ \theta) \quad \right] = 0 \tag{5.1}$$

where $\mathcal{D}^{j_i}(\hat{\boldsymbol{n}}\ \theta)$ denote the unitary irreducible representation of the rotation $R(\hat{\boldsymbol{n}}\ \theta)$ from the $SO(3)$ group. Any rotation transformation can be written in terms of the total angular momentum operator $\boldsymbol{J} = \boldsymbol{j}_1 + \boldsymbol{j}_2$ as: $R(\hat{\boldsymbol{n}}\ \theta) = \exp(i\hat{\boldsymbol{n}} \cdot \boldsymbol{J}\theta)$.

According to Schur s lemma the density operator acts as a scalar on each irreducible representation of the total angular momentum operator $\boldsymbol{J} = \boldsymbol{j}_1 + \boldsymbol{j}_2$ and therefore can be written as

$$= \sum_{J=|j_1-j_2|}^{j_1+j_2} \frac{\alpha_J}{2J+1} P_J \tag{5.2}$$

where α_J are non negative coefficients fulfilling the normalization condition $\sum_J \alpha_J = 1$ and the operator P_J is a $2J + 1$-dimensional projector onto the subspace with total angular

momentum J:

$$P_J = \sum_{M=-J}^{J} J\ M \quad J\ M \tag{5.3}$$

Here $J\ M$ are the common eigenvectors of the square of the total angular momentum $\boldsymbol{J}^2$ and its z-component J_z with eigenvalues $J(J+1)$ and M, respectively.

The simplest case corresponds to two spin-1 2 particles. There are only two invariant subspaces: $J = j_1 - j_2 = 0$ of dimension 1 and $J = j_1 + j_2 = 1$ of dimension 3. Hence, there exist only one *pure* $SO(3)$ invariant state, the singlet state represented by the density matrix $_{\text{sing}} = P_0$. The projector onto the subspace of $J = 1$, P_1 is separable and the entanglement of an arbitrary combination of the two projectors is fully characterized by the PPT criterion [Horodecki 96]. Characterization using the PPT test is also possible for rotationally symmetric states in other specific cases [Schliemann 03, Schliemann 05, Breuer 05], however bound entanglement is found already in a system with $j_1 = 1$ and $j_2 = 3$ 2 and higher dimensions [Breuer 06, Augusiak 07].

Now we move to the more complex situation of three spin-1 2 particles with angular momentum operators $\boldsymbol{j}_1$ $\boldsymbol{j}_2$ and $\boldsymbol{j}_3$. In this case we can first couple the angular momenta of the first two particles $\boldsymbol{J}_{12} = \boldsymbol{j}_1 + \boldsymbol{j}_2$ and then add the third one, which we schematically write:

$$\begin{aligned} \frac{1}{2} \otimes \frac{1}{2} \otimes \frac{1}{2} &= (0 \oplus 1) \otimes \frac{1}{2} \\ &= \left(\frac{1}{2}\right)_0 \oplus \left(\frac{1}{2}\right)_1 \oplus \frac{3}{2} \end{aligned} \tag{5.4}$$

The subscripts in the two non equivalent spin 1 2 doublets remind that the first two spins are in a singlet or in a triplet. Now in order to specify the state of the three particles one needs not only the modulus of the total angular momentum $\boldsymbol{J}$ and its component M along some axis, but also another quantum number. Here it is natural to take the modulus of $\boldsymbol{J}_{12}$. Note, however, that equally well we can begin by coupling the angular momenta $\boldsymbol{j}_1$ and $\boldsymbol{j}_3$ or $\boldsymbol{j}_2$ and $\boldsymbol{j}_3$. This ambiguity is very well known from the theory of angular momentum.

In order to express a rotationally invariant density operator in the product Hilbert space $\mathcal{H}_1 \otimes \mathcal{H}_2 \otimes \mathcal{H}_3$, we apply again the Schur s lemma which tells us that acts trivially in the subspace of total angular momentum 1 2 and 3 2. However, since in general $[\ \boldsymbol{J}_{12}] = 0$, the two subspaces $(1\ 2)_0$ and $(1\ 2)_1$ can be mixed. Therefore, we proceed as follows. Using the decomposition (5.4), we define a basis for $(1\ 2)_i$: $\pm 1\ 2\ _i$. Now we mix the two subspaces $(1\ 2)_0$ and $(1\ 2)_1$ obtaining two new orthogonal subspaces $(1\ 2)_a$ and $(1\ 2)_b$ with vectors:

$$\pm\frac{1}{2}\ _a = \cos\frac{\theta}{2}\ \pm\frac{1}{2}\ _0 + e^{i\phi}\sin\frac{\theta}{2}\ \pm\frac{1}{2}\ _1 \tag{5.5a}$$

$$\pm\frac{1}{2}\ _b = -\sin\frac{\theta}{2}\ \pm\frac{1}{2}\ _0 + e^{i\phi}\cos\frac{\theta}{2}\ \pm\frac{1}{2}\ _1 \tag{5.5b}$$

where θ $[0\ \pi]$ and ρ $[0\ 2\pi]$. The corresponding orthogonal projectors on the subspaces of total angular momentum 1 2 read:

$$P_{1/2,\alpha} = \frac{1}{2}\ _\alpha\ \frac{1}{2} + -\frac{1}{2}\ _\alpha\ -\frac{1}{2} \qquad \alpha = a\ b \tag{5.6}$$

leading to the density operator in the form

$$= \frac{p}{2}P_{1/2,a} + \frac{q}{2}P_{1/2,b} + \frac{1-p-q}{4}P_{3/2} \tag{5.7}$$

where $0 \leq p \;\; q \leq 1$. We see that 4 parameters are required to describe the set of $SO(3)$-invariant states of three spins $1 \;\; 2$, i.e., $p \;\; q \;\; \theta \;\; \rho$. This construction can be extended to higher spins by taking adequate superpositions of vectors from the subspaces of the same total spin, however the number of parameters grows dramatically, e.g., for spin-1 particles 13 variables are required.

Even though the representation based on the coupling of the angular momenta is simple and intuitive it involves nonlinear functions of parameters, which are not easy to deal with. Because of this we make a connection to another representation of rotationally symmetric states of three spin-$1 \;\; 2$ particles. We use the fact that for two level systems, the $SO(3)$ rotations are the most general unitary operations. Hence, the state invariant under rotations is also invariant under all local unitary transformations of the form $U \otimes U \otimes U$. This class of states has been completely characterized by Eggeling and Werner in [Eggeling 01]. We recall their results and establish a mapping between the two constructions.

Following [Eggeling 01] we introduce permutation operators V_{12}, V_{13} and V_{23} [1] which exchange the corresponding particles, and the two operators which cyclically permute all three particles: $V_{123} = V_{12}V_{23}$ and $V_{321} = V_{23}V_{12}$. The Hermitian operators that are used to represent the unitary invariant density matrix are then defined as

$$R_+ = \frac{1}{6}\left(\mathbb{I} + V_{12} + V_{23} + V_{13} + V_{123} + V_{321}\right) \tag{5.8a}$$

$$R_0 = \frac{1}{3}\left(2\mathbb{I} - V_{123} - V_{321}\right) \tag{5.8b}$$

$$R_1 = \frac{1}{3}\left(2V_{23} - V_{13} - V_{12}\right) \tag{5.8c}$$

$$R_2 = \frac{1}{\overline{3}}\left(V_{12} - V_{13}\right) \tag{5.8d}$$

$$R_3 = \frac{i}{\overline{3}}\left(V_{123} - V_{321}\right) \tag{5.8e}$$

Now any density matrix invariant under all unitary operators $U \otimes U \otimes U$ can be written in the following form:

$$\rho = \sum_{k=+,0,1,2,3} \frac{r_k}{4} \;\; R_k \tag{5.9}$$

where $r_k = \mathrm{tr}\rho R_k$ and the factor $1 \;\; 4$ ensures the normalization $\mathrm{tr}\rho = 1$. Comparing our representation (5.7) with the one proposed by Eggeling and Werner (5.9) we obtain the following correspondence between the parameters:

$$r_+ = 1 - p - q \tag{5.10a}$$

$$r_0 = p + q \tag{5.10b}$$

$$r_1 = \frac{1}{2}(p-q)(\cos\theta + \;\; \overline{3}\cos\rho\sin\theta) \tag{5.10c}$$

$$r_2 = -\frac{1}{2}(p-q)(\;\; \overline{3}\cos\theta - \cos\rho\sin\theta) \tag{5.10d}$$

$$r_3 = (p-q)\sin\theta\sin\rho \tag{5.10e}$$

[1] The two-particle swap operator is defined as $V_{ij} = |ij\rangle\langle ji| + |ji\rangle\langle ij|$.

From equations (5.10a) and (5.10b) one immediately sees that the operator R_+ is proportional to the projector $P_{3/2}$ and the operator R_0 to $P_{1/2} = P_{1/2,a} + P_{1/2,b}$. The three remaining matrices R_i ($i = 1\ 2\ 3$) act on the 4-dimensional subspace of spin $1\ 2$ and follow the angular momentum commutation rules, therefore are traceless. They are responsible for mixing between the two distinct spin-$1\ 2$ subspaces $(1\ 2)_0$ and $(1\ 2)_1$. Due to the above properties the description of spin-$1\ 2$ subspace resembles very much the Bloch representation of one-qubit with R_0 being the identity matrix and R_i the Pauli matrices. Hence, the coefficients r_k ($k = +\ 0\ 1\ 2\ 3$) must fulfil the following conditions in order that (5.9) represents a state:

$$r_+\ r_0 \geqslant 0 \tag{5.11a}$$

$$r_+ + r_0 = 1 \tag{5.11b}$$

$$r_1^2 + r_2^2 + r_3^2 \leqslant r_0^2 \tag{5.11c}$$

It turns out that in the case of three rotationally symmetric qubits, the PPT criterion suffices to unambiguous characterize the classes of biseparable states. However, the set of fully separable states does not coincide with the intersection $\mathcal{B}_1 \setminus \mathcal{B}_2 \setminus \mathcal{B}_3$. In [Eggeling 01] the sets $\mathcal{S}$ of fully separable and $\mathcal{B}$ of biseparable states are fully described in terms of inequalities for the coefficients r_k. In particular, the authors have proven that the set $\mathcal{S}$ is constrained by the following conditions:

$$\frac{1}{4} \leqslant r_+ \leqslant 1 \tag{5.12a}$$

$$3r_3^2 + (1 - 3r_+)^2 \leqslant (r_1 + r_+)[(r_1 - 2r_+)^2 - 3r_2^2] \tag{5.12b}$$

Analogously, the states separable with respect to partition $1\ 23$, belonging to the set $\mathcal{B}_1$, can be shown to fulfil the conditions:

$$h\ < 1 \tag{5.13a}$$

$$3(r_2^2 + r_3^2) \leqslant \begin{cases} (h+1)^2 - [h + (r_1 - r_+)]^2, & \text{if } h < 0 \\ (h-1)^2 - [h - (r_1 - r_+)]^2, & \text{if } h > 0 \end{cases} \tag{5.13b}$$

where $h = 1 + r_1 - 2r_+$. The corresponding sets $\mathcal{B}_2$ and $\mathcal{B}_3$ are found by rotating the set $\mathcal{B}_1$ by $\pm 2\pi\ \ 3$ around the axis r_0 (see figure 5.1(c)). The total set of biseparable states $\mathcal{B}$ is the convex hull of the sets $\mathcal{B}_1\ \ \mathcal{B}_2\ \ \mathcal{B}_3$. Finally, the set $\mathcal{T}$ of genuine tripartite entangled states is found as the complement of $\mathcal{B}$ in the set of all admissible parameters (5.11).

The fact that we are going to analyse ground and thermal states of real symmetric Hamiltonians, a very common situation for spin interactions, further facilitates this already simple description. It allows us to reduce the number of parameters by using the property that such states are represented by real density operators. Inspecting the representations we find that this is equivalent to putting $\rho = 0$ in (5.7) or $r_3 = 0$ in (5.9). This leaves us with three parameters and enables visualization of the sets in the space $r_1\ \ r_2\ \ r_0$ (figure 5.1). The complete set of states is a cone with symmetry axis parallel to the axis r_0. In particular figure 5.1(a) shows the set of separable states $\mathcal{S}$ and figure 5.1(b) the set of biseparable states $\mathcal{B}$. The unshaded area inside the cone in figure 5.1(b) contains genuine tripartite entangled states. Finally, figure 5.1(c) is a section of the cone for a fixed r_0. We notice that the necessary condition for a state to be tripartite entangled is $r_0 > 2\ \ 3$. In fact below this value biseparable states fill the cone completely.

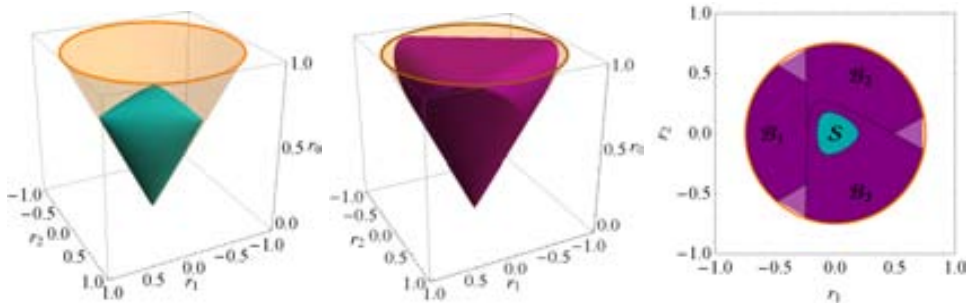

Figure 5.1: Graphical representation of the set of real rotationally invariant states and its subsets with various types of entanglement in the space of $r_1\ r_2\ r_0$.

5.2 Tripartite entanglement in rotationally-invariant spin networks

We now consider several exemplary spin systems with Heisenberg interaction

$$H = \sum_{\langle i,j \rangle} J_{ij} \boldsymbol{\sigma}_i \cdot \boldsymbol{\sigma}_j \tag{5.14}$$

where the sum over indices $i\ j$ is restricted to edges in the graph describing the system. For each case we first construct the ground and the thermal state in equilibrium at temperature T

$$\rho = \frac{e^{-\beta H}}{\mathrm{tr} e^{-\beta H}} \tag{5.15}$$

and then trace out all the spins in the network except three chosen spins $A\ B\ C$. The ground state is rotationally symmetric only if it is non-degenerate. Note that any subsystem of a rotationally invariant state is also rotationally invariant, hence the reduced density matrix can be analysed with the criterion from the previous section by computing the coefficients $r_0\ r_1\ r_2$ from equation (5.9) and checking to which set the state belongs.

5.2.1 A spin star

We start by considering a spin star network consisting of four spins, shown in figure 5.2a. The couplings are chosen so that $J_{14} = J_{24} = J$ while $J_{34} = \lambda J$. The dimensionless parameter λ fixes the ratio, positive or negative, between the couplings of the central spin with spins $1\ 2$ and 3. We trace out the central spin, choosing the three relevant spins to be $A = 1$, $B = 2$, $C = 3$. We want to understand if, and under which conditions, the central spin induces tripartite entanglement in the outer spins. A similar model has been recently studied in [Militello 11] for non rotational invariant Hamiltonians for which, however, necessary separability conditions are not known. Here, we emphasize that, although we consider a restricted class of Hamiltonians, the detection of tripartite entangled states is unambiguous.

We distinguish two cases: repulsive interaction $J > 0$ and the attractive one $J < 0$. Let us start with $J > 0$, for which we plot a complete phase diagram in figure 5.2b. In this case

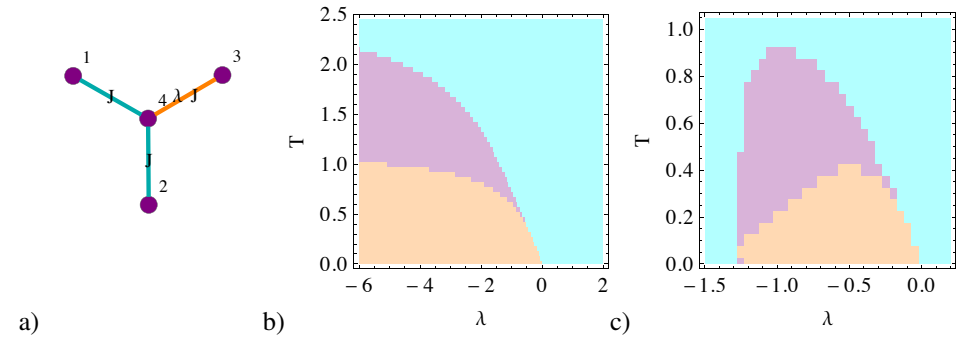

Figure 5.2: Regions of genuine tripartite entanglement, biseparability and full separability in of three outer spins of a four-spin star with inhomogeneous couplings (as depicted in picture a) We distinguish b) the repulsive interactions $J > 0$ and c) the attractive case $J < 0$. (T and λ are expressed in the units of J)

we find that independently of the choice of $\lambda > 0$ the reduced state is never genuine tripartite entangled. To see this it is sufficient to determine the coefficient r_0 for the reduced density matrix ρ_{ABC}

$$r_0 = \frac{-7 - 2\lambda + 3\sqrt{4\lambda^2 - 4\lambda + 9}}{6\sqrt{4\lambda^2 - 4\lambda + 9}}, \tag{5.16}$$

whose maximum as a function of λ is $1/3$. Since a necessary condition for a state to be genuinely tripartite entangled is $r_0 > 2/3$ we conclude that for $\lambda > 0$ the state is always biseparable or fully separable. By checking the remaining parameters we verify that the state is separable.

By looking at the eigenenergies of Hamiltonian H, we observe a level crossing at $\lambda = 0$. For $\lambda < 0$ the ground state is given by:

$$|\psi_G\rangle = \frac{1}{\sqrt{3}}|0011\rangle + \frac{1}{\sqrt{3}}|1100\rangle - \frac{1}{\sqrt{6}}(|01\rangle + |10\rangle)(|01\rangle + |10\rangle) \tag{5.17}$$

independently of the particular value of λ. The corresponding reduced density matrix of the first three spins is genuinely tripartite entangled.

Now let us consider the case $J < 0$. For $\lambda > 0$ the ground state reads:

$$|\psi_G\rangle = \frac{1}{\sqrt{6}}(|0011\rangle + |0101\rangle + |1001\rangle + |0110\rangle + |1010\rangle + |1100\rangle). \tag{5.18}$$

The reduced density matrix of the first three spins (actually of any three spins, since the state is permutationally invariant) is separable for all values of λ because $r_0 = 0$. Instead, for $-1.24 < \lambda < 0$ the ground state is genuine tripartite entangled and fully separable outside this range. The complete entanglement diagram, shown in figure 5.2c, indicates that for intermediate temperatures the state becomes biseparable, and finally as the temperature increase, fully separable.

5.2.2 A spin chain

As the second example we consider a closed ring topology for the spin chain, as depicted in figure 5.3. We study the Heisenberg Hamiltonian with dimerization:

$$J_{i(i+1)} = J[1 + (-1)^i \lambda]. \tag{5.19}$$

We choose $J > 0$ and $0 \leq \lambda \leq 1$. Analogously to the spin star, we calculate the thermal state, given in equation (5.15), of the chain. This time, however, we diagonalize the Hamiltonian numerically. We then analyse the reduced density matrix of three spins ABC marked in the figure 5.3a.

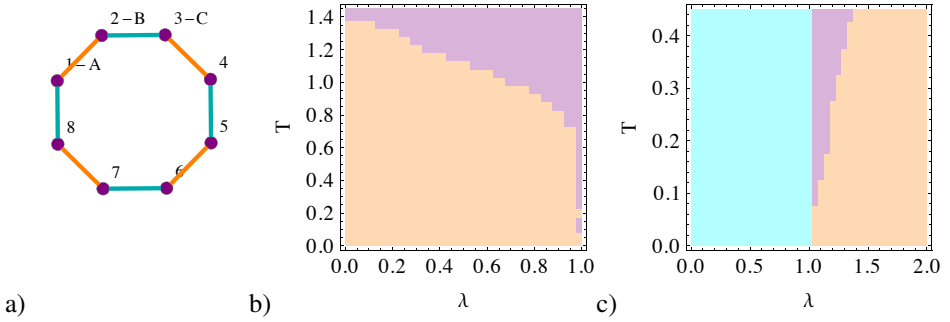

Figure 5.3: The spin chain with $L = 8$ spins. The regions of temperature and dimerization parameter λ for which the three spins ABC are in a genuine tripartite entangled, biseparable or fully separable state. The interaction constant J is b) positive and c) negative.

The case of neighbouring spins is translationally invariant, i.e., the results do not change if we shift the three spins along the chain. The resulting phase diagram as a function of the dimerization λ and the temperature T is shown in figure 5.3. Note that in the absence of dimerization, a homogeneous Heisenberg chain, the three neighbouring spins are genuinely tripartite entangled up to a temperature $k_B T \simeq 1.39J$ when they become biseparable. This agrees with the results found in [Gühne 05]. For increasing dimerization λ, the critical temperature for tripartite entanglement decreases as the system tends to form strongly correlated dimers, i.e. singlets. This pairing tendency destroys the tripartite entanglement, leaving the state biseparable for smaller temperatures. The situation is even more striking for $\lambda = 1$ for which the chain is broken and is exactly made of singlets. For this value we never observe tripartite entanglement.

The ferromagnetic case $J < 0$ and $|\lambda| < 1$ is trivial as all the spins are parallel to each other. For $\lambda > 1$ the sign of the interaction changes for alternate spins and we observe genuine tripartite entanglement in the ground state and at low temperatures and biseparability for higher T.

5.3 Tripartite entanglement in spin systems without rotational symmetry

In the previous section we have concentrated on rotationally invariant states since there we can unambiguously decide to which entanglement class a given state belongs. Here we show that the separability criterion for rotationally invariant states can be applied even for a more general class of states by the use of the *twirling map* defined for a particular group G as

$$\Pi\rho = \int_G \mathrm{d}U U\rho U^\dagger \tag{5.20}$$

If the group G consist of local operators, the twirling map preserves the separability of a state [Vollbrecht 01]. We formulate the following fact for the specific case considered in this chapter, which establishes a necessary separability criterion for any class of tripartite states.

Fact 1 (Twirling criterion)**.** Assume that the group G consists of local unitaries and consider the tripartite states ρ $\Pi\rho$. The state $\Pi\rho$ is clearly $SU(2)$ invariant; moreover

(i) if ρ is separable then $\Pi\rho$ is separable,

(ii) if ρ is biseparable then $\Pi\rho$ is separable or biseparable.

We conclude that if $\Pi\rho$ is genuine tripartite entangled then so is ρ and in what follows we demonstrate the applicability of the twirling criterion for systems with XXZ interaction Hamiltonian with magnetic field.

5.3.1 Spin-$1/2$ XXZ model

We consider the system of spin-1 2 particles with XXZ Hamiltonian describing the nearest neighbour interaction and magnetic field along direction z:

$$H_{\mathrm{XXZ}} = J\sum_{\langle i,j\rangle}\left[(\sigma_i^x\sigma_j^x + \sigma_i^y\sigma_j^y) + \lambda\sigma_i^z\sigma_j^z\right] + h\sum_i \sigma_i^z \tag{5.21}$$

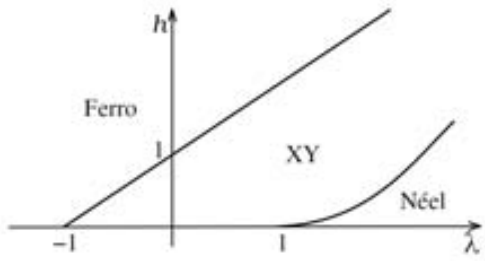

a)

Figure 5.4: Phase diagram for the XXZ model for spin 1 2. (based on [Mikeska 04])

We focus on a spin-chain geometry and $J > 0$ and in figure 5.4 we show a complete phase diagram of the system. In the absence of magnetic field for $\lambda < -1$ the attractive

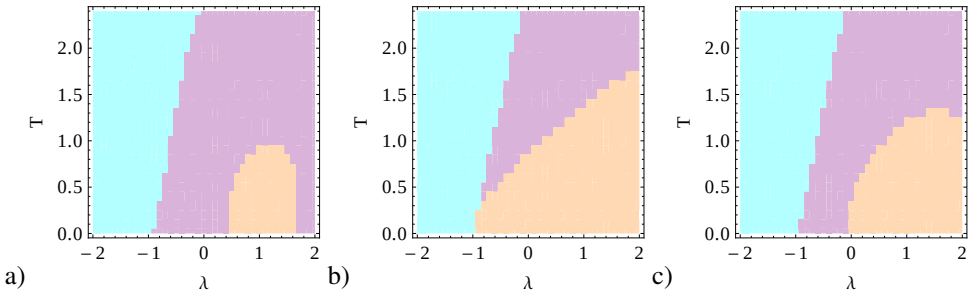

Figure 5.5: The XXZ spin chain with a) $L = 7$, b) $L = 8$, c) $L = 9$ spins.

interactions in direction z dominate over other interaction terms and all the spins are oriented along $\pm z$ (degeneracy); the ground state is, therefore, a ferromagnet. In the other extremal case, $\lambda > 1$, the repulsive interaction between z-oriented spins dominates and the system is in an anti-ferromagnetic phase, which has a long range order. The larger λ, the more the ground state resembles the classical Ising or Néel phase. For λ in the interval $(-1\ 1)$ the XY term dominates over the Z term and the system is in the XY phase. The presence of the magnetic field shifts the transition points extending the region of ferromagnetic order. It also removes the degeneracy of the ground state $\lambda < -1$.

First, we set the magnetic field to zero and determine numerically the equilibrium thermal state for the system of even ($L = 8$) and odd ($L = 7\ 9$) number of spins and test the entanglement of their reduced density matrices of three consecutive spins ρ_{ABC} using the twirling criterion, i.e., we test the separability properties of the rotationally invariant state $\Pi\rho_{\mathrm{ABC}}$. The results are presented in figure 5.5. We observe that for $\lambda < -1$, where the ground state is a ferromagnet, the twirled state is fully separable. We also expect the state ρ_{ABC} to be fully separable in this regime independently of the size of the system. For $\lambda > -1$ we notice a difference between odd and even system size. In this region the system of 8 spins has genuine tripartite entanglement for arbitrary λ and at low temperatures, whereas for 9 spins we see that in the interval $-1 < \lambda < 0$ the twirled state is biseparable and only for $\lambda > 0$ becomes tripartite entangled (we observe a similar behaviour for 7 spins). This is explained by the fact that periodic boundary conditions may cause a geometric frustration for a finite system with odd number of spins. The qualitative difference between the states with odd and even number of particles is, therefore, signalled by the presence of multipartite entanglement.

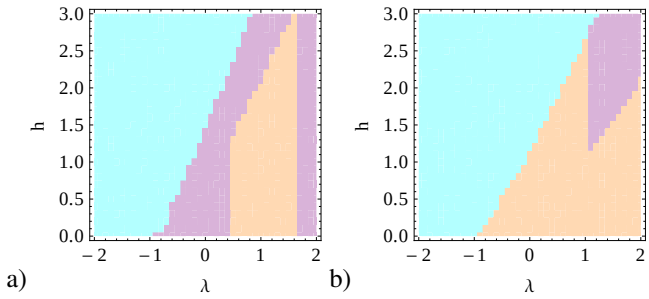

Figure 5.6: The XXZ spin chain in magnetic field with a) $L = 7$, b) $L = 8$ spins.

In figure 5.6 we depict the entanglement properties of the ground state of the XXZ model with magnetic field. For this system we also observe a qualitative difference between odd and even number of particles. As expected, the region of fully separable states coincides with the occurrence of the ferromagnetic phase. The other two phases cannot be distinguished with our method.

5.4 Conclusions

We have studied entanglement in several exemplary spin arrays with Heisenberg interaction using the necessary and sufficient separability criteria for three-qubit rotationally invariant states. We have found the range of Hamiltonian parameters and temperatures for which these systems have genuine multipartite entanglement in their ground and thermal states. Moreover, we show that the criterion for tripartite entanglement can be applied to systems that do not possess the rotational symmetry if the twirling map is used. In this case, however, it becomes only a sufficient separability test. Nevertheless, applied to a periodic spin-1 2 chain with XXZ interaction, the criterion detects genuine tripartite entanglement in its subsystems.

Chapter 6

Glass to superfluid transition for a disordered bosonic system

The presence of disorder, understood as random impurities and defects in a regular configuration, is an inherent property of real physical systems and often the fundamental factor underlying their behaviour [Akkermans 06]. One of the most noted phenomena linked to disorder is the exponential localization of the electronic wave-function in a dirty crystal. The phenomenon is named after its discoverer: the Anderson localization [Anderson 58], and occurs due to interference of paths resulting from multiple coherent scattering events from a random potential. At its heart, Anderson localization is a wave phenomenon and indeed it was first observed experimentally for classical electromagnetic and acoustic waves [Wiersma 97, Schwartz 07, Hu 08]. After a long search, Anderson localization of matter waves was finally reported for ultracold gases in one dimension (1D) [Billy 08, Roati 08], and very recently also in 3D [Kondov 11, Jendrzejewski 12].

The physics of disordered quantum systems is a very active field of research and in the past decades there have appeared an enormous literature on the topic; for reviews see, e.g., [Ando 88, Kramer 93, Fallani 08, Sanchez-Palencia 10]. Although, due to the complexity of the subject, mathematically rigorous results are still scarce, a great deal of work has been done on random Schrödinger operators, which describe the single particle behaviour (see [Kirsch 07] for an introduction to the topic). Yet, non-interacting particles in a disordered potential provide an oversimplified picture, as the theory of dirty solids (crystals) is much more complex due to long-range Coulomb interaction between particles, underlying periodic structure, interaction with phonons, magnetic effects *etc* . At this point it is important to stress the fundamental difference between disordered fermionic and bosonic systems. For fermions the crucial role is played by the Fermi energy: the question whether a given system is a conductor or an insulator depends on whether the single particle states close to Fermi level are localized or not. Bosons, in contrast, tend to condense in the lowest energy state (or states). The question whether they constitute a superfluid or an insulator reduces then to understanding if the low-energy states are localized or not (for discussion see for instance [Sanchez-Palencia 10, Lewenstein 12]). In this chapter I concentrate on bosonic systems.

A new playground for the investigation of quantum disordered systems is offered by the field of ultracold atomic gases. The vast degree of control achieved in these genuinely quantum systems enables simulation of fundamental processes underlying the properties of con-

densed matter [Lewenstein 12]. Current technology makes it possible to produce cold atomic gases following a chosen statistics (Bose or Fermi) and adjust the interaction between the particles by means of Feshbach resonances. Moreover, modern experimental techniques give a full control over the optical trapping potential and therefore allow for analysing systems with reduced dimensionality. Finally, what is most important in the present context, a controllable amount of disorder potential can be implemented in many ways, which will be discussed in more detail in section 6.1.2.

A challenging and still open problem is the understanding of the interplay between the delocalizing effect of repulsive interactions and localization in disordered bosonic systems. Experimentally, the problem has been recently addressed by a number of groups [Fallani 07, Pasienski 10, Gadway 11]. In the regime where disorder dominates over interactions, it was shown that the ground state of the bosonic system can be described by a glassy phase, called Lifshits (or Anderson) glass [Lugan 07, Deissler 10], characterized by exponentially localized and well separated "islands" in the regions of space where the potential is small. As repulsive interactions are strengthened, an increasing number of islands is populated, until their overlap becomes sufficient to establish phase coherence and transport between them. Then the gas as a whole undergoes a phase transition towards an extended super uid (SF) phase. For the gas confined in a lattice, as the interactions further increase the repulsion between particles becomes so strong that on-site density uctuations characteristic of the SF state become energetically unfavourable. In this situation the gas undergoes a transition out of the SF, first to the Bose glass phase and then into the Mott state [Giamarchi 88, Fisher 89]. Between the Lifshits and the Bose glasses there is no phase transition, nonetheless the two states are qualitatively different, in the sense that in the former the gas is fragmented into independent and distant islands, while the latter tends to extend over a large portion of the available volume.

In this chapter we will consider disorder of Bernoulli type, i.e., the potential generated by identical localized impurities randomly-distributed in a lattice. An important feature of systems with this particular disorder is that they allow for rigorous analytical estimates. In a recent paper, Bishop and Wehr [Bishop 12] have provided rigorous tight bounds on the single-particle ground state energy, as well as approximations of the ground state and excited states wave-functions for this potential in a 1D lattice. Since the shape of the low-energy states is known the results can be, at least partially, generalized to interacting 1D and 2D systems. Here we recall the work of Bishop and Wehr discussing the typical size of zero-potential islands and the energy of the localized eigenstates in 1D and conjecture the analogous properties in arbitrary dimension. Then we focus on the regime of weak to intermediate interactions and explore the properties of ground states of 1D and 2D systems by comparing the performance of three theoretical methods. The first one is a simple version of the multi-orbital Hartree–Fock method (sMOHF), a variational method based on an expansion into single-particle states. This approximation is appropriate to describe the weak interaction regime where super uidity is suppressed by disorder [Lugan 07]. The second method is the standard Gross–Pitaevskii (GP) approach, which generally yields an appropriate description for weak and moderate interactions ($\sqrt{g\ \rho} \leq\ 1$), however fails in the strong coupling regime. The third method, a multi-orbital Gross–Pitaevskii equation (MOGP), interpolates between the sMOHF and GP. It incorporates the fragmentation of the ground state achieved with sMOHF but allows for a self-consistent adjustment of the shape of specific orbitals as the GP approach [Cederbaum 03]. The results concerning the application of MOGP to disordered systems were obtained in collaboration with L. Sanchez-Palencia, P. Massignan and M. Lewenstein and have not been published.

6.1 Ultracold atomic gases in a lattice

The technological advancement in the field of ultracold atomic gases occurred over the last twenty years, during which several breakthroughs were made; the development of laser and evaporative cooling techniques, and optical trapping and manipulation of atoms being the most prominent examples. In this section I brie y review the basic tools used to create and manipulate ultracold lattice gases and parameters that can be controlled in experiments, and give a short survey of experimental implementations of disorder. Later, I shortly discuss the ideal homogeneous Bose-Hubbard model, which provides a perfect description of bosonic atoms in a lattice. Finally, I switch to description of bosons in random potentials. For complete review on the current developments in the discipline of ultracold atomic gases see, e.g., [Lewenstein 07, Bloch 08, Lewenstein 12].

6.1.1 Experimental techniques

Cooling. — Reaching the regime of temperatures on the order of nanoKelvins requires special cooling techniques, laser cooling and evaporative cooling. Laser cooling is based on momentum transfer from an atom to a scattered photon. When the laser with frequency just below the atomic resonance shines at the atomic cloud, the atoms moving towards the light source "see" the light Doppler-shifted. Fast atoms are closer to resonance than the slow ones, hence scatter more photons and loose momentum. By shining light from orthogonal directions, it is possible to slow down the atoms obtaining a velocity distribution corresponding to temperatures below 1 mK. This procedure is called Doppler cooling.

Another step, which enables to reach the microKelvin regime is a sub-Doppler cooling. There, a standing wave optical potential with modulated polarization is created. An atom moving "uphill" in this potential looses kinetic energy. Reaching the top of the potential it is reoriented through optical excitation and photon emission to an internal state that "feels" the opposite potential. In this way, moving atoms constantly run up the potential hills and their kinetic energy is converted to photon energy, lowering the temperature of the atomic cloud.

To decrease the temperature even further, to the order of nK, evaporative cooling method is used. The idea behind the procedure is to selectively release the energetic atoms from the trap by lowering the potential barrier or pumping the fast atoms to a non-trapped state. Once the hot atoms are removed, the sample rethermalizes through atomic collisions. A crucial role in evaporative cooling of diluted gases is played by Feshbach resonances (described in more detail below) which enhance the collisions rate in the sample and speed up the process.

Optical potentials. — The confinement of cold atoms in a lattice structure is achieved with optical potentials. An off-resonant oscillating electric field of a laser induces in an atom an alternating quadratic Stark shift. The energy shift of atomic levels is proportional to the square of the electric field $\Delta E(\mathbf{r}) = \alpha(\ _L)\left\langle \mathbf{E}(\mathbf{r}\ t)^2 \right\rangle$, where $\alpha(\ _L)$ is the polarizability of the atom depending on the light frequency $\ _L$. The largest shift is obtained for levels close to the resonance, for which $\alpha(\ _L)\quad 1\ \Delta$ is inversely proportional to the detuning $\Delta = \ _0 - \ _L$. We see that for a spatially varying field, a standing wave, the potential takes the form

$$V_{\mathrm{opt}}(\mathbf{r}) = \frac{I(\mathbf{r})}{\Delta} \tag{6.1}$$

and atoms are attracted towards the region of high or low intensity depending on the sign of the detuning. The potential depth is controlled by the amplitude of the field. Lattices

of various dimensionality and geometry can be built by overlapping optical standing waves along different directions. To avoid interference effects light with orthogonal polarizations or slightly different frequencies is used.

Atomic interactions. — The strength of the short range two-body interactions in a diluted ultracold gas is governed by the scattering length a_s. In such systems only the lowest angular momentum spherical wave contributes to the collision process, which is the s-wave for bosons and the p-wave for fermions. There exist atomic species (for instance, ^{6}Li, ^{40}K for fermions and ^{7}Li, ^{85}Rb for bosons) for which the interaction constant can be manipulated over a wide range of values with magnetic field. It is possible due to a magnetically-tuned Feshbach resonance which modifies the scattering length of an s-wave collision as

$$a(B) = a_{\mathrm{bg}}\left(1 - \frac{\Delta}{B - B_0}\right) \tag{6.2}$$

with a_{bg} being the off-resonant value of the scattering length, Δ denoting the width of the resonance and B_0 its position. The importance of Feshbach resonances in ultracold gases cannot be overrated. They not only provide a way to reach the strong-coupling regime, important for condensed matter physics, but also enable studies of truly non-interacting particles, a paradigm of statistical physics, by setting $B = B_0 + \Delta$.

6.1.2 Implementations of disordered potentials

Ultracold atomic gases offer a unique possibility of studying disordered systems with a well controlled strength and type of disorder. A random potential can be engineered in several ways. In what follows we review the most popular approaches (see, e.g., [Fallani 08, Lewenstein 12] for a more thorough discussion).

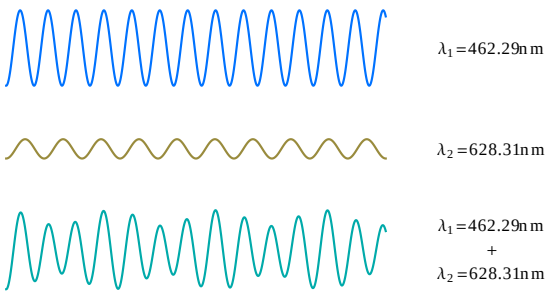

Figure 6.1: Bichromatic lattice obtained by superposing two optical standing waves of incommensurate wavelengths.

Bichromatic lattice. — The bichromatic potential depicted in figure 6.1 is created by superimposing two optical standing waves of incommensurate wavelengths, normally one having larger intensity than the other[Damski 03, Fallani 07]. This kind of pseudo-random potential takes the following value at each point:

$$V(x) = V_1 \sin^2\left(\frac{2\pi x}{\lambda_1}\right) + V_2 \sin^2\left(\frac{2\pi x}{\lambda_2} + \rho\right) \tag{6.3}$$

where $V_i > 0$ ($i = 1\ \ 2$) is the intensity of each standing wave and λ_i its wavelength. The potential can be viewed as random if the ratio $\lambda_1\ \ \lambda_2$ has an irrational value, however effectively

such lattice serves as a good realization of disorder whenever the period of the bichromatic potential is larger than the system size.

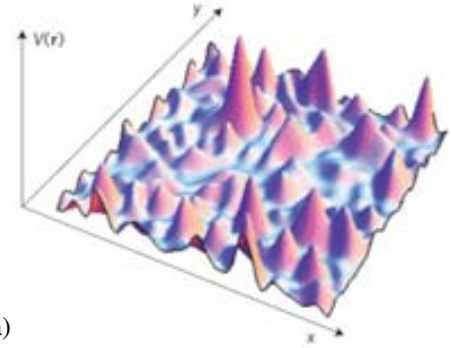

a)

Figure 6.2: A two-dimensional speckle potential [Sanchez-Palencia 10].

Speckle pattern. — An example of a truly random optical potential is the speckle pattern. It is obtained, e.g., through diffraction of a coherent laser beam on a ground-glass plate and its subsequent focusing with a converging lens. The former imprints a random phase on a light profile which afterwards leads to a random interference pattern in a focal plane of the lens. The random intensity, proportional to the optical potential, follows the exponential distribution

$$P(I(\mathbf{r})) \quad e^{-I(\mathbf{r})/\langle I\rangle} \tag{6.4}$$

The potential is then superimposed on the lattice system. Note that in this way one can produce 1D and 2D disordered patterns, however not a 3D one [Jendrzejewski 12]. Moreover, the potential amplitude on each site is not an independent random variable since the correlation length of the speckle pattern is on the order of $1\mu\mathrm{m}$.

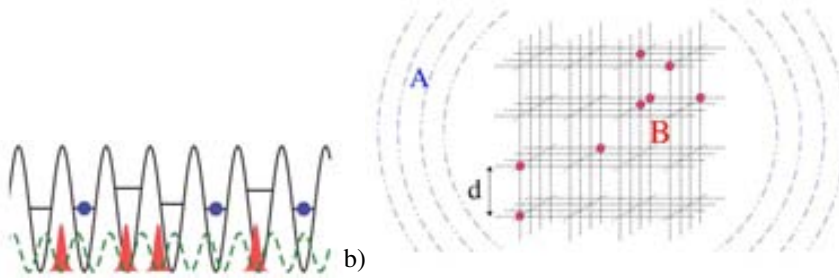

a) b)

Figure 6.3: Random impurities potential; a) the second atomic species is quenched in a secondary 1D lattice [Gadway 11]; b) 3D lattice with quenched impurities [Massignan 06].

Random impurities. — This kind of potential is ideally realized by using a two-component gas, i.e., atoms of two different kinds or internal states and a species-selective lattice which deeply traps only one of the components [Gavish 05, Massignan 06, Gadway 11]. At sufficiently low energies, the component which is not trapped experiences s-wave collisions against localized scatterers. The potential that is created in this way has only two values 0 and V, occurring with probability p and $1-p$, respectively ($1-p$ is the density of impurities).

The presence of quenched impurities may lead to a different type of disorder in the limit of weak interaction between the two atom types. Imagine two atomic species α and β, where β are frozen in random lattice sites. In this case, the presence of an impurity atom on site j may affect (i) the on-site interaction between α atoms if they "meet" in site j, and (ii) the tunnelling of αs between j and the neighbouring sites. This effectively leads to disorder in the on-site interaction and the tunnelling parameters. The occupation-dependence of the parameters of a clean homogeneous systems was studied in [Dutta 11].

6.1.3 Quantum phases in a clean bosonic system and their properties

The physical system of ultracold atoms in a lattice is described by a Hubbard Hamiltonian which, in the simplest case, contains a *hopping* part, describing the tunnelling of atoms between lattice sites, an *interaction* term containing short- and long-range couplings between atoms, and a *potential* term combining the external trapping potential, the chemical potential and the additional, e.g., disordered, potentials.

We are interested in a limited situation of N spinless bosonic atoms of a single type placed in a cubic lattice, with interactions of contact type, and at zero temperature. Such physical system is described by the ideal homogeneous Bose-Hubbard Hamiltonian

$$H_{\mathrm{BH}} = -t \sum_{\langle i,j \rangle} (b_i^\dagger b_j + b_j^\dagger b_i) + \frac{g}{2} \sum_i n_i(n_i - 1) + \mu \sum_i n_i \tag{6.5}$$

where $i\ j$ denotes the indices corresponding to the nearest neighbours, t is the tunnelling energy and g the interaction strength. We concentrate on a system with integer number of particles $\bar{n}$ per site (filling). Its behaviour depends solely on the ratio $t\ g$. In the limit of weak interactions or large tunnelling, all the bosons occupy the lowest band and are in a super uid (SF) state being gapless and compressible, and extended over the whole lattice. In the other extreme, strong on-site interactions or suppressed tunnelling, the atoms are confined to lattice sites and the energy minimum is achieved when there are exactly $\bar{n}$ bosons in each site; this state is a Mott insulator (MI) defined as a gapped and incompressible phase. The system undergoes a quantum phase transition from SF to MI at critical $t\ g$, denoted $(t\ g)_c$. Apart from the already mentioned *compressibility* and the presence of a *gap* in the excitation spectrum, the two phases can be distinguished with a number of other parameters: the *superfluid fraction*, *condensate fraction*. We define them more precisely below.

Super uid fraction. — The super uid fraction ρ_{sf} can be defined in terms of the energy change of a periodic system in response to twisted boundary conditions along one direction. For a 2D system of linear size L we impose $_{i+L,j} = e^{i\Phi}\ _{i,j}$ and express the parameter as

$$\rho_{\mathrm{sf}} = \frac{2mL^2}{\hbar^2} \frac{E(\Phi) - E(0)}{\Phi^2} \tag{6.6}$$

where $E(\Phi)$ is the energy per particle of a system with the total phase shift Φ. The super uid fraction vanishes in the Mott phase and is discontinuous at the critical point $(t\ g)_c$ (see, e.g., [Pai 96]).

Condensate fraction. — The condensate fraction describes the off-diagonal long-range order in the condensate

$$\lim_{|i-j| \to \infty} b_i^\dagger b_j\ = 0 \tag{6.7}$$

It has the interpretation of the ratio between the number of particles in the lowest energy super uid state and the total number of particles in the system, and can be computed as the largest eigenvalue of a normalized single particle density matrix defined by the equation

$$G_{ij} = \frac{b_i^\dagger b_j}{N} \tag{6.8}$$

The condensate fraction drops continuously from 1 in the limit $t\ g\ \rangle\ \ 1$ and vanishes at $(t\ g)_c$ in all dimensions.

Compressibility. — Compressibility measures the change in the number of particles with varying chemical potential

$$\kappa_s = \frac{\partial N}{\partial \mu} \tag{6.9}$$

Vanishing compressibility is the property defining the Mott insulator phase. At the MI-SF phase transition point $(t\ g)_c$ it increases discontinuously to finite values and remains finite in the SF phase.

Excitation spectrum. — A meaningful parameter in the context of excitation spectrum is whether there is a gap between the ground state and the first excited state and how does this gap scale in the neighbourhood of the phase transition point. A system is *gapped* if its excitation requires some finite amount of energy, whereas in gapless systems the ground state and excited states form a continuum. Excitation spectrum has to be analysed in the thermodynamic limit, since for finite systems the gap is always non-zero. In the point corresponding to the second order quantum phase transition all the systems become gapless. This is the case in the SF-MI transition; there the MI phase has a gap, which closes as the system approaches the critical point, while the SF phase is gapless.

Table 6.1: Summary of phases for clean bosons in a lattice, and associated properties.

	Super uid	Compressible	Gapless
SF(BEC)	Y	Y	Y
Mott insulator	N	N	N

6.1.4 Ground states of dirty bosonic systems and their properties

The properties of the system discussed in the previous section dramatically change in the presence of external random potentials. We assume the potential to be bounded, i.e., distributed in the interval $[-\Delta\ \Delta]$. In such case the ground state of the system has several universal properties, independent of the particular potential distribution. The Bose-Hubbard Hamiltonian (6.5) now takes the form

$$H_{\mathrm{BH}} = -t \sum_{\langle i,j \rangle} (b_i^\dagger b_j + b_j^\dagger b_i) + \frac{g}{2} \sum_i n_i(n_i - 1) + \sum_i (\mu + V_i) n_i \tag{6.10}$$

with V_i being a site-dependent potential. The phase diagram summarising various regimes of parameters and the corresponding phases is sketched in figure 6.4, and the most important properties of the ground state are listed in table 6.2.

Table 6.2: Summary of most common phases for dirty bosons in a lattice, and associated properties.

		Super uid	Compressible	Gapless	Fragmented
BEC		Y	Y	Y	N
Glass	Lifshits	N	Y	Y	Y
	Bose	N	Y	Y	N
Mott insulator		N	N	N	N

The first difference with respect to the clean system is the presence of an intermediate glassy phase between the SF and MI which though being compressible and gapless is not an extended super uid. The two distinguished states, the Lifshits (Anderson) and the Bose glass, belong to the same phase, however are qualitatively different. The former appears in the regime of weak interactions and is characterized by exponentially localized and well separated "islands" in the regions of space where the potential is small. Since the repulsion between the bosons is weak, the on-site density uctuations within an island can be large. In contrast, the Bose glass tends to extend over a large portion of the available volume. It arises when the repulsion between particles grows so strong that on-site density uctuations, characteristic of the super uid state, become energetically unfavourable, however before the system becomes the Mott insulator.

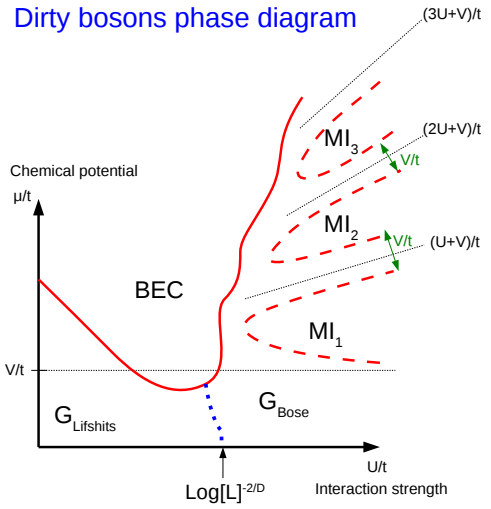

Figure 6.4: Schematic phase diagram for dirty bosons at zero temperature as a function of interactions (U) and chemical potential (μ) containing glassy (G), super uid (BEC), and Mott insulating (MI) phases. The continuous and dashed lines mark respectively the super uid-insulator and glass-Mott transition, while the dotted line indicates a crossover from the Lifshits glass (heavily fragmented) to the Bose glass (extended) region.

6.2 Description of weakly interacting many-body systems

In the limit of weak interactions, in which a macroscopic number of bosons occupy a single or few orbitals, rather than describe the lattice system with the Bose-Hubbard model one can capture its physics with a much simpler mean-field approach.

6.2.1 Multi-orbital Gross–Pitaevskii equation

Following Cederbaum and Streltsov [Cederbaum 03] we consider a system of N interacting bosons and assume that the particles condense into a number of orthonormalized orbitals. In such case the bosonic wave function is a symmetrized product of all the functions describing the individual condensates

$$\Psi(\mathbf{r}_1\ \mathbf{r}_2 \qquad \mathbf{r}_N) = \mathsf{S}\rho_1(\mathbf{r}_1)\rho_2(\mathbf{r}_2) \qquad \rho_N(\mathbf{r}_N) \tag{6.11}$$

where $\mathbf{r}_i$ is the position of each boson and S is the symmetrizing operator. Among the wave functions ρ_i ($i = 1 \qquad N$) only $1 \leq Q \leq N$ are different. They form the orbitals $_j$ ($j = 1 \qquad Q$), each occupied by N_j particles, with $\sum_{j=1}^{Q} N_j = N$. When there is a single orbital, i.e., $Q = 1$, we recover the so-called Hartree approximation, which leads to the celebrated Gross-Pitaevskii (or nonlinear Schrödinger) equation.

We are interested in finding the stationary state of the system which minimizes the mean-field energy, expressed as

$$E = \sum_i N_i \mathsf{h}_{ii} + g \sum_i \frac{N_i(N_i-1)}{2} \int \mathrm{d}\mathbf{r} \quad _i(r)\ ^4 + g \sum_i \sum_{j\neq i} N_i N_j \int \mathrm{d}\mathbf{r} \quad _i(r)\ ^2 \quad _j(r)\ ^2 \tag{6.12}$$

where $\mathsf{h}_{ii} = \int \mathrm{d}\mathbf{r} \ \ ^*_i(\mathbf{r}) H \ \ _i(\mathbf{r})$ is the mean value of the non-interacting Hamiltonian on the ith orbital and g is the interaction constant. As we assume that there is a large number of particles in each orbital, we may safely approximate $N_i(N_i-1) \approx N_i^2$ and proceed by renormalizing each $_i$ as $_i = \sqrt{N_i}\ _i$. Now the expression for energy can be rewritten in a compact form:

$$E = \sum_i h_{ii} + \sum_i \frac{g}{2} \int \mathrm{d}\mathbf{r} \quad _i(\mathbf{r})\ ^4 + g \sum_i \sum_{j\neq i} \int \mathrm{d}\mathbf{r} \quad _i(\mathbf{r})\ ^2 \quad _j(\mathbf{r})\ ^2 \tag{6.13}$$

where $h_{ii} = N_i \mathsf{h}_{ii}$. We minimize the energy with respect to the orbitals and under the constraint of fixed number of particles $\sum_i \int \mathrm{d}\mathbf{r} \quad _i(\mathbf{r})\ ^2 = N$, which leads to the following set of equations

$$\overline{\qquad}_{\ ^*_k(\mathbf{r})} \left[E - \mu \left(\sum_i \int \mathrm{d}\mathbf{r}' \quad _i(\mathbf{r}')\ ^2 - N \right) \right] = 0 \tag{6.14}$$

with μ being the Lagrange multiplier having the physical interpretation of chemical potential.

Expanding the left-hand side, we obtain:

$$\begin{aligned}
&\frac{}{{}^{*}_{k}(\mathbf{r})}\left[E-\mu\left(\sum_i\int \mathrm{d}\mathbf{r}'\quad {}_i(\mathbf{r}')^{\,2}-N\right)\right]\\
&\quad=\sum_i H\quad {}_i(\mathbf{r})\delta_{ki}+g\sum_i\sum_{j\neq i}\Big(\ {}_i(\mathbf{r})\quad {}_j(\mathbf{r})^{\,2}\delta_{ki}+\quad {}_i(\mathbf{r})^{\,2}\quad {}_j(\mathbf{r})\delta_{kj}\Big)\\
&\qquad+\frac{g}{2}\sum_i 2\quad {}_i(\mathbf{r})^{\,2}\quad {}_i(\mathbf{r})\delta_{ki}-\mu\sum_i\quad {}_i(\mathbf{r})\delta_{ki}\\
&\quad=H\quad {}_k(\mathbf{r})+g\quad {}_k(\mathbf{r})^{\,2}\quad {}_k(\mathbf{r})+2g\sum_{i\neq k}\quad {}_k(\mathbf{r})\quad {}_i(\mathbf{r})^{\,2}-\mu\quad {}_k(\mathbf{r})
\end{aligned}\tag{6.15}$$

Therefore, minimization of the energy reduces to solving the set of Q coupled Gross-Pitaevskii equations

$$\left(H+g\quad {}_k(\mathbf{r})^{\,2}+2g\sum_{i\neq k}\quad {}_i(\mathbf{r})^{\,2}\right)\quad {}_k(\mathbf{r})=\mu\quad {}_k(\mathbf{r})\qquad k=1\qquad Q\tag{6.16}$$

When there is a single orbital we recover the Gross-Pitaevskii (GP) equation

$$\left(H+g\quad (\mathbf{r})^{\,2}\right)\quad (\mathbf{r})=\mu\quad (\mathbf{r})\tag{6.17}$$

At the beginning of the section we have assumed that the orbitals are orthogonal, however we have not used this condition during the derivation of the multi-orbital Gross-Pitaevskii (MOGP) equation (6.16), they may thus lead to non-orthogonal solutions. One way to solve this problem would be to introduce additional Lagrange multipliers in equation (6.14) to account for the condition $\quad {}_i\quad {}_j\ =\delta_{ij}$, however this increases the number of variational parameters. Another possibility, convenient in numerical solution of the equations, is to enforce the orthogonality of wave functions after every integration step using, e.g., the Gram-Schmidt procedure. However, to avoid any bias towards one orbital or the other one must each time change the order of vectors in the orthogonalization algorithm.

The MOGP equation recovers the GP solution whenever it is the one with lowest possible energy since in this case the occupation of the super uous orbitals becomes zero. In this sense MOGP is the "Best Mean Field" technique [Cederbaum 03]. Moreover, there exist situations in which fragmentation of the condensate is energetically favourable, e.g., for repulsive bosons in an asymmetric double well in 1D [Streltsov 05], or when a fragmented state is a metastable solution of a problem to which no stable solution exists, e.g., for attractive bosons in 3D [Cederbaum 08]. To the best of our knowledge the method was not applied to disordered systems before. However, since the ground state of the weakly interacting system is known to be highly fragmented, one expects that the MOGP would capture the properties of the disordered system better then the standard GP equation. Indeed, we observe that separate orbitals form on the low-potential islands and the ground state of the system becomes fragmented.

6.2.2 Fixed-orbitals method

Taking into account our intuition about the behaviour of weakly interacting disordered bosons, we may simplify even further the description of such system. We fix the shape of the orbitals

to be the eigenstates of the corresponding single-particle problem and minimize the energy of the system with respect to occupation of such orbitals. The method will be referred to as the simple multi-orbital Hartree-Fock (sMOHF) approach.

We take the wave function in the Fock representation

$$\Psi \;=\prod_k \frac{(\hat{a}_k^\dagger)^{n_k}}{n_k!}\,\mathbf{0} \;=\; n_1\;\; n_2 \qquad n_L \tag{6.18}$$

where $\mathbf{0}$ is the vacuum of the system and $a_k^\dagger$ creates a particle in the kth non-interacting eigenstate ($k = 1 \qquad L$). Repulsive interactions of strength $g > 0$ yield an interaction energy given by

$$\begin{aligned}
\hat{U}_{\text{int}} &= \frac{g}{2}\left\langle \Psi \middle| \int \mathrm{d}\mathbf{r}\;\; \hat{}^\dagger(\mathbf{r})\;\hat{}^\dagger(\mathbf{r})\;\hat{}(\mathbf{r})\;\hat{}(\mathbf{r}) \middle| \Psi \right\rangle \\
&= \frac{g}{2}\sum_{\mathbf{k}} \int \mathrm{d}\mathbf{r}\;\; {}^*_{k_1}(\mathbf{r})\;\; {}^*_{k_2}(\mathbf{r})\;\; {}_{k_3}(\mathbf{r})\;\; {}_{k_4}(\mathbf{r})\;\; n_1 \qquad n_L\;\hat{a}_{k_1}^\dagger \hat{a}_{k_2}^\dagger \hat{a}_{k_3}\hat{a}_{k_4}\;\; n_1 \qquad n_L \\
&= \frac{g}{2}\sum_k \Big[n_k(n_k-1)O_{k,k} + 2\sum_{j\neq k} n_k n_j O_{k,j} \Big]
\end{aligned} \tag{6.19}$$

where in the second line $\mathbf{k} = \;\; k_1\;\; k_2\;\; k_3\;\; k_4\;$, and in the last line the only terms that survive are those with $k_1 = k_3$ and $k_2 = k_4$ or $k_1 = k_4$ and $k_2 = k_3$ (hence the factor two), and the term with $k_1 = k_2 = k_3 = k_4$. In the equation we use a short notation for the integrals, i.e., $O_{k,j} = \int \mathrm{d}\mathbf{r}\;\; {}_k(\mathbf{r})\;^2 \;\; {}_j(\mathbf{r})\;^2$.

The occupation probabilities n_k giving the ground state may now be found by minimizing the total energy subject to the constraints of normalization and positivity of all n_k:

$$E = \sum_k n_k \Big[E_k + \frac{g}{2}\sum_j (n_j - \delta_{k,j})\tilde{O}_{k,j} \Big] \tag{6.20}$$

$$\sum_k n_k = N \qquad {}_k\, n_k \geq 0$$

where we write (6.20) using $\widetilde{O} = 2O - \mathrm{Diag}(O)$ and E_k is the energy of the kth single-particle eigenstate. The minimization yields the linear system (one equation for each k):

$$\sum_j n_j \widetilde{O}_{j,k} = \frac{\mu + \gamma_k - E_k}{g} + \frac{\widetilde{O}_{k,k}}{2} \tag{6.21}$$

where the Lagrange multipliers γ_k and μ correspond to the conditions of positivity of each n_k and global normalization, respectively. Now, $\boldsymbol{\gamma}$ and μ should be adjusted following the well known Karush–Kuhn–Tucker (KKT) conditions [Boyd 04], which allow for solving the optimization problem in the case in which some of the constraints are in the form of inequalities. They read:

$$\sum_k n_k = N \;\&\; {}_k\, \gamma_k \geq 0 \;\&\; \gamma_k n_k = 0 \tag{6.22}$$

and together with (6.21) yield a nonlinear system of equations for $\mathbf{n}\;\; \boldsymbol{\gamma}\;\; \mu$.

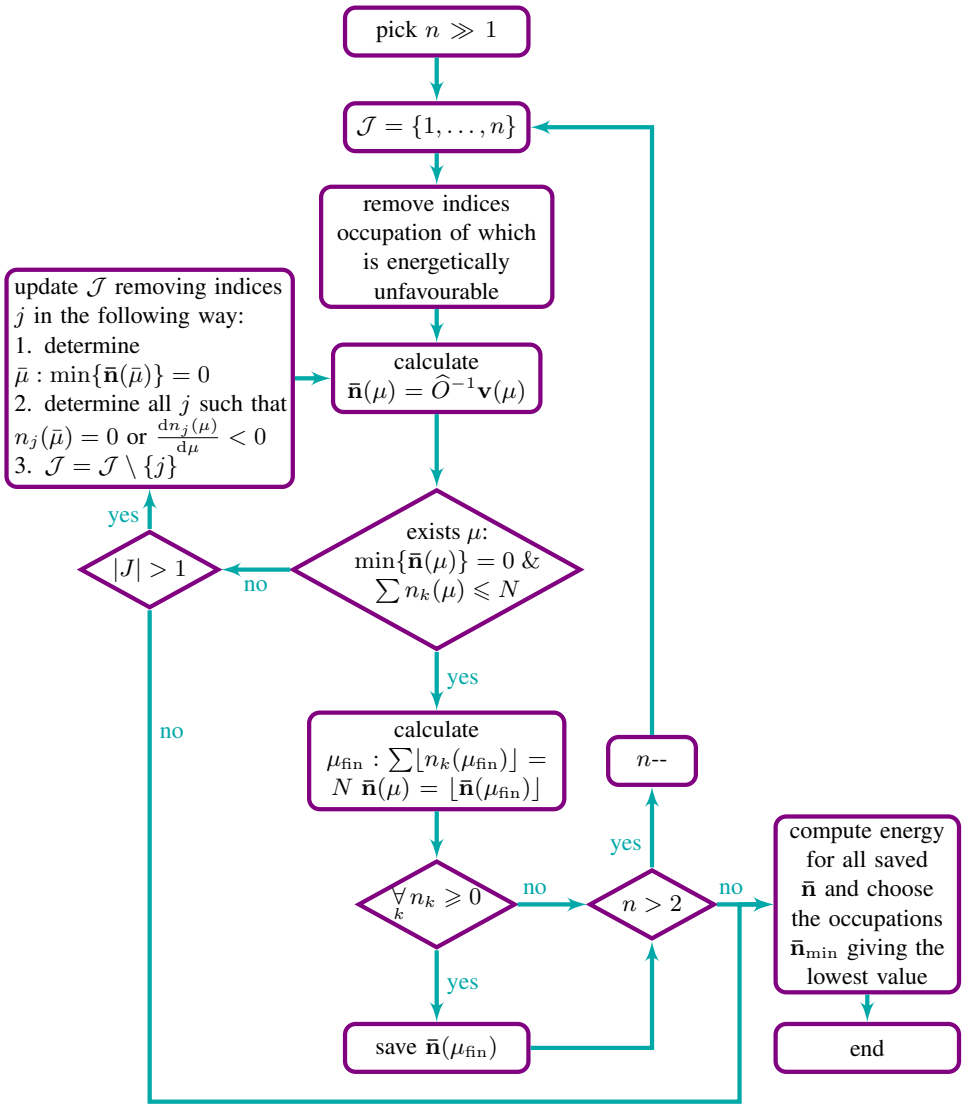

Figure 6.5: Flow diagram of the minimization algorithm

We solve the equations using the following algorithm. First we define the set of indices $\mathcal{J} = \{j : n_j > 0\}$ and using conditions (6.22) we rewrite equations (6.21) as

$$\sum_{j\in\mathcal{J}} n_j \widetilde{O}_{j,k} = \frac{\mu - E_k}{g} + \frac{\widetilde{O}_{k,k}}{2} \qquad \text{for } k \in \mathcal{J} \tag{6.23}$$

This is a system of $\mathcal{J}$ equations for occupations $n_j > 0$, which we arrange in a vector $\bar{\mathbf{n}} = [n_j]_{j\in\mathcal{J}}$. In order to write a formal solution of the problem we also define the following

vector and matrix

$$\mathbf{v}(\mu) = \left[\frac{\mu - E_j}{g} + \frac{\widetilde{O}_{j,j}}{2}\right]_{j\in\mathcal{J}} \qquad \widehat{O} = [\widetilde{O}_{k,j}]_{k,j\in\mathcal{J}} \tag{6.24}$$

We can now write the solution in the form

$$\bar{\mathbf{n}}(\mu) = \widehat{O}^{-1}\mathbf{v}(\mu) \tag{6.25}$$

and the problem reduces to finding the set $\mathcal{J}$ and adjusting the chemical potential μ to make the occupations fulfil the normalization constraint. Normally, in the weakly interacting regime only the low-energy eigenstates are occupied, which gives an indication as to how to look for the set $\mathcal{J}$. Moreover, in the search for the optimal set $\mathcal{J}$ one should take into account that moving a particle to an eigenstate which has a significant overlap with another eigenstate and higher energy (e.g., higher harmonics in a 1D well) is in most cases energetically unfavourable. The particular condition that should be applied to eliminate such eigenstates from set $\mathcal{J}$ are system-dependent and should be derived separately for each case. Our approach is summarized in the diagram in figure 6.5.

6.3 Bose gas in the random-impurities potential

In this section I am going to discuss the results published in [Stasińska 12a] concerning the properties of a bosonic gas on disordered 1D and 2D square lattices of linear dimension L. We consider the potential of randomly distributed impurities discussed in section 6.1.2 (the so-called Bernoulli potential), which on each site assumes the value:

$$V_i = \begin{cases} V > 0 & \text{with probability } 1-p \\ 0 & \text{with probability } p \end{cases} \tag{6.26}$$

with V_i being independent random variables ($i = 1 \qquad L^D$).

The use of the Bernoulli disorder is particularly appealing because its asymptotic properties become apparent even for small lattices (e.g., with $\sim 50^D$ sites). The Bernoulli potential has also optimal properties of convergence. Therefore, the random-impurities disorder is suitable for numerical simulations and due to its simple form, it allows for various analytical estimates.

6.3.1 Properties of a non-interacting gas

Let us start by discussing the properties of a non-interacting system, and in particular look at its ground state energy, and the density of low energy excited states. We consider a discretized system, i.e., the wave function is supported on equally spaced lattice sites and the 1D system Hamiltonian reads

$$H = -\Delta + V \tag{6.27}$$

with $-\Delta \ _i = 2 \ _i - \ _{i-1} - \ _{i+1}$ (we set $\hbar^2 \ 2m = 1$).

Ground state energy. — Minimization of a single-particle energy in a large 1D system with Bernoulli disorder reduces to finding the wave function minimizing the functional:

$$H \quad = \sum_{i=1}^{L}[(\ _i - \ _{i+1})^2 + V_i \ \ _i{}^2] = \qquad {}^2 + \sum_{i=1}^{L} V_i \ \ _i{}^2 \tag{6.28}$$

One observes that in order to minimize the potential term, the wave function can take non-zero values only on the sites of potential zero. On the other hand, the kinetic energy is minimized when the function is maximally spread over available volume. It turns out that the ground state of the non-interacting bosonic gas in such a potential is supported on the largest island of zero potential.

The linear size $L_{\max}^{(1\mathrm{D})}$ of the largest island scales as $L_{\max}^{(1\mathrm{D})}$ $\log L$ [Bishop 12]. The proof of this fact is based on the following observation. The probability of an island having length $k = 1\ 2$ is $P(\ = k) = p^{k-1}(1-p)$, which is the geometric distribution describing the probability of $k = 1\ 2$ failures (potential 0) until the first success (potential V). Then assuming that the number of all zero potential islands is N_{isl} we have

$$pL = \sum_{k=1}^{\infty} N_{\mathrm{isl}} k P(\ = k) = \frac{N_{\mathrm{isl}}}{1-p} \tag{6.29}$$

which tells that the total number of islands is proportional to the size of the system, namely $N_{\mathrm{isl}} = p(1-p)L$. Now the maximal size of an island $f(L)$ should scale with the system size in such way that it yields a non-zero and finite number of such islands in the limit L

$$\lim_{L\to\infty} N_{\mathrm{isl}} P(\ = f(L)) = \lim_{L\to\infty} p(1-p)Lp^{f(L)-1} = \lim_{L\to\infty} (1-p)Lp^{f(L)} = \mathrm{const} \tag{6.30}$$

The function f must be sub-linear since for $f(L)$ L or any expression polynomial in L the right-hand side of (6.30) gives 0. The correct scaling turns out to be $f(L) = \log L$ $\log p$, which is also confirmed by numerical simulations. Now, the ground-state energy is bounded from above by the energy of the first harmonic, i.e., a half-sine function, of the square well of the largest island. A lower bound of the same order was proved in [Bishop 12], showing that the minimum energy behaves asymptotically as $\pi^2\ (\log L)^2$ when L .

Similarly, one can argue that in a large D-dimensional system the ground state will occupy the largest spherical island of zero-potential sites since this shape minimizes the kinetic energy [Antal 95]. Its diameter can be shown to grow as $L_{\max}^{(\mathrm{D})}$ $(\log L)^{1/D}$, and therefore we expect the energy of the ground state to scale as E_0 $\log L^{-2/D}$. The proof of scaling of the island size is based on a similar argument as in the 1D case, although is a bit more involved. The numerical confirmation of the scaling for the 2D case is shown in the inset of figure 6.6.

Lifshits tail. — Since the disordered potential is chosen to be finite, the spectrum of the system is bounded from below. As a consequence, the spectrum is expected to exhibit a so-called Lifshits tail [Lugan 07, Simon 85], in the sense that the cumulative density of states (cDOS) $\mathcal{N}(\epsilon) = \int^{\epsilon} \mathrm{d}\epsilon'\ \mathcal{D}(\epsilon')$ behaves at low energies as

$$\mathcal{N}(\epsilon) \sim \exp\left[-c(\epsilon - V_{\min})^{-D/2}\right] \tag{6.31}$$

The cDOS and the associated Lifshits tail for the considered 2D system were obtained numerically and are shown in figure 6.6.

Excited states. — We expect that the Lifshits states lie on well-separated islands, and have almost degenerate energies since the islands linear sizes are approximately the same. This is true for 1D system, irrespectively of potential density $1-p$, as depicted in figure 6.7, where the low-energy eigenstates are shown. In a 2D system, however, the location of excited states depends on potential density. In figure 6.8 we show the ground state and

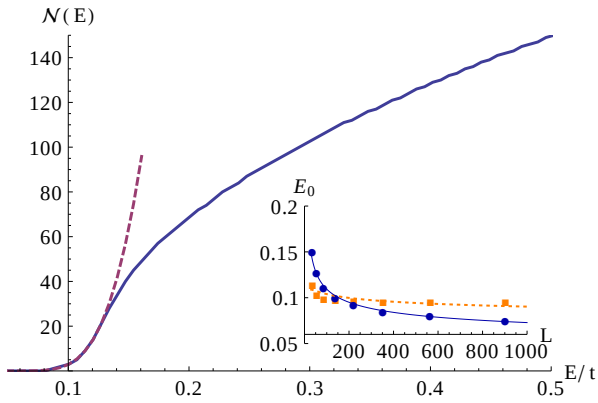

Figure 6.6: Properties of non-interacting dirty bosons in 2D. Main figure: the cumulative density of states $\mathcal{N}(\epsilon)$ shows a Lifshits tail (purple dashed line) given by (6.31). Here we have taken a 200×200 lattice, and averaged over 10 realizations. Inset: ground state energy E_0 in 2D plotted versus linear size of the system L; results for Bernoulli disorder are plotted in blue and scale as $\sim 1 \quad \log L$, while results for random-amplitude disorder (by random-amplitude disorder we understand the potential V being at each site a random variable uniformly distributed in the interval $[0 \ \Delta]$) are plotted in orange and scale as $\sim \log\log L \quad \log L$.

several eigenstates for 2D systems with moderate and low potential densities ($1 - p = 0\,6$ and $1 - p = 0\,2$). One can observe that in a finite system in the case when the scatterers are sparse, the ground state is localized on a single island however the excited states spread over several islands and overlap. This is not the case when the potential is dense, as clearly seen in the picture.

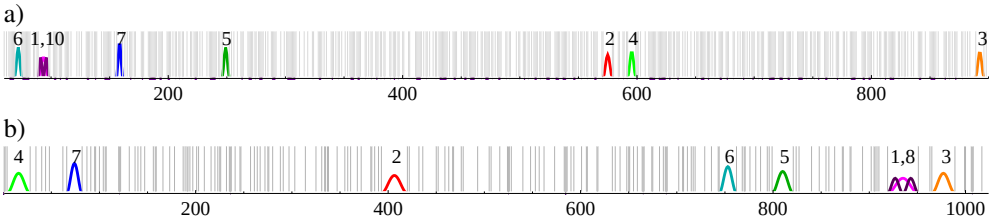

Figure 6.7: The ground state and excited states of a 1D system with a) $p = 0\,4$ and b) $p = 0\,8$. The eigenstates occupy well separated islands of zero potential in the order of length. An important point to note is that at some point an orthogonal wave function (second harmonic) on an already occupied island has lower energy than a sine wave placed on the next largest island.

The structure of excited states affects the minimisation procedure described in section 6.2.2. Whenever the eigenstates are localized on isolated islands they overlap only if they constitute different harmonics on the same island. In such case occupation of the second harmonic increases the interaction energy. Consequently, all the indices j fulfilling the following

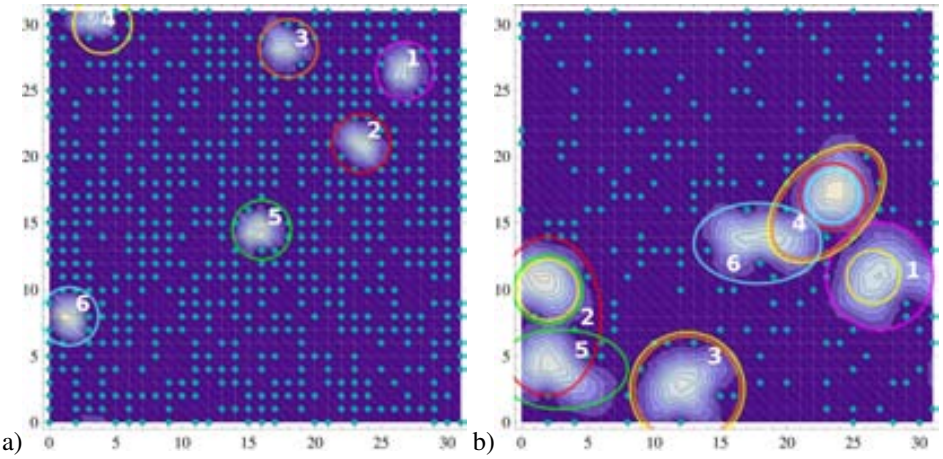

Figure 6.8: Eigenstates of a 2D system with a) $p = 0\,4$ and b) $p = 0\,8$. The eigenstates are marked by ellipsis of various colours, whenever there are several shapes of the same colour it means that the eigenstate spreads over several islands, several ellipsis of different colours surrounding the same area denote the overlap of the wave functions in this region. One observes that in the case of dense scatterers, the wave functions are situated on separate islands. On the other hand, when the potential is sparse the excited states are spread over several islands and may have significant overlap.

condition should be removed from $\mathcal{J}$

$$O_{k,k} \leqslant O_{j,j} \;\&\; O_{k,k} < O_{j,k} \tag{6.32}$$

In the case in which excited states are more extended than the ground state it may be advantageous to occupy the states with higher energy but smaller self-interaction term $gn_j(n_j - 1)O_{j,j}$.

6.3.2 Interacting case

Here we characterize the interacting system with the methods described in section 6.2. We present the numerical solutions of the sMOHF and MOGP equations (GP as a particular case of the latter), comparing the performance of the two methods. In particular, we discuss and compare the ground state energy, the super uid fraction, and the fractal dimension.

As we will see, sMOHF approach is suitable to describe a weakly-interacting system, whose ground state occupies few large islands of zero potential. The second method, the standard Gross–Pitaevskii (GP) equation, correctly describes the energy in both regimes, i.e., for weak and moderate ($g \;\rho \leq 1$) interactions. In the latter large overlaps between the islands and self-interaction on each island play an important role and the sMOHF approach fails to capture the physics of such system. We check that in 1D the MOGP method describes correctly the energy in both the regimes. Moreover, we observe that it captures the fragmentation of the ground state in the limit of weak interactions and gives the momentum distribution with much smaller zero-momentum peak than the GP equation. This, and the fact that also MOHF yields correct results in this regime confirms the intuition that the particles populate

low-lying well separated eigenstates, the Lifshits islands, that are not correlated among each other.

Before going into details, let us estimate when the sMOHF description based on non-interacting single particle states should be valid. As we have discussed, this regime corresponds to the Lifshits glass region. Let us assume that we have s filled islands of the characteristic linear size $_0 \quad \log L$, and "volume" $\quad {}^D_0$, so that the wave function is supported on a proportion of a total volume of the system

$$s \ {}^D_0 = cL^D \tag{6.33}$$

The proportionality constant c depends in general on p, $\rho = N \ L^D$ and V, which is discussed more thoroughly later in this section. Since we are interested in the weak interaction regime we can ignore this dependence.

The Lifshits glass regime occurs then for an inter-particle interaction coupling g smaller than the characteristic value $g_{\rm ch}$, at which the kinetic energy is comparable to the interaction energy. An estimate of the characteristic coupling is obtained by equating the kinetic energy per particle $\quad \pi^2 \quad {}^2_0$, with the interaction energy per particle $\quad gN \ (s \ {}^D_0)$. Using the expression (6.33) for $s \ {}^D_0$, we obtain

$$g_{\rm ch} \quad \frac{c\pi^2 L^D}{N \ {}^2_0} \quad \frac{c\pi^2}{\rho} \left(\frac{\log p}{\log L} \right)^{2/D} \tag{6.34}$$

This scaling provides a good estimate of the order of the coupling constant at which the two energies depicted in figure 6.9 start to diverge.

Below we present the results of numerical simulations. Unless otherwise noted, the results presented in this section are obtained for a system on either a 1D or a 2D lattice with 1024 or 32×32 sites, respectively, $N = 10^4$ particles, and the Bernoulli potential with $V = 5$ or $V = 50$. Where needed, we perform appropriate averages to obtain results which are independent of the particular disorder configuration.

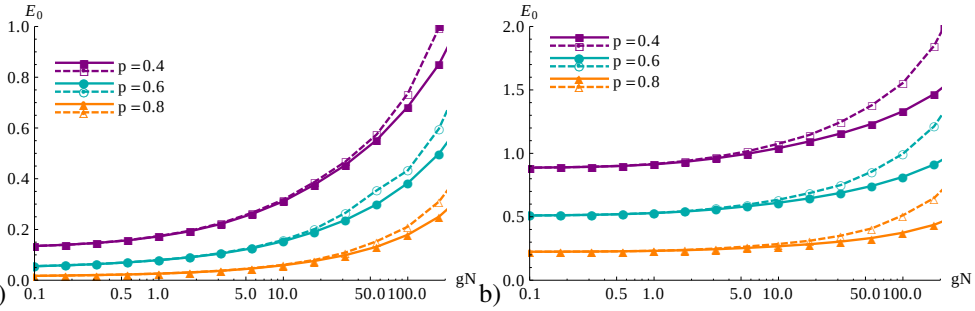

Figure 6.9: Ground state energies obtained by sMOHF (dashed) and GP (continuous) for various disorder densities p for a) 1D and b) 2D system. The value of the coupling constant at which the energies obtained by the two methods start to diverge is estimated by equation (6.34). Results obtained by averaging over 5 simulations and $V = 5$.

Energy. — In figure 6.9 we compare the energies obtained through the sMOHF approach with those obtained from the GP equation as a function of the interaction strength g (we do not observe significant energy difference between the GP and MOGP approach, therefore here we

show only the results for the former). For a coupling constant g smaller than a characteristic value $g_{\rm ch}$, the minimization of expression (6.20) and the GP equation yield the same values of energy proving that sMOHF method correctly describes the system in this limit. The characteristic value $g_{\rm ch}$ estimates the interaction strength at which the energy obtained from the sMOHF starts to differ from the one obtained through the GP equation. For values of the interaction $g \rangle \quad g_{\rm ch}$, the disorder plays a negligible role and the energy per particle saturates to the analytic value $E = \overline{E} + g\rho \ 2$, where $\overline{E}$ is a constant that depends on V and p. This analytic solution is recovered by the numerical results for the GP equation, but not by the sMOHF approach.

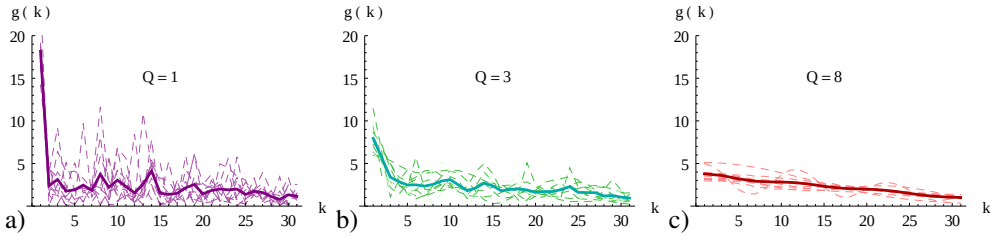

Figure 6.10: Momentum distribution $g(k)$ for 10^2 particles in a 1D lattice with 1024 sites, $g = 0\ 001$, and potential characterized by $p = 0\ 8\ V = 5$. Results averaged over 10 realizations of the potential; the strongly uctuating results for each potential are also visible in the pictures. Number of components enforced in the MOGP equation is depicted in each figure.

Momentum distribution. — In order to see that the MOGP approach provides an adequate description of fragmentation of the system, we compute the momentum distribution for the MOGP and GP wave functions defined as

$$g(k) = \frac{1}{2\pi}\frac{1}{N}\int \mathrm{d}\mathbf{r}\,\mathrm{d}\mathbf{r}' \sum_{i=1}^{Q} \ {}^{*}_{i}(r) \ {}_{i}(r')e^{-ik(r-r')} \tag{6.35}$$

We enforce MOGP wave-function to occupy fixed number of orbitals to compare several distributions. The obtained results are depicted in figure 6.10. As we may see, GP yields $g(k)$ strongly-peaked at $k = 0$, indicating that a large number of particles occupy a single and large BEC component. Instead, the MOGP gives a much lower peak, which confirms that the particles are distributed among different orbitals. The behaviour of $g(k)$ at large momentum is similar for GP and MOGP.

Super uid fraction. — We compute the super uid fraction $\rho_{\rm sf}$ solving numerically the GP equation for a periodic system with twisted boundary conditions along one direction. Our results are depicted in figure 6.11. In the regime where sMOHF provides a good description, the SF fraction is negligible because the localized single-particle eigenstates experience an exponentially small energy change due to the imposed phase shift. The region in which GP equation yields a perceptibly lower energy than sMOHF coincides with the range of interaction for which the super uid fraction $\rho_{\rm sf}$ becomes sufficiently large ($\rho_{\rm sf} \gtrsim 0\ 1$). Note that for large values of potential ($V \rangle \quad 1$), the curve of the super uid fraction levels off at intermediate values of g. This corresponds to the situation in which the wave function fills all the area of potential zero. Since the positive value of potential is high, it is energetically unfavourable to put a significant mass of a wave-function outside the zero potential region. Consequently,

as the repulsion between the particles increases the shape of the wave-function squares off to decrease the interaction energy.

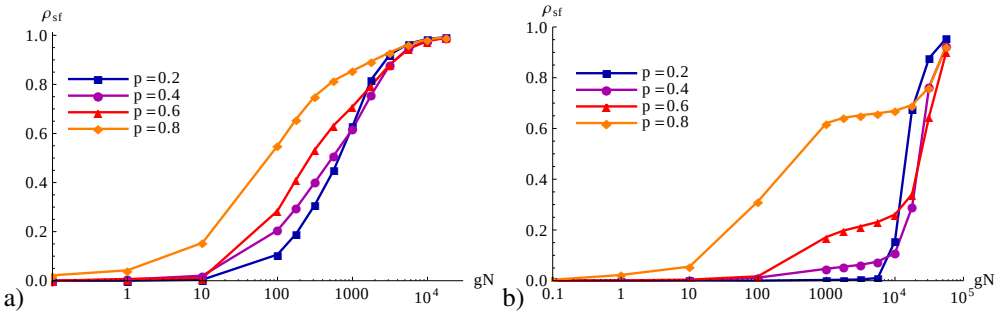

Figure 6.11: Super uid fraction $\rho_{\rm sf}$ as a function of potential density p and interaction strength g for a) $V = 5$ b) $V = 50$.

Fractal dimension. — As we have discussed in the previous sections, the ground state of a weakly-interacting gas is localized on one or several Lifshits islands. When interactions start to play an important role, the extension of the ground state increases, generally, until the gas occupies all available space. In order to provide a quantitative measure of the extension of the ground state, we calculate its fractal dimension d^* [Kramer 93], and introduce here the concept of *fractional occupation* c.

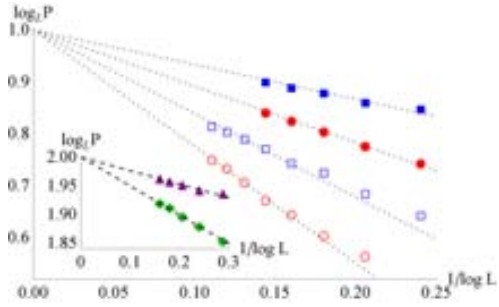

Figure 6.12: Scaling of the logarithm of the participation number $\log_L P$ versus the inverse of the logarithm of the lattice size. The slope of the lines, being the logarithm of c, allows for determining the fraction of space occupied by the state. Main figure: 1D lattice of length L, and interaction strengths $g = 0\ 1$ (empty) and $g = 10$ (filled). The potential densities are respectively $p = 0\ 4$ (red circles) and $0\ 7$ (blue squares). Inset: 2D lattice of linear size L, interaction strength $g = 10$, potential parameter $p = 0\ 6$ (green diamonds), $0\ 8$ (purple triangles).

The fractal dimension is defined as a minimum d^* such that

$$\lim_{L\to\infty} \frac{P}{L^{d^*}} = c \quad c > 0 \tag{6.36}$$

Here $P = 1 \quad \int \mathrm{d}\mathbf{r}\ \rho(\mathbf{r})\ ^4$ is the so-called "participation number" of the ground state [Kramer 93]. For an extended state such as a plane wave one finds that P is proportional to the volume of

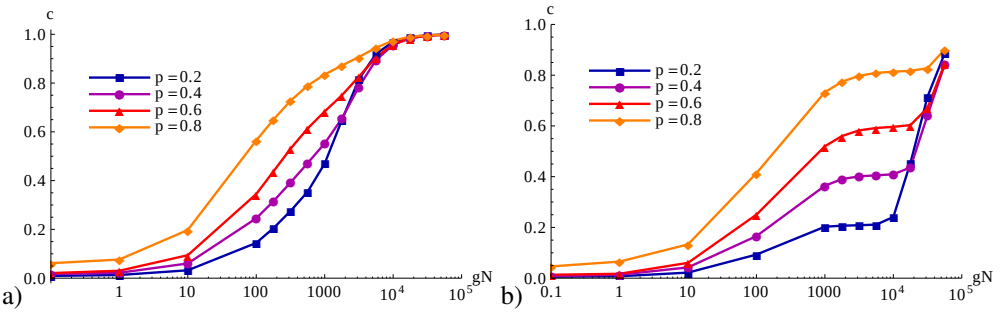

Figure 6.13: Fractional occupation c of the ground state as a function of potential density p and interaction strength g for a) $V = 5$ and b) $V = 50$. Here we have considered a 2D lattice and c was obtained by averaging over 5 potential realizations.

the system, and therefore the fractal dimension equals the Euclidean dimension, $d^* = D$. Instead, for a state which is localized in a volume Q, the participation number behaves as Q, and the corresponding fractal dimension vanishes if Q grows slower than any power of L. For instance, the ground state of the non-interacting disordered system with Bernoulli disorder is localized on an island of volume $Q \sim \log L$ which for all α grows slower then L^α giving $d^* = 0$. Hence, in general, one has $0 \leq d^* \leq D$.

Analysing the results obtained from both sMOHF and GP approaches, we find that $d^* = D$ for any $g > 0$. This may be understood as follows. Assuming that d^* is bounded strictly below D, we see that the interaction energy per particle $(gN\ 2) \int \mathrm{d}\mathbf{r}\ \rho(\mathbf{r})^{\ 4}$ diverges. Physically, there is not enough space for the particles to keep the interaction energy bounded unless they spread out through a non-zero proportion of the whole space. If $\log_L P = D - f(L)$, and $\lim_{L\to\infty} L^D\ L^{d^*} = c$, then it must be that $L^{f(L)}$ c, so $f(L) \approx \log(c)\ \log(L)$. Numerical results confirm this behaviour in both 1D and 2D. To show this, in figure 6.12 we plot $\log_L P$ as a function of $1\ \log L$ for a 1D system and a 2D system (inset).

The quantity c, which takes values between 0 and 1, can be interpreted as the fraction of space occupied by the ground state, and we will therefore refer to it as the *fractional occupation* of the ground state. We show our results for the fractional occupation in figure 6.13. For strong disorder ($V \rangle\ t$) the fractional occupation c displays at intermediate interactions a plateau at $\sim p$ which coincides with a similar plateau in the plot of the super uid fraction (*cf.* figures 6.11b and 6.13b). Due to a fairly simple structure of the system we can estimate the range of g with such behaviour of c and ρ_{sf}. We concentrate on a 1D case for simplicity.

For large interactions one may use the Thomas-Fermi approximation (neglect the kinetic energy). Suppose we choose an ansatz such that the wave function equals m $\overline{pL}$ on sites of zero potential and $\overline{1-m^2}$ $\overline{qL}$ on the remaining sites ($0 \leqslant m \leqslant 1$), then the value of m^2 minimizing the energy is $m^2 = p + pqV\ (g\rho)$. If $g\rho < pV$, the above ansatz becomes invalid, and the ground state stays exclusively on sites of zero potential. This estimates the value of g at which the plateau begins; to derive the value of g at which it finishes we compare the energy of a wave function equal to 1 $\overline{pL}$ on sites of zero potential and zero elsewhere to a wave function that is equal to 1 $\overline{L}$ everywhere. Ignoring the kinetic energy terms (which we can control by another parameter), we see that the first wave function provides a better variational ansatz if $g\rho\ 2 \leq pV$. This means that for $pV \lesssim g\rho \lesssim 2pV$, we are in an area where $c \approx p$, that is, the kinetic energy and interaction energy are balancing, but any significant support of

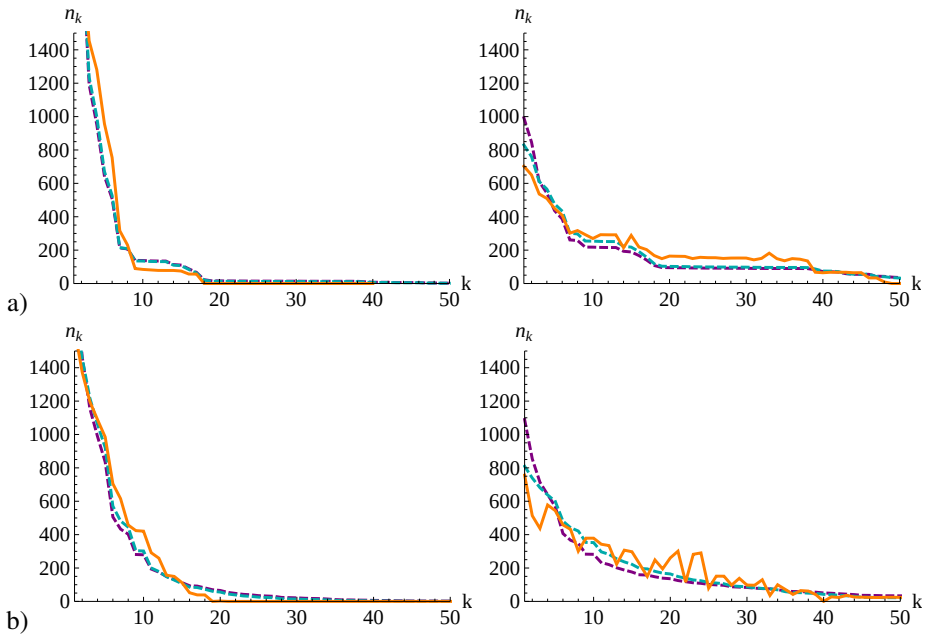

Figure 6.14: Occupations of the single particle states for the 1D system with a) $p = 0\ 4$, b) $p = 0\ 8$. In the left column $gN = 5\ 62$, in the right $gN = 50\ 6$ and the temperatures were adjusted to agree with the density profile and are slightly higher for Bose-Einstein distribution. The lines are: Boltzmann, Bose-Einstein, and sMOHF. Results averaged over 5 simulations.

the ground state on the sites occupied by scatterers is too costly. Since the wave function does not spread significantly in this regime, also the super uid fraction remains constant.

6.3.3 Comparison of temperature and interaction effects

In this section we turn to the analysis of the effects of non-zero temperature in a non-interacting system. We will see that those remind very much the effects of interactions at zero temperature.

For free boson systems, the effects of temperature may be studied by expanding arbitrary states in the basis of non-interacting eigenstates, in analogy with what we did to treat the interacting case (sMOHF). In this approximation, the average density of the gas reads

$$\rho(\mathbf{x}) = L^{-D} \sum n_k \quad {}_k(\mathbf{x})^{\,2} \tag{6.37}$$

The occupation factors depend on the statistics of the particles. Identical bosons follow the Bose–Einstein distribution

$$n_k = \frac{1}{\mathrm{e}^{(E_k-\mu)/T} - 1} \tag{6.38}$$

Distinguishable (or classical) particles would instead populate the non-interacting eigenstates following a Boltzmann distribution, $n_k = \mathrm{e}^{-(E_k-\mu)/T}$.

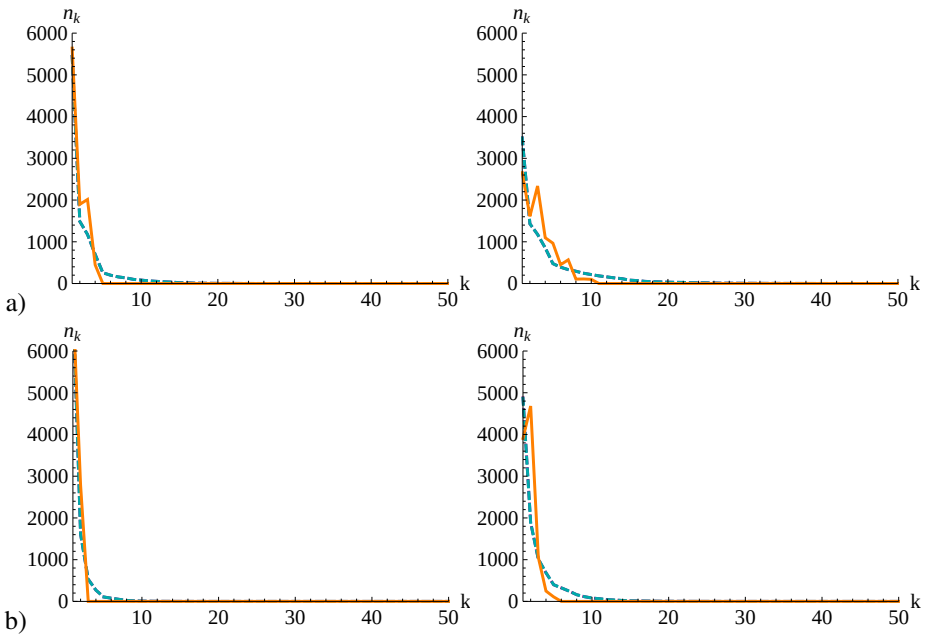

Figure 6.15: Occupations of the single particle states for the 2D system with a) $p = 0\ 4$, b) $p = 0\ 8$. In the left column $gN = 5\ 62$, in the right $gN = 17\ 8$ and the temperatures were adjusted to agree with the density profile of the interacting gas. The lines are: Boltzmann, Bose-Einstein (covered by Boltzman), and sMOHF. Results averaged over 5 simulations.

At zero temperature, only the lowest energy state has a non-zero population, i.e., $n_k = N\delta_{0,k}$. Non-zero temperatures modify the occupation probabilities, redistributing the population over the higher energy states, but we expect that for $T \leq 1$ only the lowest energy states (the Lifshits states) are populated.

We note here that in an interacting 2D Bose gas of finite extension one generally expects a crossover between two qualitatively different regimes. At very low temperatures ($T < T_C$) phase correlations in the gas decay algebraically with distance. For temperatures larger than the critical value T_C instead, phase correlations decay exponentially with distance. This switch in the decay of correlations can be traced back to the dissociation of bound vortex-antivortex pairs at $T > T_C$. The crossover becomes a real phase transition in an infinite system, and the underlying mechanism goes under the name of Berezinskii-Kosterlitz-Thouless (BKT) transition [Berezinskii 72, Kosterlitz 73].

Our approach to finite temperatures is rather crude, and is not well suited to describe the BKT physics, which requires considering both temperature and interactions at the same time. However, for the range of parameters considered in this manuscript, our model provides a qualitative, although simplified, explanation of the complementary roles played by temperature and interactions. Moreover, a similar scenario to the one considered here is present in three dimensions, where a true BEC exists at low temperatures contrary to 1D and 2D where condensation occurs only at $T = 0$, while at $T < T_c$ there are phase uctuations and a quasi-condensate is formed.

As the temperature raises, the cloud gets to occupy more and more islands; when $T \lesssim V$ it will populate only the unoccupied sites, and for $T \rangle \quad V$ it will occupy even sites inhabited by scatterers. While a classical cloud quickly spreads over various low energy states, a bosonic gas at low temperatures tends to condense in a single or few Lifshits states. Interaction effects in a bosonic cloud at $T = 0$, instead, yield at first sight a state which very much resembles the finite temperature case. Even for moderate repulsive interactions, the cloud spreads over various Lifshits states.

The occupation n_k for the three cases analysed above (Boltzmann, Bose, and interacting) are shown in figures 6.14 and 6.15 for a 1D and 2D systems, respectively. Since the lowest-energy single-particle states for a 1D system and 2D system with large or moderate potential density $1 - p$ correspond to the localized and well separated Lifshits states, a population distribution is narrow with a peak at low energies. On the other hand, in a 2D system with sparse potential peaks the excited states tend to be more extended than the ground state (*cf.* discussion in section 6.3.1), consequently their occupation lowers the interaction energy and may be more advantageous for stronger interaction. Therefore, as can be seen in figure 6.15b, the 2D interacting gas in a potential with $1 - p = 0\ 2$ has an occupation distribution with a peak at the ground state for weak interaction and at an excited state for slightly higher g.

As the temperature increases the Bose liquid tends to have narrow population distribution, while the Boltzmann and interacting distributions spread more quickly. As a result, the temperature of a Bose gas that gives the density matching the interacting case is slightly higher than the corresponding temperature for the Boltzman gas.

6.4 Conclusions

We have considered a bosonic lattice gas in the presence of Bernoulli disorder, realised, e.g., by localising in a lattice identical random scatterers. We have shown that in this case it is possible to provide precise analytical estimates of ground state wave function and energy even for the interacting case. We have compared two theoretical schemes, the simplified multi-orbital Hartree–Fock and the (multi-orbital) Gross–Pitaevskii approaches, showing how the first is very accurate in the glassy regime of strong disorder, but fails when interactions bring the system into an extended state and the super uid fraction reaches values $\rho_{sf} \gtrsim 0\ 1$.

Further, we have shown analytically that the fractal dimension for this kind of potential tends to the physical dimension of the system. As a result, we have introduced a quantity termed *fractional occupation*, which characterizes the typical extension of the system. It is expected that when the latter becomes of order p, i.e., the fraction of physical space where scatterers are absent, the system crosses over from the Lifshits to the Bose glass. Finally, we have discussed the similarities and differences between effects due to interaction and temperature. This question is of fundamental importance for ongoing experiments, since in a laboratory the two effects are often difficult to distinguish.

The numerical results presented in this chapter were obtained using software written by the author. The numerical simulations for MOGP are based on the Suzuki-Trotter algorithm for the imaginary time evolution. The algorithm used for the minimization problem of sMOHF was design for this specific application.

Chapter 7

Summary and outlook

In the thesis we have considered several physical systems in which correlations, either intrinsically present or specially engineered, play a crucial role. In particular, we have shown how the application of what we call the geometric set-up for the QND-Faraday atom-light interface facilitates generation, manipulation and detection of multipartite entanglement between atomic ensembles. Second, we have analysed the separability properties of tripartite subsystems of spin networks. We have concentrated on spin-1 2 particles and applying the necessary and sufficient separability criteria for rotationally invariant three-qubit systems we verified the presence of tripartite entanglement in ground and thermal states of Heisenberg and XXZ Hamiltonians. Finally, we have studied the properties of the system of bosons in the presence of random-impurities disorder, contributing to the understanding of the interplay between the localization caused by disorder and the counteractive effect of repulsive interactions. Due to the simplicity of the disordered potential we were able to provide several analytical estimates, e.g., assess the applicability of the simple multi-orbital Hartree-Fock description of the system.

n this thesis, I have as well consider the problem of characterization of correlations as a resource for quantum information. We have studied tasks (Bell inequalities) for which quantum and classical resources work equally well, and only more general non-signalling correlations enable one to perform them more efficiently. We have provided a systematic method for construction of such tasks, showing an intriguing connection to Unextendible Product Bases.

There are several research directions to follow. The studies of multipartite correlations in many-body systems and its connection to quantum phase transitions is at an early stage. The systems we have analysed in chapter 5 are far from the many-body limit and it would be interesting to investigate the separability properties in larger networks and higher spins, in particular spin-1 systems, with certain symmetries. For example, recent work reveals that multipartite entanglement may be a better indicator of quantum phase transitions in spin models if the interaction involves more than two spins [Bera 12].

The link between Unextendible Product Bases (UPB) and Bell inequalities that are not violated by quantum mechanics, studied in chapter 4 is also not fully understood. As it was shown in [Augusiak 12], the construction may lead to tight Bell tests, however, it is not clear which (if any) properties of a UPB decide whether a corresponding Bell inequality is tight.

Finally, the topic of Bose gas in the presence of random-impurities can be explored from

a different perspective. In chapter 6 we have concentrated on the limit of strong interaction between the Bose gas and the impurity atoms. In this case, the latter act effectively as a disordered potential. In the limit of weak interaction, however, the impurities induce disorder of a different type, i.e., they may affect (i) the on-site interaction between bosons, and (ii) their tunnelling constant. This observation may pave the way for experimental realisation of this kind of disorder, however a detailed feasibility study is still missing.

Acknowledgements

I would like to take the opportunity to thank everyone with whom I have had a pleasure to work during this four years. In the first place Anna who, apart from her knowledge and research experience, has always contributed a great deal of enthusiasm to every project. She always encouraged me to work on variety of topics and collaborate with many researchers from different groups for which I am grateful to her. I would like to thank Simone, Carles, Gabriele, Ben, Janek, Michael, Maciek, Pietro, Laurent, Toni, Chris and Jarek for all the things I have learnt from them during our collaboration. It was a terrific experience.

Special acknowledgements go to my boyfriend/collaborator Remigiusz, who was always very supportive and understanding and helped me with a good advise both in life and in research.

Last but not least, I would like to thank all the current and former GIQs and all the nice people I was meeting daily in the IFAE corridors for creating a friendly and lively atmosphere. I am going to miss You.

Bibliography

[Acín 01] A. Acín, D. Bruß, M. Lewenstein & A. Sanpera. *Classification of mixed three-qubit states*. Phys. Rev. Lett., vol. 87, page 040401, 2001.

[Acín 07] A. Acín, N. Brunner, N. Gisin, S. Massar, S. Pironio & V. Scarani. *Device-independent security of quantum cryptography against collective attacks*. Phys. Rev. Lett., vol. 98, page 230501, 2007.

[Acín 10] A. Acín, R. Augusiak, D. Cavalcanti, C. Hadley, J. K. Korbicz, M. Lewenstein, Ll. Masanes & M. Piani. *Unified framework for correlations in terms of local quantum observables*. Phys. Rev. Lett., vol. 104, page 140404, 2010.

[Acín 12a] A. Acín, M. L. Almeida, R. Augusiak & N. Brunner. *Guess your neighbour's input: No quantum advantage but an advantage for quantum theory*. In Quantum Theory: Informational Foundations and Foils. 2012.

[Acín 12b] A. Acín, S. Massar & S. Pironio. *Randomness versus nonlocality and entanglement*. Phys. Rev. Lett., vol. 108, page 100402, 2012.

[Adesso 07] G. Adesso & F. Illuminati. *Entanglement in continuous-variable systems: Recent advances and current perspectives*. J. Phys. A: Math. Theor., vol. 40, 2007.

[Akkermans 06] E. Akkermans & G. Montambaux. *Mesoscopic physics of electrons and photons*. Cambridge University Press, New York, 2006.

[Almeida] M. L. Almeida. *Private communication*.

[Almeida 10] M. L. Almeida, J. D. Bancal, N. Brunner, A. Acín, N. Gisin & S. Pironio. *Guess your neighbor's input: A multipartite nonlocal game with no quantum advantage*. Phys. Rev. Lett., vol. 104, page 230404, 2010.

[Amico 08] L. Amico, A. Osterloh & V. Vedral. *Entanglement in many-body systems*. Rev. Mod. Phys., vol. 80, page 517, 2008.

[Amselem 09] E. Amselem & M. Bourennane. *Experimental four-qubit bound entanglement*. Nat. Phys., vol. 5, page 748, 2009.

[Andersen 10] U. L. Andersen, G. Leuchs & C. Silberhorn. *Continuous-variable quantum information processing*. Laser Photonics Rev., vol. 4, page 337, 2010.

[Anderson 58] P. W. Anderson. *Absence of diffusion in certain random lattices*. Phys. Rev., vol. 109, page 1492, 1958.

[Ando 88] T. Ando & H. Fukuyama, ed. *Anderson localization*, Springer Proceedings in Physics, vol. 28, Heidelberg, 1988. Springer.

[Antal 95] P. Antal. *Enlargement of obstacles for the simple random walk*. Ann. Probab., vol. 23, page 1061, 1995.

[Aolita 11] L. Aolita, A. Roncaglia, A. Ferraro & A. Acín. *Gapped two-body hamiltonian for continuous-variable quantum computation*. Phys. Rev. Lett., vol. 106, 2011.

[Appel 09] J. Appel, P. J. Windpassinger, D. Oblak, U. B. Hoff, N. Kjærgaard & E. S. Polzik. *Mesoscopic atomic entanglement for precision measurements beyond the standard quantum limit*. Proc. Natl. Acad. Sci. U.S.A., vol. 106, page 10960, 2009.

[Audenaert 02] K. Audenaert, J. Eisert, M. Plenio & R. F. Werner. *Entanglement properties of the harmonic chain*. Phys. Rev. A, vol. 66, page 042327, 2002.

[Augusiak 06] R. Augusiak & P. Horodecki. *Bound entanglement maximally violating Bell inequalities: Quantum entanglement is not fully equivalent to cryptographic security*. Phys. Rev. A, vol. 74, page 010305, 2006.

[Augusiak 07] R. Augusiak & J. Stasińska. *Rotationally invariant bipartite states and bound entanglement*. Phys. Lett. A, vol. 363, page 182, 2007.

[Augusiak 11] R. Augusiak, J. Stasińska, C. Hadley, J. Korbicz, M. Lewenstein & A. Acín. *Bell inequalities with no quantum violation and unextendable product bases*. Phys. Rev. Lett., vol. 107, page 070401, 2011.

[Augusiak 12] R. Augusiak, T. Fritz, Ma. Kotowski, Mi. Kotowski, M. Paw owski, M. Lewenstein & A. Acín. *Tight Bell inequalities with no quantum violation from qubit unextendible product bases*. Phys. Rev. A, vol. 85, page 042113, 2012.

[Barnum 10] H. Barnum, S. Beigi, S. Boixo, M. B. Elliott & S. Wehner. *Local quantum measurement and no-signaling imply quantum correlations*. Phys. Rev. Lett., vol. 104, page 140401, 2010.

[Barrett 05a] J. Barrett, L. Hardy & A. Kent. *No signaling and quantum key distribution*. Phys. Rev. Lett., vol. 95, page 010503, 2005.

[Barrett 05b] J. Barrett, N. Linden, S. Massar, S. Pironio, S. Popescu & D. Roberts. *Nonlocal correlations as an information-theoretic resource*. Phys. Rev. A, vol. 71, page 022101, 2005.

[Bell 64] J. S. Bell. *On the Einstein–Podolsky–Rosen paradox*. Phys. Lett. A, vol. 1, page 195, 1964.

[Bennett 96] C. H. Bennett, G. Brassard, S. Popescu, B. Schumacher, J. Smolin & W. K. Wootters. *Purification of noisy entanglement and faithful teleportation via noisy channels*. Phys. Rev. Lett., vol. 76, page 722, 1996.

[Bennett 99a] C. H. Bennett, D. P. DiVincenzo, C. A. Fuchs, T. Mor, E. Rains, P. W. Shor, J. A. Smolin & W. K. Wootters. *Quantum nonlocality without entanglement*. Phys. Rev. A, vol. 59, page 1070, 1999.

[Bennett 99b] C. H. Bennett, D. P. DiVincenzo, T. Mor, P. W. Shor, J. A. Smolin & B. Terhal. *Unextendible product bases and bound entanglement*. Phys. Rev. Lett., vol. 82, page 5385, 1999.

[Bera 12] M. N. Bera & U. Sen R. Prabhu A. Sen De. *Multisite entanglement acts as a better indicator of quantum phase transitions in spin models with three-spin interactions*. arXiv:1209.1523 [quant-ph], 2012.

[Berezinskii 72] V. L. Berezinskii. *Destruction of long-range order in one-dimensional and two-dimensional systems possessing a continuous symmetry group. ii. quantum systems.* Sov. Phys. JETP, vol. 34, page 610, 1972.

[Billy 08] J. Billy, V. Josse, Z. Zuo, A. Bernard, B. Hambrecht, P. Lugan, D. Clément, L. Sanchez-Palencia, P. Bouyer & A. Aspect. *Direct observation of Anderson localization of matter waves in a controlled disorder.* Nature, vol. 453, page 891, 2008.

[Bishop 12] M. Bishop & J. Wehr. *Ground state energy of the one-dimensional discrete random Schrödinger operator with Bernoulli potential*. J. Stat. Phys., vol. 147, page 529, 2012.

[Bloch 08] I. Bloch & W. Zwerger. *Many-body physics with ultracold gases*. Rev. Mod. Phys., vol. 80, page 885, 2008.

[Bovino 05] F. Bovino, G. Castagnoli, A. Ekert, P. Horodecki, C. Alves & A. Sergienko. *Direct measurement of nonlinear properties of bipartite quantum states*. Phys. Rev. Lett., vol. 95, page 240407, 2005.

[Boyd 04] S. Boyd & L. Vandenberghe. *Convex optimization*. Cambridge University Press, New York, 2004.

[Braginsky 96] V. Braginsky & F. Khalili. *Quantum nondemolition measurements: The route from toys to tools*. Rev. Mod. Phys., vol. 68, page 1–11, 1996.

[Braunstein 05] S. L. Braunstein & P. van Loock. *Quantum information with continuous variables*. Rev. Mod. Phys., vol. 77, page 513, 2005.

[Bravyi 04] S. B. Bravyi. *Unextendible product bases and locally unconvertible bound entangled states*. Quantum Inf. Process., vol. 3, page 309, 2004.

[Breuer 05] H.-P. Breuer. *State space structure and entanglement of rotationally invariant spin systems*. J. Phys. A: Math. Gen., vol. 38, page 9019, 2005.

[Breuer 06] H.-P. Breuer. *Optimal entanglement criterion for mixed quantum states*. Phys. Rev. Lett., vol. 97, page 080501, 2006.

[Briegel 98] H.-J. Briegel, W. Dür, J. I. Cirac & P. Zoller. *Quantum repeaters: The role of imperfect local operations in quantum communication*. Phys. Rev. Lett., vol. 81, page 5932, 1998.

[Brukner 04] C. Brukner, M. Zukowski, J.-W. Pan & A. Zeilinger. *Bell's inequalities and quantum communication complexity*. Phys. Rev. Lett., vol. 92, page 127901, 2004.

[Brunner 05] N. Brunner, N. Gisin & V. Scarani. *Entanglement and non-locality are different resources*. New J. Phys., vol. 7, page 88, 2005.

[Bruß 05] D. Bruß, N. Datta, A. Ekert, L. Kwek & C. Macchiavello. *Multipartite entanglement in quantum spin chains*. Phys. Rev. A, vol. 72, page 014301, 2005.

[Bruß 11] D. Bruß & C. Macchiavello. *Multipartite entanglement in quantum algorithms*. Phys. Rev. A, vol. 83, page 052313, 2011.

[Buhrman 10] H. Buhrman, S. Massar & R. de Wolf. *Nonlocality and communication complexity*. Rev. Mod. Phys., vol. 82, page 665, 2010.

[Buluta 11] I. Buluta, S. Ashhab & F. Nori. *Natural and artificial atoms for quantum computation*. Rep. Prog. Phys., vol. 74, page 104401, 2011.

[Cavalcanti 10] D. Cavalcanti, L. Aolita, A. Ferraro, A. García-Saez & A. Acín. *Macroscopic bound entanglement in thermal graph states*. New J. Phys., vol. 12, page 025011, 2010.

[Cederbaum 03] L. Cederbaum & A. Streltsov. *Best mean-field for condensates*. Phys. Lett. A, vol. 318, page 564, 2003.

[Cederbaum 08] L. Cederbaum, A. Streltsov & O. Alon. *Fragmented metastable states exist in an attractive Bose-Einstein condensate for atom numbers well above the critical number of the Gross-Pitaevskii theory*. Phys. Rev. Lett., vol. 100, 2008.

[Cerf 05] N. Cerf, N. Gisin, S. Massar & S. Popescu. *Simulating maximal quantum entanglement without communication*. Phys. Rev. Lett., vol. 94, page 220403, 2005.

[Clarisse 06] L. Clarisse & P. Wocjan. *On independent permutation separability criteria*. Quant. Inf. Comput., vol. 6, page 277, 2006.

[Colbeck 11] R. Colbeck & A. Kent. *Private randomness expansion with untrusted devices*. J. Phys. A: Math. Theor., vol. 44, page 095305, 2011.

[Damski 03] B. Damski, J. Zakrzewski, L. Santos, P. Zoller & M. Lewenstein. *Atomic Bose and Anderson glasses in optical lattices*. Phys. Rev. Lett., vol. 91, page 080403, 2003.

[De Chiara 11] G. De Chiara, O. Romero–Isart & A. Sanpera. *Probing magnetic order in ultracold lattice gases*. Phys. Rev. A, vol. 83, page 021604, 2011.

[de Oliveira 06] T. de Oliveira, G. Rigolin, M. de Oliveira & E. Miranda. *Multipartite entanglement signature of quantum phase transitions*. Phys. Rev. Lett., vol. 97, page 170401, 2006.

[Deissler 10] B. Deissler, M. Zaccanti, G. Roati, C. D Errico, M. Fattori, M. Modugno, G. Modugno & M. Inguscio. *Delocalization of a disordered bosonic system by repulsive interactions*. Nat. Phys., vol. 6, page 354, 2010.

[Deutsch 96] D. Deutsch, A. Ekert, R. Jozsa, C. Macchiavello, S. Popescu & A. Sanpera. *Quantum privacy amplification and the security of quantum cryptography over noisy channels*. Phys. Rev .Lett., vol. 77, page 2818, 1996.

[DiVincenzo 00] D. P. DiVincenzo. *The physical implementation of quantum computation*. Fortschr. Phys., vol. 48, page 771, 2000.

[DiVincenzo 01] D. P. DiVincenzo. *Dogma and heresy in quantum computing*. Quant. Inf. Comput., vol. 1, no. Special, page 1, 2001.

[DiVincenzo 03] D. P. DiVincenzo, T. Mor, P. W. Shor, J. A. Smolin & B. Terhal. *Unextendible product bases, uncompletable product bases and bound entanglement*. Commun. Math. Phys., vol. 238, page 379, 2003.

[Duan 00a] L.-M. Duan, J. I. Cirac, P. Zoller & E. S. Polzik. *Quantum communication between atomic ensembles using coherent light*. Phys. Rev. Lett., vol. 85, page 5643, 2000.

[Duan 00b] L.-M. Duan, G. Giedke, J. I. Cirac & P. Zoller. *Inseparability criterion for continuous variable systems*. Phys. Rev. Lett., vol. 84, page 2722, 2000.

[Duan 10] L.-M. Duan & C. Monroe. *Colloquium: Quantum networks with trapped ions*. Rev. Mod. Phys., vol. 82, page 1209, 2010.

[Dutta 11] O. Dutta, A. Eckardt, P. Hauke, B. Malomed & M. Lewenstein. *Bose–Hubbard model with occupation-dependent parameters*. New J. Phys., vol. 13, page 023019, 2011.

[Dür 99] W. Dür, J. I. Cirac & R. Tarrach. *Separability and distillability of multiparticle quantum systems*. Phys. Rev. Lett., vol. 83, page 3562, 1999.

[Dür 00] W. Dür & J. I. Cirac. *Classification of multiqubit mixed states: Separability and distillability properties*. Phys. Rev. A, vol. 61, page 042314, 2000.

[Eckert 07a] K. Eckert, O. Romero-Isart, M. Rodriguez, M. Lewenstein, E. S. Polzik & A. Sanpera. *Quantum non-demolition detection of strongly correlated systems*. Nat. Phys., vol. 4, page 50, 2007.

[Eckert 07b] K. Eckert, . Zawitkowski, A. Sanpera, M. Lewenstein & E. S. Polzik. *Quantum polarization spectroscopy of ultracold spinor gases*. Phys. Rev. Lett., vol. 98, page 100404, 2007.

[Eggeling 01] T. Eggeling & R. F. Werner. *Separability properties of tripartite states with $u \otimes u \otimes u$ symmetry*. Phys. Rev. A, vol. 63, page 042111, 2001.

[Ekert 91] A. K. Ekert. *Quantum cryptography based on Bell's theorem*. Phys. Rev. Lett., vol. 67, page 661, 1991.

[Fallani 07] L. Fallani, J. Lye, V. Guarrera, C. Fort & M. Inguscio. *Ultracold atoms in a disordered crystal of light: Towards a Bose glass*. Phys. Rev. Lett., vol. 98, page 130404, 2007.

[Fallani 08] L. Fallani, C. Fort & M. Inguscio. *Bose-Einstein condensates in disordered potentials*. Adv. Atom. Mol. Opt. Phy., vol. 56, page 119, 2008.

[Fine 82] A. Fine. *Hidden variables, joint probability, and the Bell inequalities*. Phys. Rev. Lett., vol. 48, page 291, 1982.

[Fisher 89] M. P. A. Fisher, G. Grinstein & D. S. Fisher. *Boson localization and the superfluid-insulator transition*. Phys. Rev. B, vol. 40, page 546, 1989.

[Gadway 11] B. Gadway, D. Pertot, J. Reeves, M. Vogt & D. Schneble. *Glassy behavior in a binary atomic mixture*. Phys. Rev. Lett., vol. 107, page 145306, 2011.

[Gavish 05] U. Gavish & Y. Castin. *Matter-wave localization in disordered cold atom lattices*. Phys. Rev. Lett., vol. 95, page 020401, 2005.

[Giamarchi 88] T. Giamarchi & H. Schulz. *Anderson localization and interactions in one-dimensional metals*. Phys. Rev. B, vol. 37, page 325, 1988.

[Giedke 01a] G. Giedke, B. Kraus, M. Lewenstein & J. I. Cirac. *Entanglement criteria for all bipartite Gaussian states*. Phys. Rev. Lett., vol. 87, page 167904, 2001.

[Giedke 01b] G. Giedke, B. Kraus, M. Lewenstein & J. I. Cirac. *Separability properties of three-mode Gaussian states*. Phys. Rev. A, vol. 64, page 052303, 2001.

[Giedke 02] G. Giedke & J. I. Cirac. *Characterization of Gaussian operations and distillation of Gaussian states*. Phys. Rev. A, vol. 66, page 032316, 2002.

[Greif 11] D. Greif, L. Tarruell, T. Uehlinger, R. Jördens & T. Esslinger. *Probing nearest-neighbor correlations of ultracold fermions in an optical lattice*. Phys. Rev. Lett., vol. 106, page 145302, 2011.

[Gu 09] M. Gu, C. Weedbrook, N. C. Menicucci, T. Ralph & P. van Loock. *Quantum computing with continuous-variable clusters*. Phys. Rev. A, vol. 79, page 062318, 2009.

[Gühne 05] O. Gühne, G. Tóth & H. J. Briegel. *Multipartite entanglement in spin chains*. New J. Phys., vol. 7, page 229, 2005.

[Gühne 09] O. Gühne & G. Tóth. *Entanglement detection*. Phys. Rep., vol. 474, page 1, 2009.

[Hammerer 10] K. Hammerer, A. S. Sørensen & E. S. Polzik. *Quantum interface between light and atomic ensembles*. Rev. Mod. Phys., vol. 82, page 1041, 2010.

[Hastings 07a] M. Hastings. *An area law for one-dimensional quantum systems*. J. Stat. Mech.: Theor. E., vol. 2007, page P08024, 2007.

[Hastings 07b] M. Hastings. *Entropy and entanglement in quantum ground states*. Phys. Rev. B, vol. 76, page 035114, 2007.

[Horodecki 96] M. Horodecki, P. Horodecki & R. Horodecki. *Separability of mixed states: Necessary and sufficient conditions*. Phys. Lett. A, vol. 223, page 1–8, 1996.

[Horodecki 97] P. Horodecki. *Separability criterion and inseparable mixed states with positive partial transposition*. Phys. Lett. A, vol. 232, page 333, 1997.

[Horodecki 98] M. Horodecki, P. Horodecki & R. Horodecki. *Mixed-state entanglement and distillation: Is there a "bound" entanglement in nature?* Phys. Rev. Lett., vol. 80, page 5239, 1998.

[Horodecki 99] P. Horodecki, M. Horodecki & R. Horodecki. *Bound entanglement can be activated*. Phys. Rev. Lett., vol. 82, page 1056, 1999.

[Horodecki 03] P. Horodecki. *From limits of quantum operations to multicopy entanglement witnesses and state-spectrum estimation*. Phys. Rev. A, vol. 68, page 052101, 2003.

[Horodecki 09] R. Horodecki, M. Horodecki & K. Horodecki. *Quantum entanglement*. Rev. Mod. Phys., vol. 81, page 865–942, 2009.

[Horodecki 10] K. Horodecki, M. Horodecki, P. Horodecki, R. Horodecki, M. Pawlowski & M. Bourennane. *Contextuality offers device-independent security*. arXiv:1006.0468, 2010.

[Hu 08] H. Hu, A. Strybulevych, J. H. Page, S. E. Skipetrov & B. A. van Tiggelen. *Localization of ultrasound in a three-dimensional elastic network*. Nat. Phys., vol. 4, page 945, 2008.

[Hyllus 12] Ph. Hyllus, W. Laskowski, R. Krischek, C. Schwemmer, W. Wieczorek, H. Weinfurter, L. Pezzé & A. Smerzi. *Fisher information and multiparticle entanglement*. Phys. Rev. A, vol. 85, page 022321, 2012.

[Jendrzejewski 12] F. Jendrzejewski, A. Bernard, K. Mueller, P. Cheinet, V. Josse, M. Piraud, L. Pezzé, L. Sanchez-Palencia, A. Aspect & P. Bouyer. *Three-dimensional localization of ultracold atoms in an optical disordered potential*. Nat. Phys., vol. 8, page 398, 2012.

[Jozsa 03] R. Jozsa & N. Linden. *On the role of entanglement in quantum-computational speed-up*. Proc. R. Soc. London A, vol. 459, no. 2036, page 2011, 2003.

[Julsgaard 01] B. Julsgaard, A. Kozhekin & E. S. Polzik. *Experimental long-lived entanglement of two macroscopic objects*. Nature, vol. 413, page 400, 2001.

[Julsgaard 03] B. Julsgaard. *Entanglement and quantum interactions with macroscopic gas samples*. PhD thesis, University of Aarhus, Denmark, 2003.

[Julsgaard 04] B. Julsgaard, J. Sherson, J. I. Cirac, J. Fiurášek & E. S. Polzik. *Experimental demonstration of quantum memory for light*. Nature, vol. 432, page 482, 2004.

[Kaszlikowski 08] D. Kaszlikowski & A. Kay. *A witness of multipartite entanglement strata*. New J. Phys., vol. 10, page 053026, 2008.

[Khalfin 85] L. A. Khalfin & B. S. Tsirelson. *Quantum and quasi-classical analogs of Bell inequalities.* In P. Lahti, ed., Symposium of the Foundations of Modern Physics, page 441–460. World Scientific, singapore, 1985.

[Kirsch 07] W. Kirsch. *An invitation to random Schrödinger operators*. arXiv:0709.3707 [math-ph], 2007.

[Kok 07] P. Kok, K. Nemoto, T. C. Ralph, J. P. Dowling & G. J. Milburn. *Linear optical quantum computing with photonic qubits*. Rev. Mod. Phys., vol. 79, page 135, 2007.

[Kondov 11] S. S. Kondov, W. R. McGehee, J. J. Zirbel & B. DeMarco. *Three-dimensional Anderson localization of ultracold matter.* Science (New York), vol. 334, page 66, 2011.

[Korbicz 06] J. Korbicz, O. Gühne, M. Lewenstein, H. Häffner, C. Roos & R. Blatt. *Generalized spin-squeezing inequalities in N-qubit systems: Theory and experiment*. Phys. Rev. A, vol. 74, page 052319, 2006.

[Koschorreck 09] M. Koschorreck & M. W. Mitchell. *Unified description of inhomogeneities, dissipation and transport in quantum light-atom interfaces*. J. Phys. B, vol. 42, page 195502, 2009.

[Kosterlitz 73] J. M. Kosterlitz & D. J. Thouless. *Ordering, metastability and phase-transitions in 2 dimensional systems*. J. Phys. C, vol. 6, page 1181, 1973.

[Kramer 93] B Kramer & A. MacKinnon. *Localization: Theory and experiment*. Rep. Prog. Phys., vol. 56, page 1469, 1993.

[Kruse 10] J. Kruse, C. Gierl, M. Schlosser & G. Birkl. *Reconfigurable site-selective manipulation of atomic quantum systems in two-dimensional arrays of dipole traps*. Phys. Rev. A, vol. 81, page 060308, 2010.

[Kuzmich 97] A. Kuzmich, K. Mølmer & E. S. Polzik. *Spin squeezing in an ensemble of atoms illuminated with squeezed light*. Phys. Rev. Lett., vol. 79, page 4782, 1997.

[Kuzmich 00] A. Kuzmich, L. Mandel & N. P. Bigelow. *Generation of spin squeezing via continuous quantum nondemolition measurement*. Phys. Rev. Lett., vol. 85, page 1594, 2000.

[Lavoie 10] J. Lavoie, R. Kaltenbaek, M. Piani & K. Resch. *Experimental bound entanglement in a four-photon state*. Phys. Rev. Lett., vol. 105, page 130501, 2010.

[Lewenstein 01] M. Lewenstein, B. Kraus, P. Horodecki & J. I. Cirac. *Characterization of separable states and entanglement witnesses*. Phys. Rev. A, vol. 63, page 044304, 2001.

[Lewenstein 07] M. Lewenstein, A. Sanpera, V. Ahufinger, B. Damski, A. Sen(De) & U. Sen. *Ultracold atomic gases in optical lattices: Mimicking condensed matter physics and beyond*. Adv. Phys., vol. 56, page 243, 2007.

[Lewenstein 12] M. Lewenstein, A. Sanpera & V. Ahufinger. *Ultracold atoms in optical lattices: Simulating quantum many-body systems*. Oxford University Press, 2012.

[Linden 07] N. Linden, S. Popescu, A. Short & A. Winter. *Quantum nonlocality and beyond: Limits from nonlocal computation*. Phys. Rev. Lett., vol. 99, page 180502, 2007.

[Lugan 07] P. Lugan, D. Clément, P. Bouyer, A. Aspect, M. Lewenstein & L. Sanchez-Palencia. *Ultracold Bose gases in 1d disorder: From Lifshits glass to Bose-Einstein condensate*. Phys. Rev. Lett., vol. 98, page 170403, 2007.

[Madsen 04] L. B. Madsen & K. Mølmer. *Spin squeezing and precision probing with light and samples of atoms in the Gaussian description*. Phys. Rev. A, vol. 70, page 052324, 2004.

[Mandel 95] L. Mandel & E. Wolf. *Optical coherence and quantum optics*. Cambridge University Press, Cambridge, 1995.

[Masanes 11] Ll. Masanes, S. Pironio & A. Acín. *Secure device-independent quantum key distribution with causally independent measurement devices.* Nat. Commun., vol. 2, page 238, 2011.

[Massignan 06] P. Massignan & Y. Castin. *Three-dimensional strong localization of matter waves by scattering from atoms in a lattice with a confinement-induced resonance*. Phys. Rev. A, vol. 74, page 013616, 2006.

[Menicucci 06] N. C. Menicucci, P. van Loock, M. Gu, C. Weedbrook, T. Ralph & M. Nielsen. *Universal quantum computation with continuous-variable cluster states*. Phys. Rev. Lett., vol. 97, page 110501, 2006.

[Menicucci 10] N. Menicucci, X. Ma & T. Ralph. *Arbitrarily large continuous-variable cluster states from a single quantum nondemolition gate*. Phys. Rev. Lett., vol. 104, page 250503, 2010.

[Methot 07] A. A. Methot & V. Scarani. *An anomaly of non-locality*. Quantum Inf. Comput., vol. 7, page 157, 2007.

[Mikeska 04] H.-J. Mikeska & A. K. Kolezhuk. *One-Dimensional Magnetism*. In U. Schollwöck, J. Richter, D. J. J. Farnell & R. F. Bishop, ed., Lecture Notes in Physics, vol. 645, volume 83, chapitre 1, pages 1–83. Springer, 2004.

[Militello 11] B. Militello & A. Messina. *Genuine tripartite entanglement in a spin-star network at thermal equilibrium*. Phys. Rev. A, vol. 83, page 042305, 2011.

[Murao 01] M. Murao & V. Vedral. *Remote information concentration using a bound entangled state*. Phys. Rev. Lett., vol. 86, page 352, 2001.

[Napolitano 10] M. Napolitano & M. W. Mitchell. *Nonlinear metrology with a quantum interface*. New J. Phys., vol. 12, page 093016, 2010.

[Napolitano 11] M. Napolitano, M. Koschorreck, B. Dubost, N. Behbood, R. J. Sewell & M. W. Mitchell. *Interaction-based quantum metrology showing scaling beyond the Heisenberg limit.* Nature, vol. 471, page 486, 2011.

[Nielsen 00] M. A. Nielsen & I. L. Chuang. *Quantum computation and quantum information*. Cambridge University Press, 2000.

[Nielsen 04] M. A Nielsen. *Optical quantum computation using cluster states*. Phys. Rev. Lett., vol. 93, page 040503, 2004.

[Niset 06] J. Niset & N. Cerf. *Multipartite nonlocality without entanglement in many dimensions*. Phys. Rev. A, vol. 74, page 052103, 2006.

[Ohliger 10] M. Ohliger, K. Kieling & J. Eisert. *Limitations of quantum computing with Gaussian cluster states*. Phys. Rev. A, vol. 82, page 042336, 2010.

[Osborne 02] T. Osborne & M. Nielsen. *Entanglement in a simple quantum phase transition*. Phys. Rev. A, vol. 66, page 032110, 2002.

[Osterloh 02] A. Osterloh, L. Amico, G. Falci & R. Fazio. *Scaling of entanglement close to a quantum phase transition.* Nature, vol. 416, page 608, 2002.

[Pai 96] R. Pai, R. Pandit, H. Krishnamurthy & S. Ramasesha. *One-dimensional disordered bosonic Hubbard model: A density-matrix renormalization group study*. Phys. Rev .Lett., vol. 76, page 2937, 1996.

[Pasienski 10] M. Pasienski, D. McKay, M. White & B. DeMarco. *A disordered insulator in an optical lattice*. Nat. Phys., vol. 6, page 677, 2010.

[Peres 96] A. Peres. *Separability criterion for density matrices*. Phys. Rev. Lett., vol. 77, page 1413, 1996.

[Pironio 05] S. Pironio. *Lifting Bell inequalities*. J. Math. Phys., vol. 46, page 062112, 2005.

[Pironio 10] S. Pironio, A. Acín, S. Massar, A. Boyer de la Giroday, D. N. Matsukevich, P. Maunz, S. Olmschenk, D. Hayes, L. Luo, T. A. Manning & C. Monroe. *Random numbers certified by Bell's theorem.* Nature, vol. 464, page 1021, 2010.

[Pironio 11] S. Pironio, J.-D. Bancal & V. Scarani. *Extremal correlations of the tripartite no-signaling polytope*. J. Phys. A: Math. Theor., vol. 44, page 065303, 2011.

[Pitowsky 01] I. Pitowsky & K. Svozil. *Optimal tests of quantum nonlocality*. Phys. Rev. A, vol. 64, page 014102, 2001.

[Popescu 94] S. Popescu & D. Rohrlich. *Nonlocality as an axiom*. Found. Phys., vol. 24, page 379, 1994.

[Pérez-Delgado 11] C. Pérez-Delgado & P. Kok. *Quantum computers: Definition and implementations*. Phys. Rev. A, vol. 83, page 012303, 2011.

[Roati 08] G. Roati, C. D Errico, L. Fallani, M. Fattori, C. Fort, M. Zaccanti, G. Modugno, M. Modugno & M. Inguscio. *Anderson localization of a non-interacting Bose-Einstein condensate.* Nature, vol. 453, page 895, 2008.

[Romero-Isart 12] O. Romero-Isart, M. Rizzi, C. Muschik, E. S. Polzik, M. Lewenstein & A. Sanpera. *Quantum memory assisted probing of dynamical spin correlations*. Phys. Rev. Lett., vol. 108, page 065302, 2012.

[Roscilde 09] T. Roscilde, M. Rodríguez, K. Eckert, O. Romero-Isart, M. Lewenstein, E. S. Polzik & A. Sanpera. *Quantum polarization spectroscopy of correlations in attractive fermionic gases*. New J. Phys., vol. 11, page 055041, 2009.

[Saffman 10] M. Saffman, T. Walker & K. Mølmer. *Quantum information with Rydberg atoms*. Rev. Mod. Phys., vol. 82, page 2313, 2010.

[Sanchez-Palencia 10] L. Sanchez-Palencia & M. Lewenstein. *Disordered quantum gases under control*. Nat. Phys., vol. 6, page 87, 2010.

[Sangouard 11] N. Sangouard, C. Simon, H. de Riedmatten & N. Gisin. *Quantum repeaters based on atomic ensembles and linear optics*. Rev. Mod. Phys., vol. 83, no. 1, page 33, 2011.

[Schliemann 03] J. Schliemann. *Entanglement in su(2)-invariant quantum spin systems*. Phys. Rev. A, vol. 68, page 012309, 2003.

[Schliemann 05] J. Schliemann. *Entanglement in su(2)-invariant quantum systems: The positive partial transpose criterion and others*. Phys. Rev. A, vol. 72, page 012307, 2005.

[Schlosser 11] M. Schlosser, S. Tichelmann, J. Kruse & G. Birkl. *Scalable architecture for quantum information processing with atoms in optical microstructures*. Quantum Inf. Process., vol. 10, page 907, 2011.

[Schwartz 07] T. Schwartz, G. Bartal, S. Fishman & M. Segev. *Transport and Anderson localization in disordered two-dimensional photonic lattices.* Nature, vol. 446, page 52, 2007.

[Sherson 05] J. Sherson & K. Mølmer. *Entanglement of large atomic samples: A Gaussian-state analysis*. Phys. Rev. A, vol. 71, page 033813, 2005.

[Sherson 06] J. F. Sherson, H. Krauter, R. K. Olsson, B. Julsgaard, K. Hammerer, J. I. Cirac & E. S. Polzik. *Quantum teleportation between light and matter.* Nature, vol. 443, page 557–60, 2006.

[Shor 03] P. W. Shor, J. A. Smolin & A. V. Thapliyal. *Superactivation of bound entanglement*. Phys. Rev. Lett., vol. 90, page 107901, 2003.

[Simon 85] B. Simon. *Ground state energy of the one-dimensional discrete random Schrödinger operator with Bernoulli potential*. J. Stat. Phys., vol. 38, page 66, 1985.

[Simon 00] R. Simon. *Peres-Horodecki separability criterion for continuous variable systems*. Phys. Rev. Lett., vol. 84, page 2726, 2000.

[Singer 10] K. Singer, U. Poschinger, M. Murphy, P. Ivanov, F. Ziesel, T. Calarco & F. Schmidt-Kaler. *Colloquium: Trapped ions as quantum bits: Essential numerical tools*. Rev. Mod. Phys., vol. 82, page 2609, 2010.

[Smolin 01] J. A. Smolin. *Four-party unlockable bound entangled state*. Phys. Rev. A, vol. 63, page 032306, 2001.

[Stasińska 09] J. Stasińska, C. Rodó, S. Paganelli, G. Birkl & A. Sanpera. *Manipulating mesoscopic multipartite entanglement with atom-light interfaces*. Phys. Rev. A, vol. 80, page 062304, 2009.

[Stasińska 12a] J. Stasińska, P. Massignan, M. Bishop, J. Wehr, A. Sanpera & M. Lewenstein. *Glass to superfluid transition in dirty bosons on a lattice*. New J. Phys., vol. 14, page 043043, 2012.

[Stasińska 12b] J. Stasińska, S. Paganelli & A. Sanpera. *Beyond pure state entanglement for atomic ensembles*. New J. Phys., vol. 14, page 033034, 2012.

[Stasińska 12c] J. Stasińska, B. Rogers, G. De Chiara & A. Sanpera. *Glass to superfluid transition in dirty bosons on a lattice*. New J. Phys., vol. 14, page 043043, 2012.

[Streltsov 05] A. Streltsov & L. Cederbaum. *Properties of fragmented repulsive condensates*. Phys. Rev. A, vol. 71, page 063612, 2005.

[Sørensen 98] J. Sørensen, J. Hald & E. S. Polzik. *Quantum noise of an atomic spin polarization measurement*. Phys. Rev. Lett., vol. 80, page 3487, 1998.

[Takeuchi 06] M. Takeuchi, T. Takano, S. Ichihara, Y. Takasu, M. Kumakura, T. Yabuzaki & Y. Takahashi. *Paramagnetic Faraday rotation with spin-polarized ytterbium atoms*. Appl. Phys. B, vol. 83, page 107, 2006.

[Tóth 07] G. Tóth, C. Knapp, O. Gühne & H. J. Briegel. *Optimal spin squeezing inequalities detect bound entanglement in spin models*. Phys. Rev .Lett., vol. 99, page 250405, 2007.

[Tóth 12] G. Tóth. *Multipartite entanglement and high-precision metrology*. Phys. Rev. A, vol. 85, page 022322, 2012.

[van Loock 00] P. van Loock & S. L. Braunstein. *Multipartite entanglement for continuous variables: A quantum teleportation network*. Phys. Rev. Lett., vol. 84, page 3482, 2000.

[van Loock 03] P. van Loock & A. Furusawa. *Detecting genuine multipartite continuous-variable entanglement*. Phys. Rev. A, vol. 67, page 052315, 2003.

[van Loock 07] P. van Loock, C. Weedbrook & M. Gu. *Building Gaussian cluster states by linear optics*. Phys. Rev. A, vol. 76, page 032321, 2007.

[Verstraete 04a] F. Verstraete, M. Popp & J. I. Cirac. *Entanglement versus correlations in spin systems*. Phys. Rev. Lett., vol. 92, page 027901, 2004.

[Verstraete 04b] F. Verstraete, D. Porras & J. I. Cirac. *Density matrix renormalization group and periodic boundary conditions: A quantum information perspective*. Phys. Rev. Lett., vol. 93, page 227205, 2004.

[Vidal 02] G. Vidal & R. F. Werner. *Computable measure of entanglement*. Phys. Rev. A, vol. 65, page 032314, 2002.

[Vidal 03a] G. Vidal. *Efficient Classical Simulation of Slightly Entangled Quantum Computations*. Phys. Rev. Lett., vol. 91, page 147902, 2003.

[Vidal 03b] G. Vidal, J. I. Latorre, E. Rico & A. Kitaev. *Entanglement in quantum critical phenomena*. Phys. Rev. Lett., vol. 90, page 227902, 2003.

[Vidal 04] G. Vidal. *Efficient simulation of one-dimensional quantum many-body systems*. Phys. Rev. Lett., vol. 93, page 040502, 2004.

[Vollbrecht 01] K. Vollbrecht & R. F. Werner. *Entanglement measures under symmetry*. Phys. Rev. A, vol. 64, page 062307, 2001.

[Vollbrecht 02] K. G. H. Vollbrecht & M. M. Wolf. *Conditional entropies and their relation to entanglement criteria*. J. Math. Phys., vol. 43, page 4299, 2002.

[Wallach 02] N. R. Wallach. *An unentangled Gleason's theorem*. In S. J. Lomonaco Jr. & H. E. Brandt, ed., Contemporary Mathematics: Quantum Computation and Information, volume 305, 2002.

[Wang 02] X. Wang. *Threshold temperature for pairwise and many-particle thermal entanglement in the isotropic Heisenberg model*. Phys. Rev. A, vol. 66, page 044305, 2002.

[Weedbrook 12] C. Weedbrook, S. Pirandola, R. García-Patrón, N. Cerf, T. Ralph, J. Shapiro & S. Lloyd. *Gaussian quantum information*. Rev. Mod. Phys., vol. 84, page 621, 2012.

[Wei 03] T.-Ch. Wei & P. Goldbart. *Geometric measure of entanglement and applications to bipartite and multipartite quantum states*. Phys. Rev. A, vol. 68, page 042307, 2003.

[Werner 89] R. F. Werner. *Quantum states with Einstein-Podolsky-Rosen correlations admitting a hidden-variable model*. Phys. Rev. A, vol. 40, page 4277, 1989.

[Werner 01a] R. F. Werner & M. Wolf. *All-multipartite Bell-correlation inequalities for two dichotomic observables per site*. Phys. Rev. A, vol. 64, page 032112, 2001.

[Werner 01b] R. F. Werner & M. M. Wolf. *Bound entangled Gaussian states*. Phys. Rev. Lett., vol. 86, page 3658, 2001.

[Wiersma 97] D. S. Wiersma, P. Bartolini, A. Lagendijk & R. Righini. *Localization of light in a disordered medium*. Nature, vol. 390, page 671, 1997.

[Wolfgramm 10] F. Wolfgramm, A. Cerè, F. A. Beduini, A. Predojević, M. Koschorreck & M. W. Mitchell. *Squeezed-light optical magnetometry*. Phys. Rev. Lett., vol. 105, page 053601, 2010.

[Yukawa 08] M. Yukawa, R. Ukai, P. van Loock & A. Furusawa. *Experimental generation of four-mode continuous-variable cluster states*. Phys. Rev. A, vol. 78, page 012301, 2008.

[Zhang 06] J. Zhang & S. L. Braunstein. *Continuous-variable Gaussian analog of cluster states*. Phys. Rev. A, vol. 73, page 032318, 2006.

[Zhang 09] J. Zhang, G. Adesso, C. Xie & K. Peng. *Quantum teamwork for unconditional multiparty communication with Gaussian states*. Phys. Rev. Lett., vol. 103, page 070501, 2009.

[Zhang 11] J. Zhang. *Continuous-variable Gaussian unlockable bound entangled state*. Phys. Rev. A, vol. 83, page 052327, 2011.

[Śliwa 03] C. Śliwa. *Symmetries of the Bell correlation inequalities*. arXiv:quant-ph/0305190, 2003.

[Štelmachovic 04] P. Štelmachovic & V. Bu ek. *Quantum-information approach to the Ising model: Entanglement in chains of qubits*. Phys. Rev. A, vol. 70, page 032313, 2004.

[Zyczkowski 98] K. Zyczkowski, P. Horodecki, A. Sanpera & M. Lewenstein. *Volume of the set of separable states*. Phys. Rev. A, vol. 58, page 883, 1998.